
EXPERIMENTAL VALIDATION AND NUMERICAL MODELLING OF TRAIN-BRIDGE DYNAMICS



by

ing. P. Boersma

UNIVERSITY OF TWENTE

Faculty of Engineering Technology (ET)

Mechanical Engineering

Department of Mechanics of Solids, Surfaces and Systems (MS³)

Dynamics Based Maintenance (DBM) Research group

**EXPERIMENTAL VALIDATION AND
NUMERICAL MODELLING OF
TRAIN-BRIDGE DYNAMICS**

A thesis submitted to the University of Twente in accordance with the
requirements of the degree of Master of Science in Mechanical
Engineering

AUTHOR:

ing. P. Boersma
s2428288

Enschede, The Netherlands
11.10.2023

THESIS SUPERVISORS:

dr. ir. R. Loendersloot
dr. ir. A.A. Meghoe

EXAMINATION COMMITTEE:

dr. ir. M.H.M. Ellenbroek

Acknowledgement

First and foremost, I want to thank my supervisors dr. ir R. Loendersloot and dr. ir. A. A. Meghoe, for their supervision throughout this thesis. The meetings have significantly enriched my knowledge, and I am grateful for their advice, feedback and overall assistance with the report.

Special appreciation goes to ing. Z.A.J. Lok for the assistance with electronics and advice regarding the experiments. I am also thankful for the provision of space in the Dynamics Lab for the experimental setup.

I would like to acknowledge ing. N.T.M. Spikker from the workshop for the design advice related to manufacturing. Additionally, I would like to acknowledge K. Wissink of Geerding and D.R.F. de Kinkelder for their assistance and expertise throughout the manufacturing process.

I would like to express my appreciation to the members of my examination committee. I am also thankful to the DBM group for their tips and feedback during our monthly meetings. Last but not least, I would thank all my friends and fellow students for their support.

Summary

Structural Health Monitoring (SHM) plays a crucial role in maintenance strategies aimed at ensuring structural health and safety in bridges. While prior research has focused on numerical research, experimental validation of train-bridge dynamics has lagged behind. To enhance the understanding of train-bridge interactions, the overarching goal is to establish an experimental setup and related experiments for validating numerically calculated train dynamics.

The realisation of the experimental setup involves scaling down the Boyne Viaduct to a laboratory-scale prototype using the similarity analysis. It has been demonstrated that a relaxed model, allowing for deviations in damping coefficient and inertia terms, has proven acceptable behaviour in terms of frequency and mass ratios, yielding the ratio between train and bridge. The setup was designed based on its intended functions, with concepts evaluated against design requirements and success criteria to identify the optimal concept. Validation of the design against the Boyne Viaduct confirmed compliance with these ratios.

To enhance the benchmark numerical model, which comprises a dual suspended mass, link connectors are introduced to realise the bogie model. A more accurate numerical representation of the half-train model and the train model is achieved by incorporating a velocity ramp in the boundary condition and ensuring a neutral position of train components after applying the train body mass.

Experimental validation has not yet been completed. Enhancements to the validation, such as increasing bridge and train masses and varying spring coefficients, are proposed. The current method of determining natural frequencies, using the roving hammer technique, was found inaccurate, indicating the need for a more precise approach in future studies. Using the shaker method, despite its added experimental complexity, is recommended. This approach ensures consistent results and reduces local geometric bouncing, leading to more accurate results.

The numerical simulations reveal that the modal analysis aligns with the dynamic analysis. Moreover, during the train's passage over the bridge, known as the traverse phase, resonance frequencies vary due to the time-dependent mass distribution of the train on the bridge. Additionally, simulations indicate that uneven axle spacing leads to asymmetrical behaviour of these resonance frequencies.

The results of the dynamic analysis exhibit spikes in the frequency content. An inverse relation between velocity and the number of spikes has been found, along with the position of the spikes shifting further along the bridge by higher velocities. These numerically generated spikes are likely related to the train's velocity and element edge length. Additionally, there seems to be a correlation with the frequency ratio, and it is assumed that axle spacing may also influence this behaviour revolving the spikes. Nevertheless, these factors require further validation.

The DMU train configuration only reveals the bridge's fundamental frequency. The bogie's bouncing frequency remains hidden because of the train's high damping coefficient, which filters out the vibration information from the response. This high damping, along with inadequate train-bridge interaction resulting from low mass, leads to insufficient bridge excitation, causing the absence of the bogie's bouncing frequency. The insufficient bridge excitation also results in minimal change in the bridge's fundamental frequency. SHM methods focus on detecting changes in the bridge's fundamental frequency during the traverse phase, and with minimal changes render this train configuration unsuitable for SHM methods.

It has been found that the amplitude ratio between the train and the bridge for modes changes during the traverse phase. This change is suspected to be connected to the distribution of kinetic energy, providing information into the prominent resonance

frequency in the results. However, additional research in this area is necessary to explore possibilities and effectiveness in this area. Similarly, further investigation is required when introducing multiple carriages to study resonance. The next phase towards enhancing structural safety and method validation entails introducing damage into both the experimental setup and numerical environment.

Contents

List of Figures	xx
List of Tables	xxii
1 Introduction	1
1.1 Background	1
1.2 Research problem	6
1.3 Research aim, objectives, questions and hypothesis	6
1.4 Approach	8
1.5 Limitations	8
1.6 Structure	10
2 Theoretical framework	11
2.1 Scaling methods	11
2.2 Similarity analysis	11
2.3 Closing Remarks	16
3 Experimental setup	17
3.1 Development	17
3.2 Implementation similarity analysis and relaxation	17
3.3 Design	19
3.3.1 Bridge	20
3.3.2 Train	20
3.3.3 Motor system	21
3.3.4 Support	21
3.3.5 Validation	22
3.4 Experiments and setup	23
3.4.1 Natural frequency analysis	23
3.4.2 Modal analysis	24
3.4.3 Dynamic	25
3.5 Closing remarks	26
4 Numerical modelling	27
4.1 Development	27
4.2 Model	28
4.3 Simulations	31
4.4 Closing remarks	32
5 Results and discussion	33
5.1 Simulations locomotive	33
5.1.1 Natural frequency	33
5.1.2 Modal analysis	33
5.1.3 Dynamic analysis	35
5.2 Variation study of the bogie variant	38
5.2.1 Velocity	39
5.2.2 Remaining quantities	40

5.3	Simulations DMU	42
5.4	Experiments	43
5.4.1	Natural frequency	44
5.4.2	Modal analysis	46
5.4.3	Dynamic analysis	47
5.5	Simulations experimental setup	47
5.5.1	Modal analysis	48
5.5.2	Dynamic analysis	49
5.6	Closing remarks	50
6	Conclusions	51
7	Recommendations	53
	References	55
	Appendices	59
A	Boyne Viaduct	61
B	Train configurations	63
C	Similarity analysis	65
C.1	Implementation of the complete similarity	65
C.2	Relaxation of the similarity analysis	67
D	Equations of motion: train-bridge problem	69
E	Development of the experimental setup	71
E.1	Function analysis	71
E.2	Design requirements	71
E.3	Success criteria	71
F	Concepts and assessment	73
F.1	Morphological chart	73
F.2	Concepts	73
F.3	Concept assessment	76
G	Design details	79
G.1	Design, production and materials	79
G.2	Bridge structure	80
G.3	Train	81
G.4	Motor system	82
G.5	Challenges	82
H	Validation experimental setup	83
H.1	Validation prototype and design	83
H.2	Validation model and design	84
I	Settings experiments	85
I.1	Natural frequency analysis	85
I.2	Dynamic analysis	86
J	Numerical model development	87
J.1	Train	87
J.2	Bridge	89
K	Simulations locomotive	91

L	Variation study: Velocity	93
M	Simulations DMU	95
N	Experimental results	97
O	Simulations experimental setup	99

Acronyms

This chapter presents the abbreviations used in this thesis.

2D	Two-Dimensional
3D	Three-Dimensional
BCM	Bridge Condition Monitoring
DAQ	Data Acquisition
DI	Damage Identification
DMU	Diesel multiple unit
FSA	Fixed Sensor Approach
IF	Instantaneous Frequency
MAC	Modal Assurance Criterion
MCFM	Moving Constant Force Model
MHFM	Moving Harmonic Force Model
MIMO	Multiple Input Multiple Output
MISO	Multiple Input Single Output
MMM	Moving Mass Model
MSA	Moving Sensor Approach
MSDMM	Moving Spring-Damping-Mass Model
NI	National Instruments
SHM	Structural Health Monitoring
TAVBM	Two-Axle Vehicle-Bridge Model
TBDIM	Train-Bridge Dynamic Interaction Model
TTBDIM	Train-Track-Bridge Dynamic Interaction Model
WF	Weight Factor
WSST	Wavelet SynchroSqueezed Transform

List of Symbols

This chapter outlines the symbols utilised in this thesis, distinguishing between Roman and Greek symbols.

Roman symbols

A_{bridge}	The bridge's cross-sectional area	m^2
C_{p}	The damping coefficient of the primary suspension	Nsm^{-1}
C_{s}	The damping coefficient of the secondary suspension	Nsm^{-1}
E_{bridge}	Young's modulus of Elasticity of the bridge's material	Nm^{-2}
$f_{i,\text{bridge}}$	The i^{th} fundamental frequency of the bridge	Hz
f_{train}	The train's bouncing frequency	Hz
I_{bridge}	The bridge's area moment of inertia	m^4
J_{b}	The bogie's mass moment of inertia	kgm^2
J_{tb}	The train's body mass moment of inertia	kgm^2
J_{w}	The wheel's mass moment of inertia	kgm^2
K_{p}	The stiffness coefficient of the primary suspension	Nm^{-1}
K_{s}	The stiffness coefficient of the secondary suspension	Nm^{-1}
K_{train}	The train's suspension system for a single degree of freedom system.	Nm^{-1}
L_{b}	The distance between the secondary suspension systems	m
L_{bridge}	The bridge's span length	m
L_{wb1}	The distance between wheel 1 and wheel 2	m
L_{wb2}	The distance between wheel 2 and wheel 3	m
M_{b}	The bogie's mass	kg
M_{bridge}	The bridge's mass	kg
M_{tb}	The train's body mass	kg
M_{train}	The train's mass	kg
M_{w}	The wheel's mass	kg
R_{w}	The wheel's radius	m
v_{critical}	The critical train's velocity dependent on the driving frequency	ms^{-1}
x_{train}	The train's position along the bridge	m

Greek symbols

$\eta_{\text{frequency}}$	The ratio of the train's bouncing frequency to the bridge's fundamental frequency	-
$\eta_{\text{frequency.body}}$	The ratio of the body's bouncing frequency to the bridge's fundamental frequency	-
$\eta_{\text{frequency.bogie1}}$	The ratio of the first bogie's bouncing frequency to the bridge's fundamental frequency	-
$\eta_{\text{frequency.bogie2}}$	The ratio of the second bogie's bouncing frequency to the bridge's fundamental frequency	-
η_{mass}	The ratio of the train's mass to the bridge's mass	-
$\eta_{\text{mass.body}}$	The ratio of the body's mass to the bridge's mass	-
$\eta_{\text{mass.bogie}}$	The ratio of the bogie's mass to the bridge's mass	-
$\eta_{\text{mass.wheel}}$	The ratio of the wheel's mass to the bridge's mass	-
ρ_{bridge}	The density of the bridge's material	kgm^{-3}

List of Figures

1.1	The history of the development of modelling methods.	1
1.2	An overview of models to be validated, wherein the number of axles can be varied while maintaining the same underlying model.	6
1.3	Thesis approach.	9
2.1	Physical quantities involved in the example problem.	13
3.1	Most suitable solution for (a) function 1 being rotational arm, (b) function 2 being slots, (c) function 3 being extern closed-loop or (d) function 4 being weights.	17
3.2	Graphical representation of the model to be scaled, incorporating the relevant physical quantities.	18
3.3	Representation of the (a) experimental setup or (b) subsystems in the experimental setup.	19
3.4	Connections in the bridge structure for (a) the top section or (b) the rail section.	20
3.5	Representation of the train's subsystems.	20
3.6	Representation of the bogie's subsystems.	21
3.7	Representation of the motor system and its subsystems.	21
3.8	Representation of the (a) support within the design or (b) support and its subsystems	22
3.9	Schematic overview of the setup for experimentally determining the natural frequencies.	23
3.10	Sensor and strike location(s) for the various subsystems.	24
3.11	Schematic overview of the setup for the dynamics analyses.	25
3.12	Switch and sensor locations on the experimental setup during the dynamic experiments.	25
4.1	Four stages during the model development of the train part.	27
4.2	Numerical train models encompassing the bogie variant, half-train variant and train variant corresponding to the locomotive train configuration and experimental setup.	28
4.3	Numerical train models encompassing the bogie variant, half-train variant and train variant corresponding to the DMU train configuration.	29
4.4	Bridge model and the phase separation employed in the dynamic analysis.	30
5.1	Modal analysis of the bogie variant across the bridge.	34
5.2	Mode shapes retrieved from the stepwise eigenfrequency analyses show that the bogie and the bridge move (a) in-phase or (b) out-of-phase (courtesy R. Loendersloot).	34
5.3	Modal analysis of the half-train variant across the bridge.	35
5.4	Modal analysis of the train variant across the bridge.	35
5.5	Vertical acceleration response of the mid-span node excited by the bogie variant traversing the bridge with a velocity of 10 m/s.	36

5.6	A comparison for the bogie variant between the modal analysis, and the dynamic analysis based upon the vertical acceleration of the mid-span node and a velocity of 10 m/s.	37
5.7	Amplitude of modes according the bogie variant.	37
5.8	A comparison for the half-train variant between the modal analysis, and the dynamic analysis based upon the vertical acceleration of the mid-span node and a velocity of 10 m/s.	38
5.9	A comparison for the train variant between the modal analysis, and the dynamic analysis based upon the vertical acceleration of the mid-span node and a velocity of 10 m/s.	38
5.10	The extracting of a spike's location from the result of a dynamic simulation based upon the vertical acceleration of the mid-span node and a velocity of 30 m/s.	39
5.11	Number of spikes retrieved from the vertical acceleration response of (a) the traverse phase of the the mid-span node or (b) the entrance phase of the bogie node.	40
5.12	Spike locations retrieved from the vertical acceleration response of (a) the traverse phase of the the mid-span node or (b) the entrance phase of the bogie node.	41
5.13	Difference between consecutive spikes retrieved from the vertical acceleration response of (a) the traverse phase of the the mid-span node or (b) the entrance phase of the bogie node.	41
5.14	A comparison for the bogie variant between the modal analysis, and the dynamic analysis based upon the vertical acceleration of the mid-span node and a velocity of 10 m/s.	42
5.15	A comparison for the bogie variant between the modal analysis, and the dynamic analysis based upon the vertical acceleration of the mid-span node, a velocity of 10 m/s and by equating the damping coefficient to the locomotive.	43
5.16	A comparison for the bogie variant between the modal analysis, and the dynamic analysis based upon the vertical acceleration of the mid-span node, a velocity of 10 m/s, and by equating the damping coefficient and mass ratio to the locomotive.	44
5.17	A comparison for the bogie variant between the modal analysis, and the dynamic analysis based upon the vertical acceleration of the mid-span node, a velocity of 10 m/s, and by equating the damping coefficient, mass ratio and frequency to the locomotive.	44
5.18	Modal analysis of the bogie variant across the bridge.	46
5.19	Dynamic analysis of the bogie variant based upon experimental data from the vertical acceleration of the mid-span node.	47
5.20	A comparison for the bogie variant between experimental results and numerical results of the modal analysis.	48
5.21	Dynamic analysis of the bogie variant based upon the vertical acceleration response of the mid-span node with a gravitational constant of 396.177 m/s^2 and a material damping coefficient (β) of 0.000025.	49
5.22	Dynamic analysis of the bogie variant based upon the vertical acceleration response of the mid-span node with the bogie mass and the spring stiffness multiplied by 40.	50
A.1	Boyne Viaduct in Drogheda, County Louth, Ireland.	61
A.2	Schematic representation of the Boyne Viaduct.	61
B.1	Schematic representation of (a) the 201 Class locomotive or (b) the diesel multiple unit (DMU) carriage train.	63

C.1	Effect of varying the primary and secondary damping coefficients on the frequency component of (a) the body or (b) the bogie.	68
D.1	Representation for obtaining the equations of motion for the problem.	69
E.1	Function tree regarding the design of the experimental setup.	71
F.1	Morphological chart for the design of the experimental setup.	73
F.2	Representation of concept 1 for (a) the bogie's design (b) the complete design.	74
F.3	Representation of concept 2 for (a) the bogie's design (b) the complete design.	74
F.4	Representation of concept 3 for (a) the bogie's design (b) the complete design.	74
F.5	Representation of concept 4 for (a) the bogie's design (b) the complete design.	75
F.6	Representation of concept 5 for (a) the bogie's design (b) the complete design.	75
G.1	A section view of the bogie and its main components.	81
I.1	Tools employed for obtaining the natural frequency of (a) the body or (b) the bogie.	85
J.1	The four stages of the model development of the train part.	87
J.2	Crash cases with the velocity boundary condition applied at the wheel node (node 2) for (a) before simulation or (b) during simulation.	88
J.3	Crash cases with the velocity boundary condition applied at wheel (node 2) and a kinematic constraint applied to all nodes w.r.t. degree of freedom 6 for (a) before simulation or (b) during simulation.	88
J.4	Crash case after solely adding the secondary suspension system for (a) before simulation or (b) during simulation.	89
K.1	A comparison for the bogie variant between the modal analysis, and the dynamic analysis based upon the vertical acceleration of the quarter node and a velocity of 10 m/s.	91
K.2	A comparison for the bogie variant between the modal analysis, and the dynamic analysis based upon the vertical acceleration of the three-quarter node and a velocity of 10 m/s.	91
K.3	A comparison for the bogie variant between the modal analysis, and the dynamic analysis based upon the vertical acceleration of the first wheel and a velocity of 10 m/s.	92
K.4	A comparison for the bogie variant between the modal analysis, and the dynamic analysis based upon the vertical acceleration of the bogie and a velocity of 10 m/s.	92
L.1	Dynamic simulation of the bogie variant with a velocity of 5 m/s.	93
L.2	Dynamic simulation of the bogie variant with a velocity of 23 m/s.	93
L.3	Dynamic simulation of the bogie variant with a velocity of 24 m/s.	94
L.4	Dynamic simulation of the bogie variant with a velocity of 25 m/s.	94
M.1	A comparison for the bogie variant between the modal analysis, and the dynamic analysis based upon the vertical acceleration of the mid-span node, a velocity of 10 m/s, and by equating the damping coefficient, mass ratio and frequency to the locomotive, and introducing unequal axle spacing.	95

M.2	A comparison for the half-train variant between the modal analysis, and the dynamic analysis based upon the vertical acceleration of the mid-span node and a velocity of 10 m/s.	96
M.3	A comparison for the train variant between the modal analysis, and the dynamic analysis based upon the vertical acceleration of the mid-span node and a velocity of 10 m/s.	96
N.1	Modal analysis of the half-train variant across the bridge.	97
N.2	Modal analysis of the train variant across the bridge.	97
N.3	Dynamic analysis of the half-train variant based upon experimental data from the vertical acceleration of the mid-span node.	98
N.4	Dynamic analysis of the train variant based upon experimental data from the vertical acceleration of the mid-span node.	98
O.1	Modal analysis of the half-train variant across the bridge.	99
O.2	Modal analysis of the train variant across the bridge.	99

List of Tables

1.1	Overview of research related to the experimental validation of train models regarding DI.	5
2.1	Physical quantities and their fundamental dimensions occurring in the example problem.	13
2.2	Dimensionless products of the example problem.	15
2.3	Input values for determining the remaining prototype quantities using the dimensionless products.	15
2.4	Output values of the remaining prototype quantities	15
2.5	Frequency and mass ratio for the model and the prototype for the specific problem.	16
3.1	Input and output values, denoted by gray-filled cells, of the similarity analysis with prototype values corresponding to the experimental setup.	18
3.2	Frequency and mass ratios between model and SOLIDWORKS design with associated differences. The model represents the Boyne Viaduct and concerning locomotive train configuration.	22
3.3	Equipment for experimentally determining the natural frequencies.	24
3.4	Equipment for the dynamic experiments.	25
3.5	Equipment employed for the associated experiments.	26
4.1	Quantities employed in the numerical models.	29
4.2	Coordinate values employed in the numerical train models.	30
4.3	Frequency and mass ratios of the numerical models.	30
5.1	Natural frequency analysis per train variant.	33
5.2	Natural frequencies per train variant obtained experimentally.	45
A.1	Properties of the Boyne Viaduct.	62
C.1	Physical quantities and their fundamental dimensions occurring in the experimental setup.	66
C.2	Dimensionless products for the train-bridge problem.	66
C.3	Input and output values, denoted by gray-filled cells, of the similarity analysis with prototype values corresponding to the experimental setup.	67
E.1	Design requirements regarding design of the experimental setup.	72
F.1	Assessment of mimicking the dynamic behaviour on the success criteria.	76
F.2	Assessment of the guidance on the success criteria.	77
F.3	Assessment of the motor system on the success criteria.	77
F.4	Assessment of the fixating of the bridge on the success criteria.	78
H.1	Validation of the physical quantities between the prototype (similarity analysis) and SOLIDWORKS design with associated differences.	83
H.2	Frequency and mass ratios between prototype (similarity analysis) and SOLIDWORKS design with associated differences.	84

H.3	Frequency and mass values of both the model (Boyne Viaduct) and SOLIDWORKS design.	84
I.1	Measurement settings for the Sound and Vibration Measurement System.	86

1 | Introduction

Structural Health Monitoring (SHM), including Bridge Condition Monitoring (BCM), maintenance strategies, and dynamic behaviour analysis, have all demonstrated as fundamental factor for ensuring structural health and safety. To quantify the bridge's condition, methods to perform Damage Identification (DI) are essential.

There has been an lack of experimental validation and research concerning the effect of train dynamics on bridges, as well as whether increasing the complexity improves DI. This gap is particularly relevant during the period of a train passing a bridge, namely the traverse phase, which is a nonstationary process due to the time-dependent mass distribution of the train on the bridge, i.e. transient behaviour. Addressing this gap is essential as gaining a more profound understanding of the impact of train dynamics, along with experimental validation, will aid on identifying the bridge condition and development of maintenance strategies.

This research aims to identify and evaluate the influence of train dynamics in an effort to bridge the gap between the field experiments and the numerical results. This is achieved by developing an experimental setup with various train variants and developing a more advanced numerical model containing complex train dynamics.

This chapter will discuss the background of the study, followed by the identification of the research problem. It continues with the research aims, objectives, questions and hypothesis. Finally, the approach, limitations and structure will be provided.

1.1 Background

Bridges are subjected to repeated (dynamic) traffic loading and exposure to environmental conditions, leading to structural deterioration. The structural integrity must be monitored, analysed and assessed so that maintenance strategies can be established and performed accordingly. In order to analyse the structural integrity of bridges, models are required that describe the system's actual behaviour and subsequently describe the connection between dynamic behaviour and failure mechanisms. This thesis focuses on the former aspect.

Models

During the early 20th century, extensive research has been conducted in the field of model development pertaining to trains, bridges, tracks and their interactions. The development of models utilised in earlier studies has been represented in fig. 1.1.

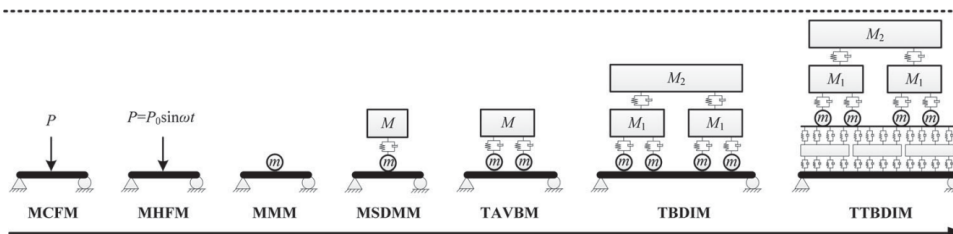


Figure 1.1: The history of the development of modelling methods. MCFM: Moving Constant Force Model, MHFM: Moving Harmonic Force Model, MMM: Moving Mass Model, MSDMM: Moving Spring-Damping-Mass Model, TAVBM: Two-Axle Vehicle-Bridge Model, TBDIM: Train-Bridge Dynamic Interaction Model, TTBDIM: Train-Track-Bridge Dynamic Interaction Model [1].

In the early stages, the problem was modelled as Moving Constant Force Model (MCFM) or Moving Harmonic Force Model (MHFM), which capture the dynamic characteristics (vertical behaviour) of the bridge. However, these models neglect the dynamic interaction between bridge and passing train, making them only applicable by a low mass ratio (defined as the train's mass divided by that of the bridge) and when the dynamic behaviour of the train is of lesser importance [1]. The Moving Mass Model (MMM) considers the influence of the train but does not accommodate the dynamic behaviour of the moving train [1]. A clear distinction is that MCFM represents a stationary process, while the MMM pertains to a nonstationary process. The Moving Spring-Damping-Mass Model (MSDMM) is capable to study the dynamic interaction between a moving train and a bridge, while including the vibration absorbing effect of the train's suspension system [1].

The MSDMM can be expanded further to describe the actual behaviour, as depicted in fig. 1.1. These extension serve for various purposes, including train running safety, DI or riding comfort. Montenegro et al. [2] offers a review on train running safety on bridges. This paper demonstrates that research within this field utilises three-dimensional (3D) models to adequately analyse derailment caused by crosswinds, earthquakes, track eccentricities, etc. It is emphasised that 3D modelling should only be included when aforementioned motivations are deemed relevant [3]. Moreover, for train running safety and comfort, the models employed are supported by detailed 3D representation of both the track and train, incorporating train dynamics. Notable, 3D modelling is frequently disregarded in DI due to its irrelevance and the aim to simplify the problem, a pursuit shared by this thesis.

Incorporating flexible elements into the train model has been found to have a limited impact on the bridge's response [4]. However, such considerations become more relevant when addressing concerns related to derailment [5]. Expanding the bridge construction with additional track structure has shown to have minimal practical effects on both bridge displacement and acceleration, while a greater effect has been observed in the train responses [6, 7]. An extended track model has to be incorporated in research regarding riding comfort [8]. Regarding frequency content, track models up to approximately 10-15 Hz exhibit negligible effects, with the track model acting as a filter beyond 15 Hz [9]. Moreover, rail irregularities have been observed to exert minimal influence on the vertical displacement of the bridge [10] and its acceleration [11]. Rail irregularities primarily impact the train's vertical response and the bridge's lateral responses, where these metrics are not directly related to DI [6, 11, 12]. Consequently, in this thesis, flexible elements within the train model, an extended track model, and rail irregularities are excluded for these reasons.

Damage identification

DI is a process that involves the detection of damage, the localisation of damage, and the assessment of the severity of damage [13]. The coupled dynamic response between the bridge and a passing train has been extensively employed to facilitate DI. This is achieved through either analysing the bridge response (referred to as direct methods) or the train response (referred to as indirect methods) [14]. Direct methods (Fixed Sensor Approach (FSA)) rely on the installation of numerous vibration sensors on the bridge structure itself. Moreover, FSA is inherently tailored for a specific bridge, posing challenges when transitioning between different bridges [15]. Conversely, indirect methods (Moving Sensor Approach (MSA)), as originally proposed by Yang [16], utilise vibration data recorded by a moving train to determine the bridge's dynamic properties. This approach minimises the amount of sensors for collecting response data [15]. A comparison between FSA and MSA reveals that MSA exhibits greater sensitivity to changes compared to FSA [17]. However, MSA introduces complexity through the incorporation of additional suspension systems in contrast to FSA. For this reason, this thesis employs the FSA method.

Dynamic response

The bridge's dynamic response when excited by a moving train can be divided into three phases: the entrance, the traverse and the leaving phase, as illustrated in fig. 4.4. The entrance phase corresponds to the time before the train enters the bridge but does not provide additional insights into the bridge's dynamic analysis [18].

The leaving phase corresponds to a stationary process in which no external force is present due to the absence of the train. This phase leads to a free vibration response that decays over time, due to the bridge's material damping. Environmental conditions, such as temperature, can influence modal parameters like natural frequency due to stiffness variations [19]. Temperature-induced expansion and contraction can lead to frequency shifts [20–22]. Moreover, modal parameters obtained from free vibrations represent averaged characteristics (global features) and may not be sensitive to localised damage [23]. Consequently, changes in natural frequency caused by environmental factors may be mistaken for damage, making the leaving phase less suitable for DI. Nevertheless, this phase will be employed in the data processing stage to determine and validate the bridge's fundamental frequency.

Conversely, the traverse phase is a nonstationary process (transient problem) due to the time-dependent mass distribution induced by the moving train on the bridge. The concept of utilising the traverse phase, which corresponds to the forced vibration response, is rooted in the idea that damage can manifest as a local singularity in the signal [24–27]. This approach was previously proposed by Mostafa et al. [18], where changes in the dynamic properties of the bridge structure due to damage are amplified by the presence of a moving vehicle. So, the traverse phase will be the main focus for obtaining results in this research.

Damage detection techniques

Several distinct techniques have been developed for the purpose of detecting damage in bridges, and these can be classified into the following categories: model-based techniques, data-driven methods, modal-based techniques, time-frequency analyses, and influence lines.

1. Model-based techniques involve the adjustment of numerical models to align them with physical models and their comparison with experimental data [28].
2. Data-driven methods rely on the collection of real-world sensor data and the utilisation of artificial intelligence to identify damage by detecting deviations from the baseline behaviour [29].
3. Modal-based techniques focus on acquiring modal properties of the bridge structure, such as natural frequencies, modal damping, mode shapes, modal curvatures, modal strain energy, and modal flexibility [19].
4. Time-frequency analyses are centered on deriving time-dependent properties resulting from a moving force (e.g., a train) on the bridge and employ nonstationary processes to extract information from the acquired signals [19].
5. Influence lines represent a static property that describes how a point varies under the influence of a unit load at different positions [30].

Model-based methods are less suitable due to the challenge associated with obtaining an accurate numerical model that represents the bridge structure [31], making it a time-consuming iterative process. On the other hand, data-driven methods do not rely on a physical model but depend on a substantial amount of measured data, which may be impractical for small-scale experiments. Modal properties are susceptible to noise contamination, and these techniques are mainly concerned with

stationary problems. In contrast, the train-bridge problem is inherently nonstationary [19], making it less suitable. The advantage of utilising the influence lines lies in their ability to provide static bridge information at any section of the bridge. However, these techniques do not account for dynamic properties induced by moving forces. The time-frequency analysis relies on instantaneous properties such as frequency [14] or force [32], and it holds promise due to the nonstationary behaviour.

Numerical research

Mostafa et al. [18] examined various techniques for extracting Instantaneous Frequencies (IFs) from the acceleration response of the traverse phase, employing a simplified sprung mass model. The study determined that the Wavelet SynchroSqueezed Transform (WSST) effectively separates frequency components and accurately localises them in time. However, the influence of train parameters such as mass and suspension system on IFs, and the dynamic interaction between the train and the bridge, remains unclear. Additionally, it is uncertain whether increasing signal complexity enhances DI.

A method for DI has been proposed, which involves constructing damage indices using the bridge's natural frequencies derived from the free vibration response, coupled with obtaining the IFs through the WSST applied to the bridge's forced vibration response [14]. This method employs a Moving Mass Model (MMM) and has demonstrated its ability to detect damage. Both studies are centered around a case study involving the Boyne Viaduct in Ireland (refer to appendix A), and two train configurations traversing the bridge: a 201 Class locomotive and a Mark 3 railway coach (refer to appendix B). The present study builds upon the prior work of Mostafa et al. [14] and focuses on the same methodology, bridge, and train configurations.

The impact of various train models and parameters on the bridge's response has been investigated. It was found that a higher damping ratio leads to a reduced dynamic response of the bridge [33]. Majka and Hartnett [34] investigated the impact of the frequency parameter, the mass parameter, and speed parameter on the bridge's response using an extended 3D train model. The frequency parameter is defined as the ratio of the train's frequency to the bridge's fundamental frequency, while the speed parameter is defined as the ratio between the train's driving frequency and the bridge's fundamental angular frequency. The study concluded that a stiffer suspension system, represented by a higher frequency parameter, led to a marginal decrease in the bridge's response. In contrast, increasing the mass parameter resulted in a higher bridge's acceleration response.

Bridges are typically modelled as beams using either the Euler-Bernoulli beam theory or the Timoshenko beam theory [35]. The Timoshenko beam theory considers shear distortion and rotational inertia, making it suitable for cases with low aspect ratios (length over thickness). While both theories provide accurate results for slender beams, the accuracy of the Euler-Bernoulli beam theory diminishes as the aspect ratio decreases. Moreover, at low frequencies, both theories yield similar dynamic responses. However, for higher frequencies, the Timoshenko beam theory is considered more reliable, particularly above approximately 500 Hz [36].

Experimental research

An overview of laboratory experiments employing both direct and indirect methods for validation is presented in table 1.1. Both approaches are included because the only distinction lies in the sensor placement, resulting in a similar experiment setup for both methods. Thus, the papers listed in this table provide insights into the experiment setup and describe which models have already been validated.

These studies reveal that, in general, response measurements are taken at the mid-

span of the bridge. This choice is motivated by the fact that the most significant changes typically occur at this location in an undamaged bridge. Furthermore, the majority of these studies primarily focuses on acceleration response measurement for two reasons: 1) acceleration measurements exhibit high sensitivity to changes, especially in the presence of damage, which predominantly alters the stiffness. 2) the acquisition of acceleration data is straightforward through the use of accelerometers. Hence, this thesis also places emphasis on utilising the acceleration response in comparison to [14, 18]. Although this thesis does not incorporate DI, the damage sensitive features provides insight into the methods currently employed in research.

Table 1.1: Overview of research related to the experimentally validation of train models regarding DI.

Literature study	Analysis method ¹	Moving model ²	Measured response	Damage sensitive feature
Cai et al. [30]	Direct	mass	x, ε	Influence lines
Huseynov et al. [37]	Direct	4A	\ddot{x}	Rotation influence line
Zhang et al. [38]	Indirect	mass	\ddot{x}	Instantaneous frequency
Chen et al. [39]	Direct	mass	x	Deflection influence line
Wang et al. [40]	Direct	2A	ε	Strain influence line
Yu et al. [26]	Direct	1A	-	Wavelet coefficient
Zhang et al. [27]	Direct	2A	x, \ddot{x}	Phase trajectory
McGetrick and Kim [41]	Indirect	2SA	\ddot{x}	Wavelet coefficient
Zhang et al. [42]	Indirect	HF	\ddot{x}	Operating deflection shape
Cerda et al. [43]	Indirect	2SA	\ddot{x}	Instantaneous frequency
Pakrashi et al. [44]	Direct	2A	ε	Wavelet coefficient, Wavelet phase
Marchesiello et al. [45]	Direct	16A	\ddot{x}	Instantaneous indicators
Zhu and Law [46]	Direct	2A	x	Wavelet coefficient

¹ Direct: sensor placement at bridge, indirect: sensor placement on train

² HF: Harmonic Force, 2SA: Two consecutively connected Suspended Axles

An overview of models to be validated is shown fig. 1.2. These validations have predominantly focused on simplified train models, such as MMMs or models incorporating multiple single suspended axles, as outlined in table 1.1. Notably, this implies that dual suspended models and single carriage models have not yet undergone experimental validation. The advantage of dual suspended models lies in their close resemblance to an actual single train carriage, facilitating a link to field experiments. Consequently, for advancing research in DI, the primary focus centers on validating the ‘train’ model, as depicted in fig. 1.2.

To gain deeper insights into the impact of train dynamics, it would be beneficial to employ intermediate models for validation. These intermediate models include the ‘bogie’ model and ‘half-train’ model. Their selection is based on their strong alignment with the characteristics of an actual train, and intermediate models can be derived from the advanced train model. Conversely, the force model, MMM, and

single axle models have not been pursued as they do not account for the influence of train dynamics, as previously discussed. Furthermore, the pursuit of a more representative train model has led to the exclusion of the single suspended mass and dual suspended mass models, along with the rigid bogie model.

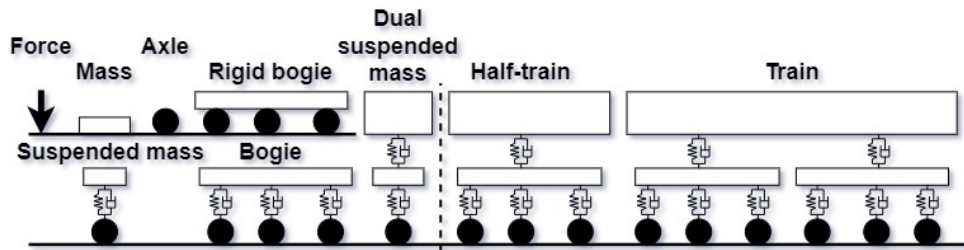


Figure 1.2: An overview of models to be validated, wherein the number of axles can be varied while maintaining the same underlying model.

1.2 Research problem

Research gap

Previous studies on DI have predominantly focused on numerical research aimed at developing methods based on simplified 2D train models for detecting damage, while there has been an absence of experimental validation. These numerical studies frequently disregard the influence of train dynamics, such as mass and suspension, due to the simplicity of the train models employed. Consequently, the impact of train dynamics on DI remains undetermined.

Reason to fill the gap

Existing research lacks the proper validation of numerically calculated train dynamics. Additionally, research lacks how train dynamics affect IFs and the dynamic interaction between trains and bridges. Moreover, the question of whether increasing the complexity of signal enhances DI remains undetermined. It is important to address this gap, as gaining a more profound understanding of the impact of train dynamics will aid on identifying the bridge condition and development of maintenance strategies.

1.3 Research aim, objectives, questions and hypothesis

Research aim

Given the research gap regarding experimental validation, this study aims to fill this gap by developing an experimental setup for validating numerically calculated train dynamics. To accomplish this validation, the development of advanced numerical models containing complex train dynamics must be constructed.

Research objectives

To achieve the aim, three activities must be undertaken, as defined in the following three research objectives:

- Realisation of the experimental setup and associated experiments.

- Realisation of more advanced numerical models incorporating train dynamics.
- Validation of train dynamics for experimental results against numerical results.

Research questions

These research objectives give rise to the following main research question:

- **How to realise an experimental setup that is capable of capturing and validating numerically calculated train dynamics?**

The main research question is divided into sub-questions that will lead to the answer of the main research question, namely:

- Which scaling technique is most suitable for this mechanical problem and how does this technique function?
- How can the guidance system between train and bridge be designed in terms of reliability, functionality and robustness?
- How can an experimental setup be designed that is capable of applying and controlling the train's motion along a predefined distance?
- How can the dynamic behaviour of the train be implemented into the experimental setup?
- What is a suitable method for performing the concerned experiments, and how can the experiments be set up in terms of equipment to acquire data?
- How to realise more realistic numerical train models that incorporate train dynamics, while ensuring a viable solution in terms of computational time, stability, and accuracy?
- Which train configuration, concerning the Boyne Viaduct, is most suitable for capturing and validating train dynamics?

Hypothesis

The thesis is expected to demonstrate the feasibility of obtaining experimental data through a laboratory-scale prototype. Additionally, it is anticipated that the experimental data will exhibit behaviour similar to both the numerical results of the actual model and the scaled prototype. However, the experimental data is likely to contain more noise compared to the simulations, leading to worse results.

As discussed earlier, a decrease in the bridge's amplitude response yields from two factors, namely: 1) reduced train-bridge interaction due to low mass, and 2) a stiffer suspension, corresponding with higher train frequency and frequency ratio. Notably, the DMU train configuration is known for its lower mass and stiffer primary suspension in comparison to the locomotive train configuration. This results in that the lower mass may yield in inadequate train-bridge interaction, leading to insufficient bridge excitation. This contributes less favorable to DI and SHM.

Furthermore, it is expected that the advanced models will exhibit behaviour similar to previously used models in terms of resonance frequency visibility and the trend of resonance frequencies during the traverse phase. Additionally, it is expected that the advanced models will result in additional resonance frequencies due to more subsystems. Finally, during the traverse phase, differences in behaviour are expected due to the presence of the secondary suspension system. This leads to alterations in the bouncing behaviour due to the separation between both masses, and changes the bridge's excitation.

1.4 Approach

A strategic research approach has been developed and is depicted in fig. 1.3. In the end, this thesis relies on validating numerically calculated train dynamics against experimental results. This validation is conducted through three variants: the bogie, the half-train, and the train variant, with the first two being simplified representations of a single train carriage. Furthermore, simulations are executed to determine the most suitable train configuration for DI, and a variation study is conducted to investigate the observed behaviour in the results.

This research encompasses three analyses, both in experiments and simulations: the natural frequency analysis, the modal analysis and the dynamic analysis. The first analysis aims to validate the natural frequencies of the train's subsystems in the experimental setup against the SOLIDWORKS model, and it also serves to validate the numerical model functions as intended. The modal analysis provides insights into the impact of train dynamics on the bridge concerning the bridge's natural frequency. This analysis involves a stepwise natural frequency analysis with varying the train's position along the bridge. The dynamics analysis is particularly important for validation, as it forms the basis for the DI method developed by Mostafa et al. [14]. This analysis reveals the dynamic interaction between train and bridge, yielding instantaneous properties.

To validate the numerically calculated train dynamics against experimental results, it is essential to have both an experimental setup and a numerical model. The experimental setup should be a laboratory-scale version to ensure cost-effectiveness and flexibility. The development of a scaled setup requires the selection of the most suitable scaling method, accompanied by an understanding of the underlying theoretical principles.

The development of the experimental setup is inspired by Oskam et al. [47]. The development involves generating concepts based on functions, followed by their evaluation against the design requirements and success criteria to identify the optimal concept. Subsequently, the scaling method is applied using MATLAB, leading to the final design in SOLIDWORKS. Moreover, the experiments are designed in terms of methodology, equipment, and settings.

The numerical model development builds upon a previously simplified model as outlined by Mostafa et al. [18]. This development employs Abaqus software for modelling. The emphasis in this development lies in the integration of train dynamics to establish the train variants and simplifying the velocity boundary condition to a single node. Appropriate simulation settings are established to ensure valid results.

Following the development and execution of both the experimental setup and associated experiments, as well as the numerical model and simulations, the final stage involves data processing. Data processing for experimentally determining the natural frequencies is performed using FEMtools v4.2.0, while data processing for the dynamic analyses is carried out in MATLAB R2021B using the WSST function. This function transforms the bridge's acceleration response into frequency content, representing IFs. Further information about the WSST function can be found in Mostafa et al. [14].

1.5 Limitations

To specify and narrow down the scope of the current study, only the following points will be included:

- **Bridge:** This study focuses on the Boyne Viaduct, an 80-meter railway bridge in Ireland, where track structures, rail irregularities, 3D modelling and flexible

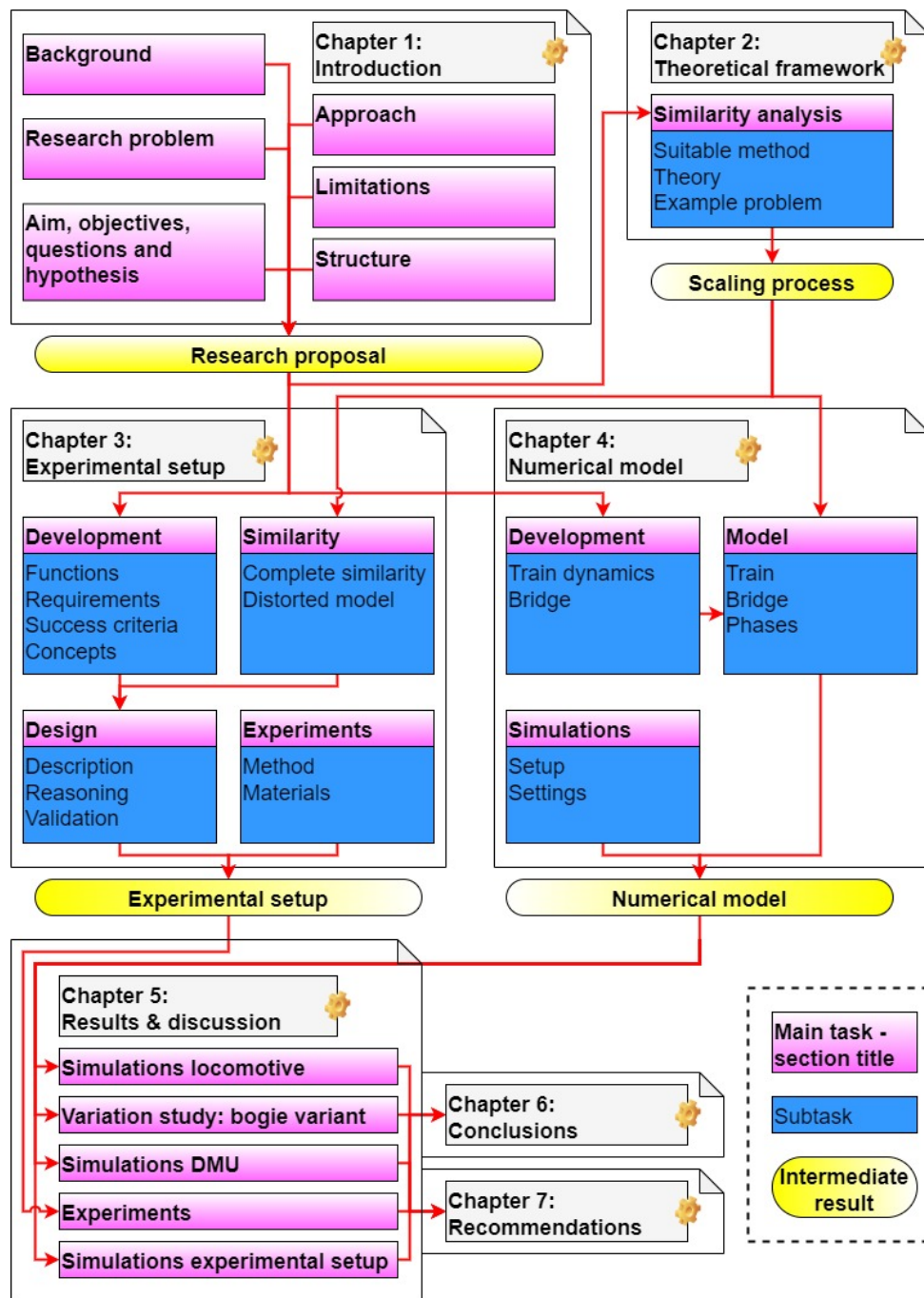


Figure 1.3: Thesis approach.

elements within the train model are not included.

- **Train:** The train configurations traversing the bridge, namely: locomotive and DMU train, are represented as three variants, namely: 'bogie', 'half-train' and 'train'. The latter represents a single train carriage.
- **Analyses:** This study includes only the following analyses: frequency analysis, modal analysis and dynamic analysis.
- **Data processing:** Data processing is performed by obtaining the IFs from the vertical acceleration response of the bridge's mid-span node using the WSST

function. Finding the optimal combination of settings for the WSST function is beyond the scope of this study.

- **Damage identification:** DI is not included, however, damage allocation is considered in the design of the experimental setup for future work.
- **Experimental setup:** The setup is a scaled-down prototype of the Boyne Viaduct. The train variants are grafted upon the locomotive.
- **Experiments:** All three variants have been tested experimentally with the three analyses all with constant quantities, no variation study.
- **Set up experiments:** In the dynamic analysis, accelerometers are attached to the bridge. A detailed research into the most suitable sensor type and location, as well as data acquisition system, is not included.
- **Numerical model:** The advanced 2D model is based upon the Boyne Viaduct and the train variants are grafted upon both the locomotive and DMU train configuration.
- **Simulations:** The locomotive-based variants are subjected to all analyses, while the DMU-based variants are exclusively subjected to the dynamic analysis. The locomotive-based bogie variant is subjected to a variation study by varying velocity, mass, inertia, spring and damper coefficient.
- **Settings simulation:** Determining a viable solution is considered in terms of computational time, stability and accuracy. Nevertheless, a study into the optimum combination of the various settings is excluded.

1.6 Structure

In chapter 1, the context of the study has been introduced. The research gap and the reason to fill the gap has been addressed. The research aim, objectives, questions and hypothesis have been identified. The approach and limitations of the study have also been discussed.

In chapter 2, the most suitable method for scaling a model to a prototype is presented. This chapter delves into the theory behind the scaling method and illustrates its application through a relatively basic example problem.

In chapter 3, the development of the experimental setup is presented. The scaling method of chapter 2 is applied to scale the Boyne Viaduct to a laboratory-scale prototype and validated based on the mass and frequency ratios. The chapter provides a description of the choices made in the final design and outlines the experimental methodology, equipment, and settings for all three analyses.

In chapter 4, the development of the numerical model is outlined. This chapter contains the model description, the simulation description and settings.

In chapter 5, the results and discussion of both experiments and simulations are covered. These results are divided into sections covering simulations related to locomotive and DMU train configuration, as well as a variation study involving the bogie variant grafted upon the locomotive train configuration. Moreover, experimental results from the scaled experimental setup and simulations concerning the scaled version are examined.

In chapter 6, the answer to the main research questions is provided and this chapter offers specific conclusions drawn from this study.

In chapter 7, the recommendations are elaborated on, which are grouped into experimental validation, future experimental work and numerical simulations.

2 | Theoretical framework

This chapter discusses the most suitable method for scaling a mechanical problem, expounds upon the underlying theory of this scaling method, and applies the theory to a practical problem. The aim is to identify an appropriate scaling method for scaling an experimental setup and to provide insight into implementing similarity through a practical application of the theory.

2.1 Scaling methods

Several scaling methods are available for scaling of a structure (model) into a scaled-down representation (prototype). These methods can either rely on: 1) similarity-based scaling (similarity analysis), 2) specific scaling, focusing on certain aspects such as geometry, kinematics, dynamics, or material; or 3) ratio-based scaling [48]. All these methods consider scaling the dimensions, but the latter two are simplified versions of complete scaling.

Similarity analysis strives to achieve complete similarity between the model and the prototype, resulting in identical behaviour. However, challenges arise when multiple length scales or numerous identical quantities are required, leaving no room for any form of scaling [48]. These issues can be addressed through the utilisation of relaxed models, which deviate from complete similarity for the less critical quantities.

Specific scaling offers flexibility in the scaling process and simplifies it, as is done in [49]. Nevertheless, this method does not guarantee that the prototype's behaviour mirrors that of the model. This implies that unaccounted-for quantities can exert significant influence on the results, leading to erroneous behaviour.

Ratio-based scaling closely resembles specific scaling, emphasising important ratios in the problem. While this approach simplifies the problem, it remains uncertain whether the prototype behaves similarly to the model. To mitigate this issue, numerical simulations can be performed alongside the scaling process to verify the behaviour. However, achieving the correct quantities may involve a time-consuming trial-and-error process.

For this thesis, complete similarity-based scaling has been selected as the most suitable method. This choice is supported by constructing the experimental setup prior to numerical modelling. This approach allows to address unforeseen challenges and aligns with the goal of this thesis, which is experimental validation. However, numerical validation of alternative scaling methods can not be conducted prior to the construction of the experimental setup.

2.2 Similarity analysis

Similarity denotes an unique relation between model and prototype, both governed by the same physical principles while varying in size [48]. The model represents a physical object intentionally designed and constructed to specific dimensions, while the prototype serves as a scaled-down representation of this model. The condition of similarity can be achieved through a process known as dimensionless analysis, grounded in the idea that all physics relations are expressed through dimensionally homogeneous equations [48]. Dimensionless analysis is a technique for reducing the number of independent quantities by means of a set of dimensionless products. By expressing all quantities in terms of these dimensionless products, it becomes possible to describe the system's behaviour.

The mathematical method employed for conducting dimensionless analysis is the Buckingham Pi theorem [50]. This method is extensively applied in engineering, particularly in the domain of fluid mechanics. The theorem states that if a system can be defined by n independent physical quantities and k fundamental dimensions (such as mass, length and time), then the number of independent dimensionless products equals $i = n - k$ [50]. Such a product is a so-called ‘pi-product’ and denoted by the Greek letter Π . In any given problem, multiple quantities are essential to depict the phenomenon of interest. In accordance to this theorem, taking all involved quantities into account ensures complete similarity.

It is noteworthy that this approach is rooted in dimensions rather than quantities. Furthermore, the method solves a system of equations featuring indeterminate prototype variables. Initially, the number of unknowns exceeds the number of equations. Through selecting a subset of prototype variables and deriving dimensionless products, the system becomes solvable. This ensures that the remaining prototype variables can be determined. This process encompasses four steps:

- Step 1: Identify the physical system to be analysed
- Step 2: Identify n relevant independent quantities and their k basic dimensions
- Step 3: Choose n dimensionally independent quantities to derive i dimensionless products
- Step 4: Solve the i remaining prototype quantities based on i dimensionless products, n model quantities and k prototype quantities (self-selected)

In the initial step, two approaches may be employed to identify the system: 1) using relevant equations or 2) using a graphical representation of the system. Nevertheless, it is essential to list all quantities to ensure similarity. Ratios and constant values may be disregarded, as these remain consistent between model and prototype.

The second step revolves around the dimension of physical quantities. A problem can be characterised by a set of physical quantities. These quantities each possess specific dimensions, quantified by units and magnitude. There exist seven primary dimensions, also known as basic, fundamental or independent quantities. Among mechanical problems, only three quantities are required to define all other physical quantities, namely: mass (M), length (L) and time (T). All other dimensions can be derived as combinations of these primary dimensions and are referred to as secondary dimensions [48]. For instance, velocity is a secondary quantity derived as a combination of length and time ($L \cdot T^{-1}$).

In accordance with the k basic dimensions and n independent quantities, a function exists with i dimensionless products (Π_i) [50]. When deriving these dimensionless products, it is essential to select independent, non-repeating quantities that encompass all dimensions. Additionally, these quantities must ensure that the determinant of the function is non-zero. It should be noted that the choice of quantities for deriving the dimensionless products is inherently arbitrary.

In the final step, the remaining unknown prototype quantities are determined. During this process, the model’s dimensionless products are equated to those of the prototype. A problem encompasses both model and prototype quantities, resulting in a total of $2 \cdot n$ quantities involved. Among these, there are n prototype quantities that must be determined, while there exist only i dimensionless numbers. Consequently, it becomes necessary to (arbitrarily) choose k model quantities (keeping in mind that $n - k = i$).

Example problem

To enhance understanding of the scaling method, its theory is applied to a specific problem closely resembling the actual scenario. This problem is depicted in fig. 2.1, illustrating a simply supported beam with a sprung mass connected to the ground. In

this problem, it is essential to maintain identical frequency and mass ratios between the beam and the sprung mass. This problem serves as a comparable representation of the actual case, where the train is simplified as a single sprung mass without considering its velocity.

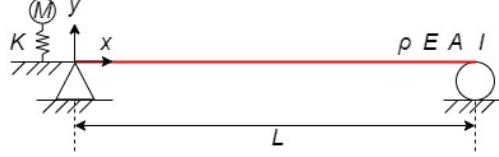


Figure 2.1: Physical quantities involved in the example problem.

There are seven physical quantities ($n = 7$) and three fundamental dimensions ($k = 3$), as is shown in table 2.1. This yields in $i = 7 - 3 = 4$ dimensionless products.

Table 2.1: Physical quantities and their fundamental dimensions occurring in the example problem.

Physical quantity	Symbol	Unit	Dimension ¹
Young's modulus of Elasticity	E_{bridge}	Nm^{-2}	$ML^{-1}T^{-2}$
Area moment of inertia	I_{bridge}	m^4	L^4
Length	L_{bridge}	m	L
Material density	ρ_{bridge}	kgm^{-3}	ML^{-3}
Cross-sectional area	A_{bridge}	m^2	L^2
Train mass	M_{train}	kg	M
Spring coefficient	K_{train}	Nm^{-1}	MT^{-2}

¹ M : Mass, L : Length, T : Time

As there are three fundamental quantities, it follows that the derivation of dimensionless products requires the selection of three specific quantities. Opting for fewer quantities would lead to an indeterminate system, while selecting more quantities would result in an overdetermined system. For the initial dimensionless product, the quantities E_{bridge} , ρ_{bridge} , and L_{bridge} have been arbitrarily chosen, primarily due to their shared dimensions. Alternative combinations are also viable, provided they satisfy the criteria of a non-zero determinant, non-repeating quantities, inclusion of all fundamental dimensions at least once, and independence of the chosen quantities. The determinant is expressed as:

$$\begin{Bmatrix} E_{\text{bridge}} \\ \rho_{\text{bridge}} \\ L_{\text{bridge}} \end{Bmatrix} = \begin{bmatrix} 1 & -1 & -2 \\ 1 & -3 & 0 \\ 0 & 1 & 0 \end{bmatrix} \begin{Bmatrix} M \\ L \\ T \end{Bmatrix} \Rightarrow \det \begin{bmatrix} 1 & -1 & -2 \\ 1 & -3 & 0 \\ 0 & 1 & 0 \end{bmatrix} = -2 \quad (2.1)$$

where this equation is derived directly from table 2.1. It can be concluded that a unique solution exists, affirming the independence of the chosen quantities.

Having established that these three quantities (E_{bridge} , ρ_{bridge} and L_{bridge}) can be utilised, the dimensionless analysis can be performed for the remaining physical quantities. An example is provided to transform M_{train} into a dimensionless product according the following process:

$$\Pi_i = Q_1^{\alpha_i} Q_2^{\beta_i} \dots Q_k^{\phi_i} P_i = 1 \quad (2.2)$$

where k denotes three, as there are three fundamental quantities in mechanical problems, namely M , L and T . P_i denotes the quantities that should be made dimensionless, in this case M_{train} . For the entire process, P_i comprising all quantities except the three selected for the analysis, namely E_{bridge} , ρ_{bridge} , and L_{bridge} . Each fundamental quantity (Q_k) is associated with its respective power term, denoted by ϕ_i , where ϕ_i

represents a distinct exponents for each term. The newly formed Π -term has as intrinsically quality to be equal to unity. This arises from the fact that all dimensions (units) within a dimensionless product can be eliminated, resulting in the numerical value 1. This can be verified by substituting the dimensions from table 2.1 in table 2.2.

Returning at the example problem, the Q -terms and P -term can be expressed as

$$\begin{aligned} Q_1 &= E_{\text{bridge}} = M^1 L^{-1} T^{-2} \\ Q_2 &= \rho_{\text{bridge}} = M^1 L^{-3} T^0 \\ Q_3 &= L_{\text{bridge}} = M^0 L^1 T^0 \\ P_1 &= M_{\text{train}} = M^1 L^0 T^0 \end{aligned} \quad (2.3)$$

where P_1 represents the first variable targeted for scaling, for which a dimensionless product is to be found.

The subsequent step involves determining the values of α_1 , β_1 and γ_1 to ensure that the product Π_1 equals unity. Substituting these terms yields:

$$\Pi_1 = (M^1 L^{-1} T^{-2})^{\alpha_1} (M^1 L^{-3} T^0)^{\beta_1} (M^0 L^1 T^0)^{\gamma_1} (M^1 L^0 T^0) = 1 \quad (2.4)$$

Rearranging the equation yields:

$$\Pi_1 = (M^{\alpha_1 + \beta_1}) (L^{-\alpha_1 - 3\beta_1 + \gamma_1}) (T^{-2\alpha_1}) (M^1 L^0 T^0) = 1 \quad (2.5)$$

For this equation to hold true, the sum of all powers of M must equal unity, those of L as well, as evidently those of T . Hence:

$$\begin{aligned} \alpha_1 + \beta_1 + 1 &= 0 \\ -\alpha_1 - 3\beta_1 + \gamma_1 &= 0 \\ -2\alpha_1 &= 0 \end{aligned} \quad (2.6)$$

This can be expressed in matrix-vector formulation to solve for α_1 , β_1 and γ_1 , resulting in:

$$\begin{bmatrix} 1 & 1 & 0 \\ -1 & -3 & 1 \\ -2 & 0 & 0 \end{bmatrix} \begin{Bmatrix} \alpha_1 \\ \beta_1 \\ \gamma_1 \end{Bmatrix} = \begin{Bmatrix} -1 \\ 0 \\ 0 \end{Bmatrix} \quad (2.7)$$

Solving this matrix-vector formulation yields the values of the unknowns, with $\alpha = 0$, $\beta = -1$ and $\gamma = -3$. Substituting these results into eq. (2.4) and employing eq. (2.3) produces the following dimensionless product:

$$\Pi_1 = M_{\text{train}} \cdot \frac{1}{\rho_{\text{bridge}} L_{\text{bridge}}^3} \quad (2.8)$$

The same procedure is applied to the remaining quantities, resulting in the four dimensionless products, as listed in table 2.2.

In total, there are seven prototype quantities that are yet to be determined. The model, representing the bridge in fig. 2.1, is constructed using steel and features geometric dimensions that have been arbitrarily selected. Similarly, the quantities regarding to the sprung mass have also been chosen arbitrarily, as indicated in the fourth column of table 2.3.

In this system, four dimensionless products have been derived, as illustrated in table 2.2. Consequently, three quantities must be assigned specific values, after which the remaining four can be determined. It has been decided that the same material

Table 2.2: Dimensionless products of the example problem.

Dimensionless products	
$\Pi_1 = M_{\text{train}} \cdot \frac{1}{\rho_{\text{bridge}} L_{\text{bridge}}^3}$	$\Pi_2 = K_{\text{train}} \cdot \frac{1}{E_{\text{bridge}} L_{\text{bridge}}}$
$\Pi_3 = A_{\text{bridge}} \cdot \frac{1}{L_{\text{bridge}}^2}$	$\Pi_4 = I_{\text{bridge}} \cdot \frac{1}{L_{\text{bridge}}^4}$

Table 2.3: Input values for determining the remaining prototype quantities using the dimensionless products.

Quantity	Unit	Dimension ¹	Model	Prototype ²
E_{bridge}	Nm ⁻²	$ML^{-1}T^{-2}$	$205 \cdot 10^9$	$205 \cdot 10^9$
I_{bridge}	m ⁴	L^4	1.22	TBD
L_{bridge}	m	L	80	2
ρ_{bridge}	kgm ⁻³	ML^{-3}	7850	7850
A_{bridge}	m ²	L^2	0.15	TBD
M_{train}	kg	M	40000	TBD
K_{train}	Nm ⁻¹	MT^{-2}	$1.0 \cdot 10^7$	TBD

¹ M : Mass, L : Length, T : Time² TBD: to be determined

will be employed for the scaled bridge (prototype), resulting in identical values for E_{bridge} and ρ_{bridge} . Furthermore, the decision has been made to reduce the length L_{bridge} by a factor of 40 (arbitrarily), as is shown in table 2.3. The train's mass in the prototype can be determined as follows:

$$\begin{aligned}
 (\Pi_1)_{\text{model}} &= (\Pi_1)_{\text{prototype}} \\
 M_{\text{train,m}} \cdot \frac{1}{\rho_{\text{bridge,m}} L_{\text{bridge,m}}^3} &= M_{\text{train,p}} \cdot \frac{1}{\rho_{\text{bridge,p}} L_{\text{bridge,p}}^3} \quad (2.9) \\
 M_{\text{train,p}} &= 0.625
 \end{aligned}$$

The same method is applied to the other three quantities, leading to the remaining model quantities as presented in table 2.4. From this simplified problem, it becomes evident that dividing the length by a factor of 40 does not proportionally affect all other quantities.

Table 2.4: Output values of the remaining prototype quantities

M_{train}	K_{train}	A_{bridge}	I_{bridge}
0.625 kg	$2.5 \cdot 10^5 \text{ Nm}^{-1}$	$9.375 \cdot 10^{-5} \text{ m}^2$	$4.765625 \cdot 10^{-7} \text{ m}^4$

As stated at the start of this problem, the interest lies in the frequency and mass ratios. To ensure complete similarity, these ratios will be examined, although this step is not an official component of the similarity analysis.

The bridge's fundamental frequency, denoted as $f_{n,\text{bridge}}$ and often referred to as the natural frequency for a simply supported beam, is determined using

$$f_{n,\text{bridge}} = n^2 \frac{\pi}{2} \sqrt{\frac{EI}{\rho AL^4}} \quad (2.10)$$

The natural frequency for the sprung mass, denoted as f_{train} , is determined using

$$f_{\text{train}} = \frac{1}{2\pi} \sqrt{\frac{K_{\text{train}}}{M_{\text{train}}}} \quad (2.11)$$

The frequencies, masses and their respective ratios are calculated for both the model and prototype, as depicted in table 2.5. This table reveals that both cases exhibit similar ratios and, consequently, similar behaviour, despite having distinct frequency and mass values.

Table 2.5: Frequency and mass ratio for the model and the prototype for the specific problem.

Quantity	Unit	Model	Prototype
f_{train}	Hz	2.516	100.658
f_{bridge}	Hz	3.578	143.079
$\eta_{\text{frequency}}$	-	0.70	0.70
M_{train}	kg	40000	0.625
M_{bridge}	kg	94200	1.472
η_{mass}	-	0.42	0.42

2.3 Closing Remarks

The goal of this chapter was to identify an appropriate scaling method for scaling an experimental setup and to provide insight into implementing similarity through a practical application of the theory. In the process, a sub-question is answered, namely:

- Which scaling technique is most suitable for this mechanical problem and how does this technique function?

The most suitable scaling method for this mechanical problem is the application of a similarity-based scaling method, known as the similarity analysis. This choice is predicated on the fact that the prototype exhibits behaviour similar to that of the model. Moreover, this choice aligns with the sequence of constructing the experimental setup before engaging in numerical modelling. This method relies on the Buckingham Pi theorem as a mathematical framework within dimensionless analysis. Additionally, this method involves solving a system of equations, which is executed through a four-step process.

Furthermore, a relatively basic example was employed to highlight the different steps involved in this method. This method will be applied in chapter 3 to a more comprehensive case involving the scaling of the Boyne Viaduct, an 80-meter railway bridge located in Ireland, and the concerned train models to a laboratory-scale prototype.

3 | Experimental setup

The chapter's goal is to develop an experimental setup, and accommodate details regarding the experiments. To maintain focus on the aim of this thesis, which is the development of an experimental setup for validating numerically calculated train dynamics, this chapter exclusively focuses on the relevant steps in this development. The chapter's goal is achieved by outlining the development of the experimental setup, incorporating the implementation of the similarity analysis. Subsequently, it delves into the various subsystems integrated into the design. Finally, this chapter addresses the experiments, encompassing the method and the equipment employed.

3.1 Development

The experimental setup must serve several functions, with the main function being to mimic the train-bridge dynamics. For the setup, this main function can be subdivided into four functions: 1) mimicking of dynamic behaviour (suspension), 2) guidance, 3) movement of the train, and 4) fixation. More details regarding these function and the function tree can be found in appendix E.1. These functions, and their respective names, are recurrently referenced throughout this chapter.

The design requirements, also referred to as functional requirements, are based on the aforementioned functions. Three design requirements are important for the setup: 1) the train dynamics must be accurately represented, 2) the setup must function correctly, and 3) vibrations from the surroundings and motor must not interfere with the measurement data. The complete overview can be found in appendix E.2.

The success criteria, also referred to as realisation requirements, are derived from the design requirements and serve as the basis for selecting the most suitable concept. These success criteria encompass factors such as reliability, robustness, feasibility, and functionality. The complete overview can be found in appendix E.3.

A morphological overview has been made, presenting potential solutions for each function, resulting in five concepts. All concepts must initially be evaluated against the design requirements. Concepts that satisfy these requirements are subsequently assessed against the success criteria, leading to the optimal concept. This assessment concludes that the optimal design comprises a combination of solutions derived from different concepts. The solutions that form the optimal design are graphically represented in fig. 3.1 and this process is elaborated in appendix F.

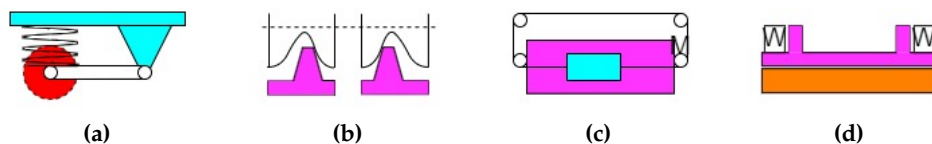


Figure 3.1: Most suitable solution for (a) function 1 being rotational arm, (b) function 2 being slots, (c) function 3 being extern closed-loop or (d) function 4 being weights.

3.2 Implementation similarity analysis and relaxation

The scaling method, outlined in chapter 2, is implemented to scale the Boyne Viaduct and locomotive train configuration to a laboratory-scale prototype. A representation of the model to be scaled, along with its physical quantities, is depicted in fig. 3.2.

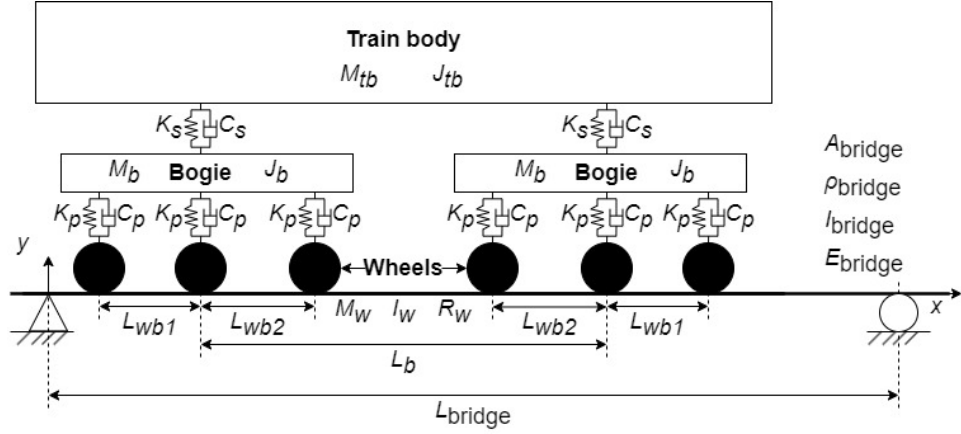


Figure 3.2: Graphical representation of the model to be scaled, incorporating the relevant physical quantities.

The physical quantities presented in fig. 3.2 are accompanied by their respective fundamental dimensions, as outlined in table 3.1. The input for the similarity analysis encompasses all model quantities, according to Bowe [51], along with three self-selected prototype quantities, namely E_{bridge} , ρ_{bridge} , and L_{bridge} . The output of the similarity analysis comprises the prototype quantities, excluding the self-selected ones, with these output values are highlighted in gray within this table. The design of the experimental setup is predicated upon all prototype quantities. A detailed elaboration of conducting the similarity analysis and reasoning behind the choices made during this process can be found in appendix C.

Table 3.1: Input and output values, denoted by gray-filled cells, of the similarity analysis with prototype values corresponding to the experimental setup.

Quantity	Unit	Dimension ¹	Model	Prototype
E_{bridge}	Nm^{-2}	$ML^{-1}T^{-2}$	$2.050 \cdot 10^{11}$	$2.050 \cdot 10^{11}$
I_{bridge}	m^4	L^4	1.220	$4.586 \cdot 10^{-7}$
L_{bridge}	m	L	$8.077 \cdot 10^1$	2.000
ρ_{bridge}	kgm^{-3}	ML^{-3}	$7.850 \cdot 10^3$	$7.850 \cdot 10^3$
A_{bridge}	m^2	L^2	$1.500 \cdot 10^{-1}$	$9.197 \cdot 10^{-5}$
M_{tb}	kg	M	$6.448 \cdot 10^4$	$9.780 \cdot 10^{-1}$
J_{tb}	kgm^2	ML^2	$2.002 \cdot 10^6$	$1.864 \cdot 10^{-2}$
M_{b}	kg	M	$1.018 \cdot 10^4$	$1.546 \cdot 10^{-1}$
J_{b}	kgm^2	ML^2	$1.155 \cdot 10^4$	$1.075 \cdot 10^{-4}$
M_{w}	kg	M	$4.520 \cdot 10^3$	$6.862 \cdot 10^{-2}$
J_{w}	kgm^2	ML^2	$4.520 \cdot 10^3$	$4.208 \cdot 10^{-5}$
C_{p}	Nsm^{-1}	MT^{-1}	$4.000 \cdot 10^5$	2.453
K_{p}	Nm^{-1}	MT^{-2}	$1.470 \cdot 10^6$	$3.640 \cdot 10^4$
C_{s}	Nsm^{-1}	MT^{-1}	$2.0000 \cdot 10^4$	$1.226 \cdot 10^1$
K_{s}	Nm^{-1}	MT^{-2}	$6.300 \cdot 10^5$	$1.560 \cdot 10^4$
R_{w}	m	L	$5.080 \cdot 10^{-1}$	$1.258 \cdot 10^{-2}$
L_{wb1}	m	L	1.689	$4.182 \cdot 10^{-2}$
L_{wb2}	m	L	2.019	$5.000 \cdot 10^{-2}$
L_{b}	m	L	$1.341 \cdot 10^1$	$3.320 \cdot 10^{-1}$

¹ M : Mass, L : Length, T : Time

The similarity analysis is carried out under the assumption of complete similarity, although achieving complete similarity is not a prerequisite for obtaining valid re-

sults. A more relaxed or distorted model can also suffice, wherein prototype quantities deviate from those determined during the similarity analysis. This thesis focuses on achieving similarity in the frequency and mass ratios between the train and the bridge. Consequently, these ratios are considered important values to meet and are regarded as the output among the prototype quantities.

The input values, which carry significant weight in this analysis, encompass all quantities except for quantities related to inertia and damping. Variation studies conducted using both MATLAB and Abaqus have revealed that these quantities exert a lesser influence on the frequency ratio, as elaborated upon in more detail in appendix C. This suggests that deviating from these less influential values allows for greater flexibility during the design phase and accelerating the process, while still ensuring the validity of the experimental setup.

3.3 Design

Based on the optimal concept and in accordance with the similarity analysis, the final design has been developed and is depicted in fig. 3.3. The manufacturing process involves the utilisation of a CNC laser cutting machine equipped with both a fiber laser and a CO₂ laser, a CNC press brake, a lathe, and a milling machine. The design is constructed using galvanised steel with a plate thickness of 0.5 mm, considering factors such as processability, price, and availability. Further details regarding design, production, and material selection can be found in appendix G.1.

The complete design comprises four subsystems: the bridge, the train, the motor system, and the support, as illustrated in fig. 3.3. In this figure, the arrows represent the timing belt used for the movement of the train. Subsequent sections elaborate upon the various subsystems, along with choices made.

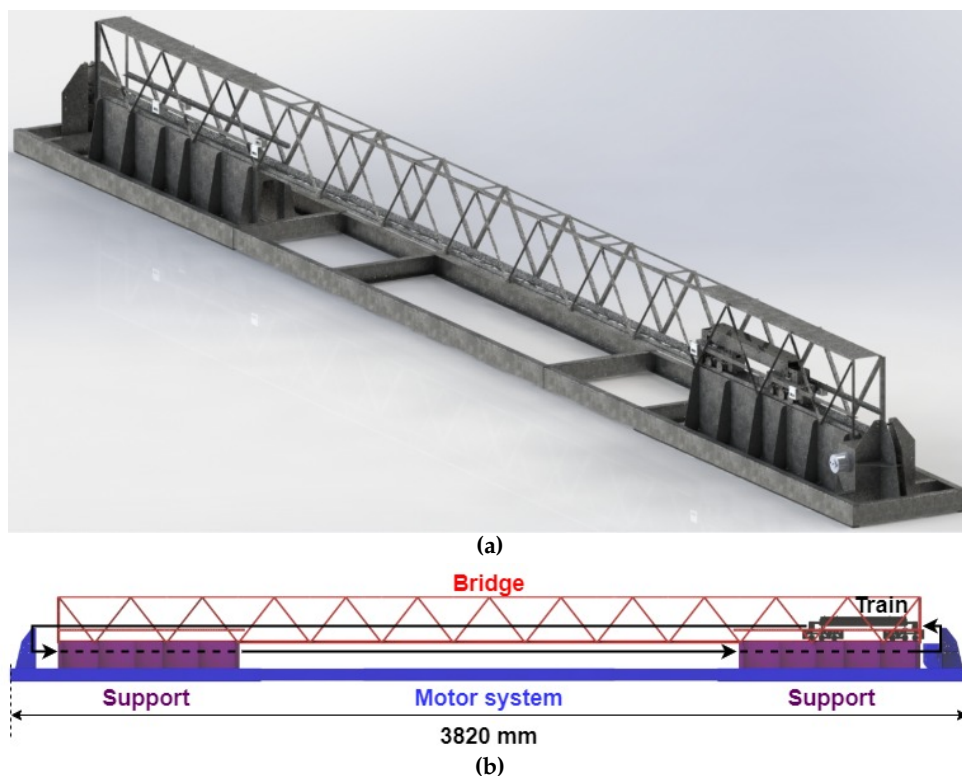


Figure 3.3: Representation of the (a) experimental setup or (b) subsystems in the experimental setup.

3.3.1 Bridge

The experimental setup incorporates a truss structure, similar to the Boyne Viaduct, as illustrated in fig. 3.3. The selection of a truss structure aligns with the requirements derived from the similarity analysis, which call for a relatively small cross-sectional area (A_{bridge}) and a relatively high area moment of inertia (I_{bridge}). A relatively low A_{bridge} is achieved by using relatively small beams that limit the structure's cross-sectional area, while obtaining a substantial I_{bridge} results from the placement of beams at a distance from the centroidal axis.

For practical reasons, related to the press brake's capacity and the availability of tools, the bridge has been partitioned into several segments for both the top and rail sections, as illustrated in fig. 3.4. The rail connector closely follows to the contour of the rail component, ensuring precise alignment of the rails and facilitating a smooth transition. The bridge is assembled through bolting, allowing for a detachable connection, which permits future damage investigation by simply removing bolts or replacing parts. Moreover, L-shaped pillars, as depicted in the figure, connect the upper segment with the rails, providing stiffness in both lateral and torsional directions. Stress calculations indicate that failure is unlikely to occur, and therefore, meeting the similarity analysis is leading, as can be seen in appendix G.2.

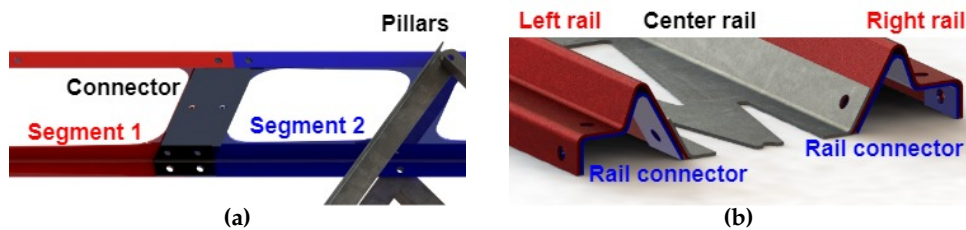


Figure 3.4: Connections in the bridge structure for (a) the top section or (b) the rail section.

3.3.2 Train

The train components are illustrated in fig. 3.5, the bogie component are depicted in fig. 3.6, and more details can be found in appendix G.3. The control arm is positioned horizontally by adjusting the installation height, determined by the compression length of the springs due to the train mass. As the springs compress, primarily vertical motion occurs, with a minor horizontal motion for small angles. It is assumed that spring compression remains small, making this a valid assumption. To achieve the desired mass, a strip (added mass) has been added to the train body. It should be noted that this strip, along with its mass, remains adjustable in future research. The train's wheels are grooved and equipped with radii to facilitate guidance and prevent derailment, ensuring the establishment of point-to-surface contact.

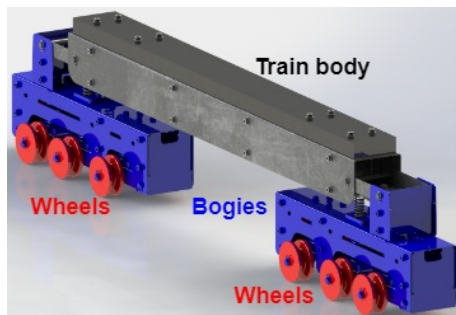


Figure 3.5: Representation of the train's subsystems.

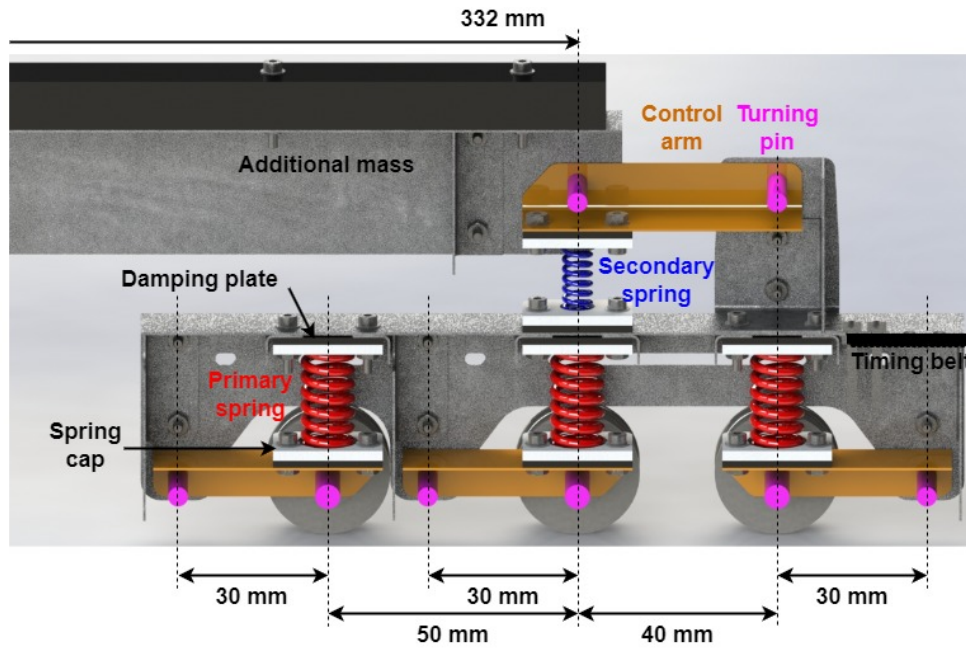


Figure 3.6: Representation of the bogie's subsystems.

3.3.3 Motor system

The motor system is designed to move the train along the bridge, as illustrated in fig. 3.7. The framework consists of longitudinal and lateral U-profiles, creating a robust and consistent separation between both sides with a fixed distance. Damping plates have been integrated into the system to prevent motor-induced vibrations on bridge measurements. The train's motion is ensured by a combination of pulleys and a timing belt. An electric motor with 41.3 W has been selected based on a maximum velocity of 2.0 m/s and an entrance length of 0.3 m due to practical reasons. More information on this selection can be found in appendix G.4.

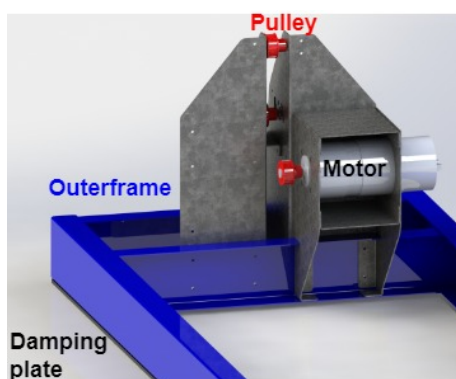


Figure 3.7: Representation of the motor system and its subsystems.

3.3.4 Support

The support serves two primary functions: 1) establishing a robust base structure that simulates a fixed boundary condition, and 2) creating a vertical clearance between the table and bridge to accommodate the timing belt. The rails are designed to align precisely with the support, as depicted in fig. 3.8. Side pillars have been

introduced to enhance lateral stiffness. Additionally, damping plates have been incorporated into the design to prevent the transmission of vibrations between the environment and the system.

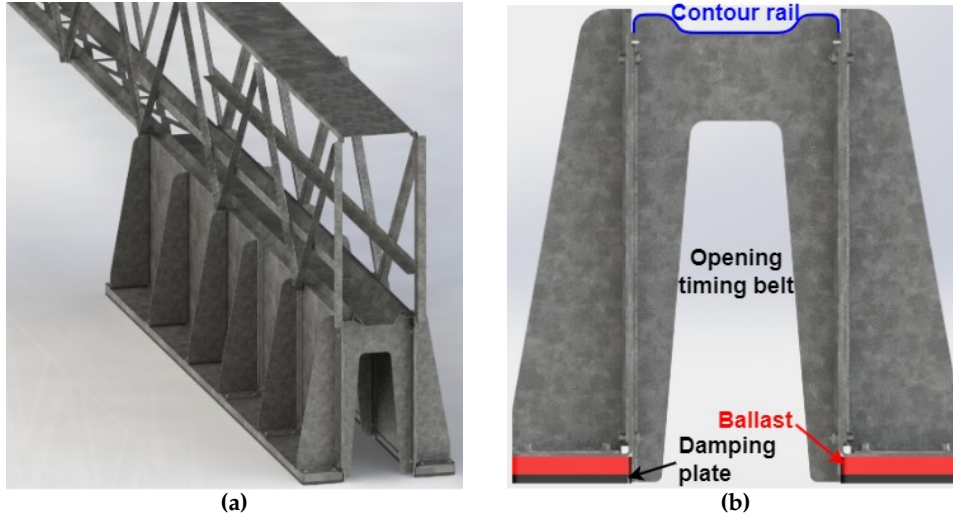


Figure 3.8: Representation of the (a) support within the design or (b) support and its subsystems

3.3.5 Validation

The final design undergoes evaluation through two validation phases. The first validation step entails a comparison between the physical quantities of the prototype derived from the similarity analysis and those of the SOLIDWORKS design. A difference is observed in the values of I_{bridge} and A_{bridge} , attributed to the constraints imposed by the press brake's minimum dimensions, as can be seen in appendix H.1. While this results in a difference in the bridge's mass, the bridge's fundamental frequency remains consistent, thus deemed acceptable.

The second, and more crucial, validation step focuses on ensuring the similarity of frequency and mass ratios between the model and design. The results are presented in table 3.2, and this validation step is similar to the one conducted in chapter 2 for the simplified problem. The frequencies and bridge's mass are determined in appendix H.2. The frequency ratios exhibit minimal difference, with the ratio between the bridge and the bogie approaching unity. In contrast, the mass ratios exhibit a greater deviation. However, this deviation is considered acceptable since the primary concern lies in the natural frequencies of the system. Minor variations in mass still yield satisfactory results, particularly concerning the train-to-bridge interaction, which influences the bridge's excitation.

Table 3.2: Frequency and mass ratios between model and SOLIDWORKS design with associated differences. The model represents the Boyne Viaduct and concerning locomotive train configuration.

Quantity	Unit	Model	Design	Difference
$\eta_{\text{frequency.body}}$	-	0.187	0.188	0.64%
$\eta_{\text{frequency.bogie1}}$	-	1.007	1.006	0.03%
$\eta_{\text{frequency.bogie2}}$	-	1.008	1.011	0.29%
$\eta_{\text{mass.body}}$	-	0.678	0.646	4.65%
$\eta_{\text{mass.bogie}}$	-	0.107	0.101	5.42%
$\eta_{\text{mass.wheel}}$	-	0.048	0.045	5.11%

The train's velocity is dependent upon two criteria to prevent resonance [52]. One of these criteria is associated with the driving frequency, which determines the duration of the train on the bridge and yields a velocity in m/s of

$$v_{\text{critical}} = 2 \cdot f_{n,\text{bridge}} \cdot L_{\text{bridge}} = 560.392 \quad (3.1)$$

The resulting velocity value is considerably high, making the occurrence of resonance based on this criterion highly unlikely. This criteria becomes more prominent when conducting research on high-speed trains.

The second criterion is dependent upon the presence of a repetitive action within the system, such as carriage length. However, since only a single carriage is under investigation, this recurring action does not take place. The brief occurrence of a repeating distance between the wheels is of such short duration that it does not need to be considered in this research.

3.4 Experiments and setup

3.4.1 Natural frequency analysis

The system's natural frequencies were determined using the roving hammer approach with a stationary sensor due to practical reasons. The roving hammer technique belongs to the category of Multiple Input Single Output (MISO) systems, where multiple striking locations serve as inputs, while a single sensor records the response. Employing multiple striking points enables the reconstruction of mode shapes, which are relevant for understanding the bridge's vibration behaviour.

An alternative method within the MISO systems involves the use of a shaker. Unlike the prior technique, a shaker allows control over the frequency and amplitude of excitation, while providing consistent and repeatable excitation forces. However, this method requires sequential attachment of the shaker to multiple points, or the use of multiple sensors, making it more complex than the roving hammer technique.

Conversely, a Multiple Input Multiple Output (MIMO) system employs multiple sensors in combination with either the roving hammer technique or multiple shakers. This method is even more complex compared to MISO systems. Opting for a MISO system is valid since the aim of these experiments is to verify the system's natural frequencies, rather than achieving the highest level of accuracy.

A schematic overview of the setup for the roving hammer technique is presented in fig. 3.9, while the equipment specifications are detailed in table 3.3. Data was sampled via a Data Acquisition (DAQ) system, which connects with the modal hammer, accelerometer, and computer. The Sound and Vibration Measurement System v4.2.0 software was employed, and its settings can be found in appendix I.1. The same appendix provides information on the tools used to obtain these natural frequencies.

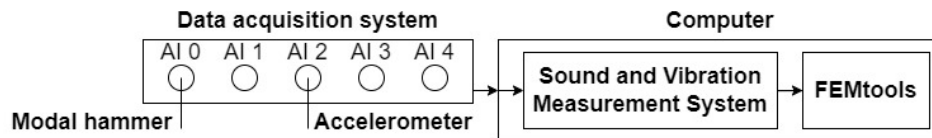


Figure 3.9: Schematic overview of the setup for experimentally determining the natural frequencies.

The structure was subjected to strikes at various predetermined locations using a modal hammer, and both these striking locations and sensor locations are illustrated in fig. 3.10. The number and position of these locations are dependent upon the mode shapes to be extracted. In this case, a limited number of striking locations is adequate to visualise the behaviour, being the bridge's first fundamental frequency.

Table 3.3: Equipment for experimentally determining the natural frequencies.

Equipment	Brand	Model	S/N ¹	Sensitivity
DAQ system	NI ²	4431	14287F7	-
Modal hammer	Meggitt	2302-10	3727	21.12 mV/N
Accelerometer	Isotron	256-100	13906	9.191 mV/m/s ²

¹ S/N stands for Serial Number.

² NI stands for National Instruments.

These locations are specifically chosen at positions where the structure exhibits high stiffness to minimise the local geometric bouncing and enhance result quality.

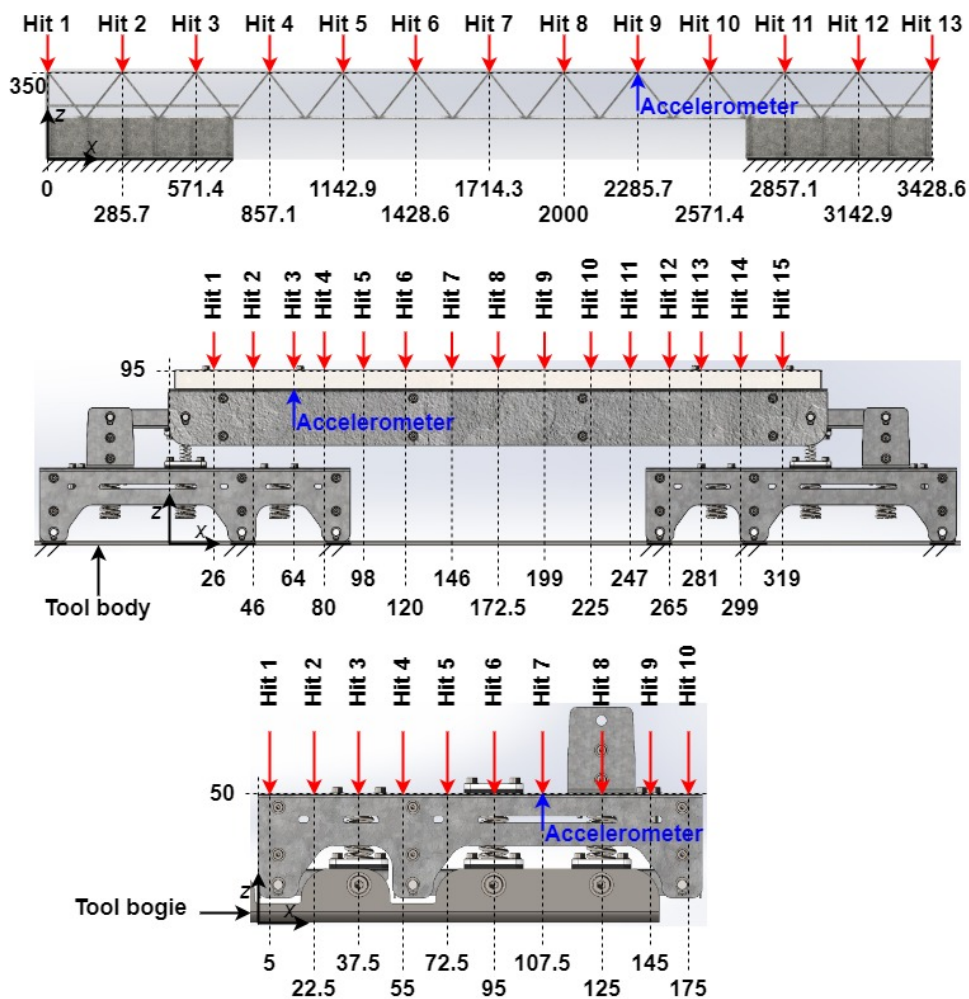


Figure 3.10: Sensor and strike location(s) for the various subsystems.

3.4.2 Modal analysis

The modal analysis entails multiple frequency analyses, with varying the train's position along the bridge's length. The experiments were carried out with the train positioned at locations 1, 3, 5, 7, 9, 11, and 13 on the bridge, as illustrated in fig. 3.10. As previously mentioned, the reason to perform the modal analysis at specific locations is influenced by the number and type of modes to be extracted. However, in

this case, the focus lies on observing the behaviour of the bridge's first fundamental frequency specifically during the traverse phase. Consequently, a limited number of train positions in combination with the predetermined striking locations is adequate to visualise the behaviour.

3.4.3 Dynamic

A schematic overview of the setup for the dynamic analysis is depicted in fig. 3.11, while the equipment specifications are presented in table 3.4. Data was sampled via a DAQ system, which connects with the accelerometers, switches, power supply, motor and computer. A control system in LabVIEW has been developed to control the system and the settings of the experiment are detailed in appendix I.2.

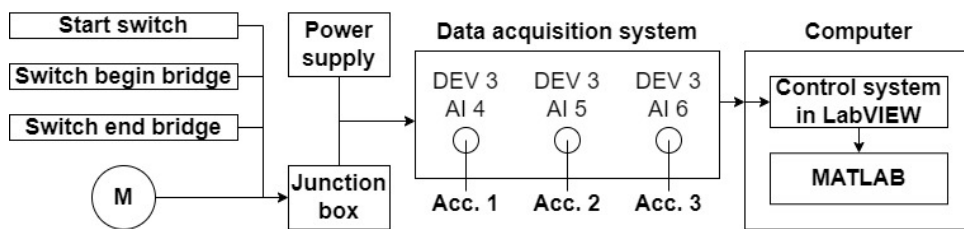


Figure 3.11: Schematic overview of the setup for the dynamics analyses.

Table 3.4: Equipment for the dynamic experiments.

Equipment	Brand	Model	S/N ¹	Sensitivity
DAQ system	NI ²	PXIe-1062Q	313BC19	-
Electric motor	RS PRO	420-631	-	-
Roller Lever Switch	Omron	SS-5GL2	2132H1	-
Power supply	RS PRO	180-8851	-	-
Accelerometer 1	Isotron	256-100	13909	9.410 mV/m/s ²
Accelerometer 2	Isotron	256-100	13906	9.191 mV/m/s ²
Accelerometer 3	Isotron	256-100	13904	9.578 mV/m/s ²

¹ S/N stands for Serial Number.

² NI stands for National Instruments.

The experiment is controlled and monitored by a LabVIEW-based control system. This control panel regulates the train's movement and data processing. Data is collected through multiple accelerometers attached to the bridge's underside corresponding to 1/4, 1/2, and 3/4 of the bridge's length, as depicted in fig. 3.12. Switches are positioned on both sides of the free-hanging bridge section, which are activated as the train passes. The activation times are recorded, enabling the determination of the train velocity. The end switch ensures that the train stops before reaching the end of the setup. The panel displays the motor voltage throughout the experiment, providing insights into the train's velocity. The software registers a voltage drop when the switch is triggered, and this signal is employed to determine if a constant train velocity has been reached prior to entering the bridge.



Figure 3.12: Switch and sensor locations on the experimental setup during the dynamic experiments.

3.5 Closing remarks

The goal of this chapter was to develop an experimental setup, and to provide the method and setup of the experiments. In this process, several sub-questions are answered, namely:

- How can the guidance system between train and bridge be designed in terms of reliability, functionality and robustness?

The optimal design for the guidance system involves implementing a slot system. This system combines the self-centering effect of conical wheels while incorporating an additional flange to prevent derailment.

- How can an experimental setup be designed that is capable of applying and controlling the train's motion along a predefined distance?

An external motor system is employed to apply the motion of the train. This motor system operates in closed-loop manner, enabling bidirectional movement of the train. Control of this system is executed through a LabVIEW software program.

- How can the dynamic behaviour of the train be implemented into the experimental setup?

A rotational arm equipped with compression springs is employed to mimic the dynamic behaviour of the train. This approach remains valid for small angles and under the assumption that the train's compression is minimal.

- What is a suitable method for performing the concerned experiments, and how can the experiments be set up in terms of equipment to acquire data?

Experiments aimed at determining the system's natural frequencies are conducted by employing the roving hammer technique (MISO system). The dynamic analysis was carried out by moving the train along the bridge and collecting data using accelerometers. The equipment employed for each experiment is listed in table 3.5.

Table 3.5: *Equipment employed for the associated experiments.*

Natural frequencies	Modal analysis	Dynamic analysis
DAQ system	DAQ system	DAQ system
Modal hammer	Modal hammer	Electric motor
Accelerometer	Accelerometer	Roller Lever Switch
-	-	Power supply
-	-	3 Accelerometers

Moreover, the experiments are executed using an experimental setup comprising a rotational arm to mimic the train's dynamic behaviour, a slot system to guide the train along the rails, an external motor system to drive the train, and weights for fixing the bridge. A similarity analysis has been applied to the current experimental setup, revealing that a relaxed model, allowing for deviations in damping coefficient and inertia terms, still produces valid results. Furthermore, it has been observed that variations in the train's velocity do not induce resonance. Additionally, details regarding the final design choices have been provided and subsequently validation in terms of frequency and mass ratios has been performed.

4 | Numerical modelling

This chapter revolves around the numerical study. The aim is to provide details how the results are generated in terms of model and simulation. This is achieved by the model's development, its description, and the elaboration of the simulations.

4.1 Development

The numerical model's development builds upon a simplified train-bridge model established in a prior study aimed at assessing the effectiveness of time-frequency analysis techniques [18]. This 2D model serves as starting point for further development and is referred to as the benchmark model. The bridge is segmented into three sections: the entrance section, the bridge section, and the leaving section. Fixed boundary conditions are applied along the entire entrance and leaving sections whereas the bridge section incorporates boundary conditions consistent with those of a simply supported beam. The train is represented as a sprung mass system, encompassing both spring and damper components.

A model that incorporates train dynamics has been developed through a four-stage process, as depicted in fig. 4.1. This section provides a concise overview of the development stages, with a detailed description available in appendix J.

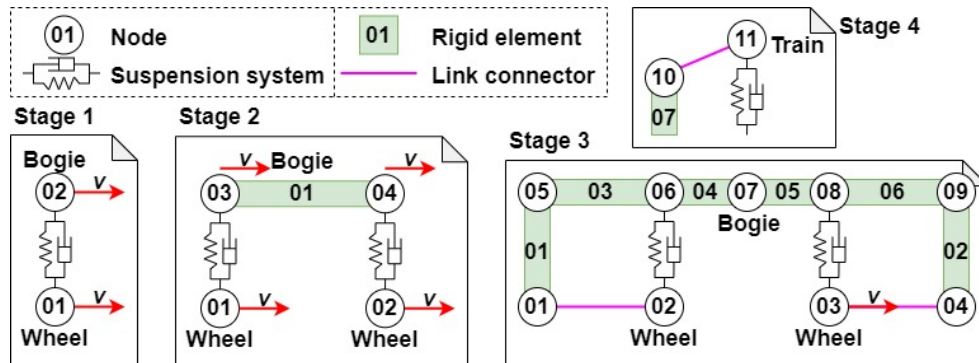


Figure 4.1: Four stages during the model development of the train part.

In the initial stage, adjustments are made to the benchmark model's parameters to align with those of the Boyne Viaduct and the corresponding train configuration. Additionally, separate parts are allocated for both the bridge and the train. A representation of this stage is available in fig. 4.1.

Extending the basic sprung mass model to a more realistic bogie model is achieved through the introduction of the model depicted in stage 3 in fig. 4.1. This model allows to apply the velocity boundary condition to a single wheel rather than to all nodes within the bogie, due to the inclusion of link connectors. These connectors maintain a fixed distance between nodes [53], permitting only rotational motion within the model. This motion can be observed in stage 3, where node 2 revolves around node 1, with this motion being constrained by the suspension system connecting nodes 2 and 6. This concept aligns with the experimental setup and, by ensuring the neutral position is attained and applying small rotations, this approach yields a valid case. To achieve a single (rigid) motion of the bogie, rigid elements are combined within a rigid body, connecting all degrees of freedom among the elements and nodes in the collection. This model employs rigid elements instead of flexible ones because: 1) adding flexible element has minimal influence on the bridge's response [4], and 2) maintaining model simplicity.

Finally, expanding the bogie model into a more realistic train model is realised by the introduction of the model presented in stage 4 in fig. 4.1. This model introduces the secondary suspension system in addition to the previously developed model in stage 3. Making this additional suspension system functional involves: 1) introducing a ramp in the allocation of the velocity boundary condition, ensuring a reduction in the initial acceleration of the model, and 2) ensuring that the neutral position is achieved after applying the train body mass load to the spring, as demonstrated in fig. 4.1. This guarantees that sufficient room is available to absorb motion during the early stages of the simulation.

A bridge is typically characterised as a slender structure, subject to transverse forces, with a length that is significantly greater than its other two dimensions. Beam elements are designed to model structures in which one dimension is significantly larger than the other two, rendering them well-suited for this type of problem.

4.2 Model

The newly developed models have been expanded to align with the train configurations and experimental setup. The models corresponding to the locomotive train configuration and experimental setup are illustrated in fig. 4.2, where the experimental setup is based on the SOLIDWORKS design. Meanwhile, the models corresponding to the DMU train configuration are depicted in fig. 4.3. The values of the quantities used in these models are detailed in table 4.1, with the locomotive and DMU quantities following those described by Bowe [51]. Additionally, the coordinate values employed for these models are provided in table 4.2.

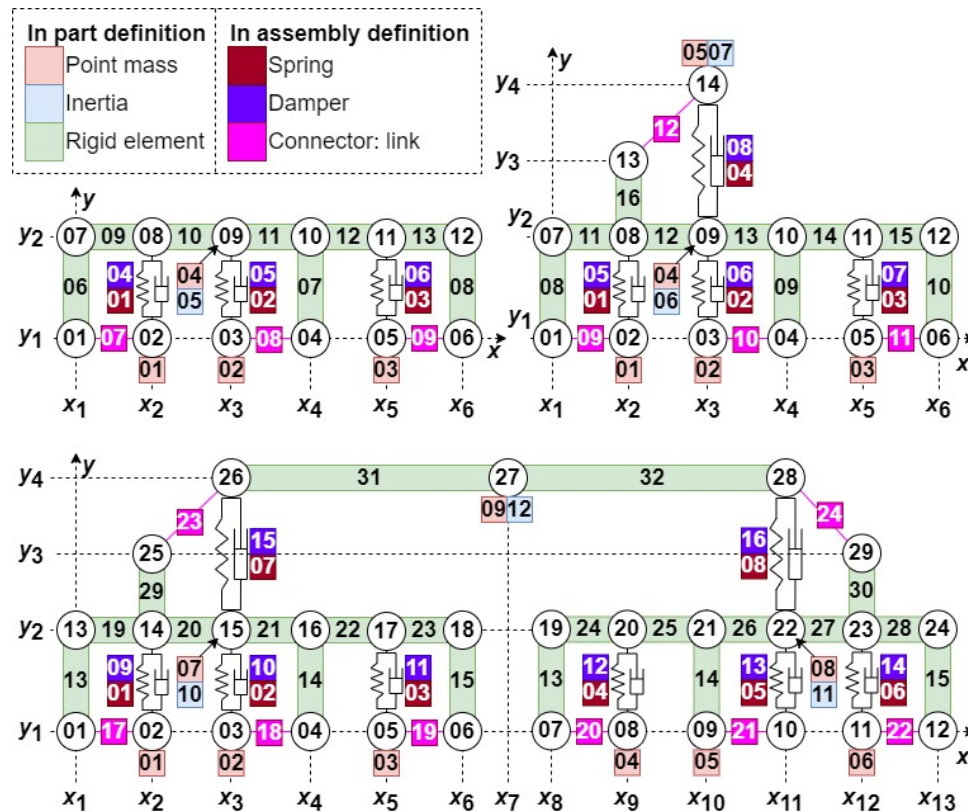


Figure 4.2: Numerical train models encompassing the bogie variant, half-train variant and train variant corresponding to the locomotive train configuration and experimental setup.

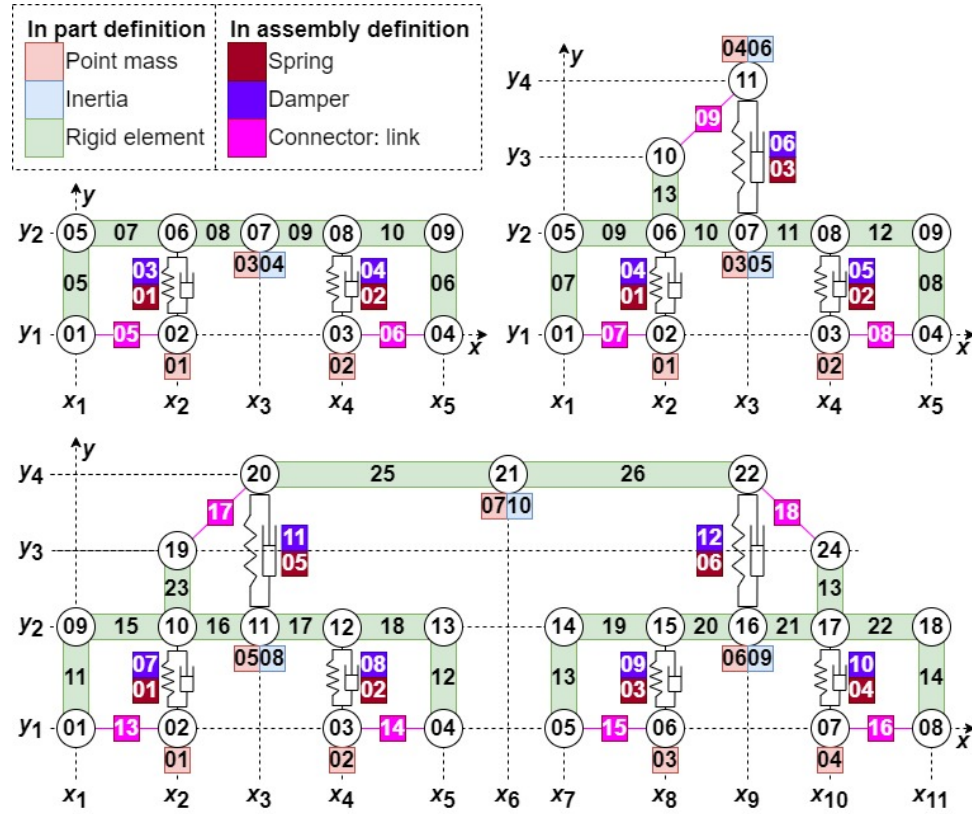


Figure 4.3: Numerical train models encompassing the bogie variant, half-train variant and train variant corresponding to the DMU train configuration.

Table 4.1: Quantities employed in the numerical models.

Quantity	Unit	Locomotive	DMU	Experimental setup
E_{bridge}	Nm^{-2}	$2.050 \cdot 10^{11}$	$2.050 \cdot 10^{11}$	$2.050 \cdot 10^{11}$
I_{bridge}	m^4	1.220	1.220	$4.586 \cdot 10^{-7}$
L_{bridge}	m	$8.077 \cdot 10^1$	$8.077 \cdot 10^1$	2.000
ρ_{bridge}	kgm^{-3}	$7.850 \cdot 10^3$	$7.850 \cdot 10^3$	$7.850 \cdot 10^3$
A_{bridge}	m^2	$1.500 \cdot 10^{-1}$	$1.500 \cdot 10^{-1}$	$9.197 \cdot 10^{-5}$
M_{tb}	kg	$6.448 \cdot 10^4$	$3.574 \cdot 10^4$	$9.872 \cdot 10^{-1}$
J_{tb}	kgm^2	$2.002 \cdot 10^6$	$1.284 \cdot 10^6$	$1.084 \cdot 10^{-2}$
M_{b}	kg	$1.018 \cdot 10^4$	$3.150 \cdot 10^3$	$1.546 \cdot 10^{-1}$
J_{b}	kgm^2	$1.155 \cdot 10^4$	$1.760 \cdot 10^3$	$4.685 \cdot 10^{-4}$
M_{w}	kg	$4.520 \cdot 10^3$	$1.500 \cdot 10^3$	$6.887 \cdot 10^{-2}$
J_{w}	kgm^2	$4.520 \cdot 10^3$	$1.500 \cdot 10^3$	$1.649 \cdot 10^{-6}$
C_{p}	Nsm^{-1}	$4.000 \cdot 10^3$	$3.241 \cdot 10^4$	2.453
K_{p}	Nm^{-1}	$1.470 \cdot 10^6$	$3.185 \cdot 10^6$	$3.630 \cdot 10^4$
C_{s}	Nsm^{-1}	$2.000 \cdot 10^4$	$2.624 \cdot 10^4$	$1.226 \cdot 10^1$
K_{s}	Nm^{-1}	$6.300 \cdot 10^5$	$5.660 \cdot 10^5$	$1.610 \cdot 10^4$

The frequency and mass ratios are depicted in table 4.3. These ratios are derived from the quantities provided in table 4.2. The frequencies are determined using MATLAB, employing the matrices listed in appendix B. These ratios highlight the distinctions between the locomotive and DMU train configurations. Notably, the DMU exhibits significantly lower mass ratios compared to the locomotive, and the bogie's frequency ratios of the DMU deviate from unity, unlike the locomotive train.

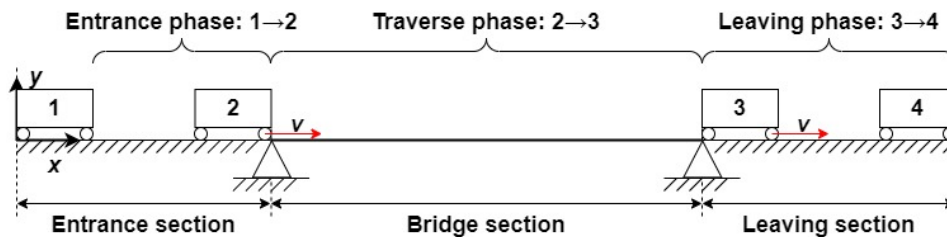
Table 4.2: Coordinate values employed in the numerical train models.

Quantity	Loco [m]	DMU [m]	Experimental setup [m]
x_1	0	0	0
x_2	1.21	1.20	0.03
x_3	2.90	2.50	0.07
x_4	4.11	3.80	0.10
x_5	4.90	5.00	0.12
x_6	6.11	10.50	0.15
x_7	9.605	16.00	0.236
x_8	13.10	17.20	0.322
x_9	14.31	18.50	0.352
x_{10}	15.10	19.80	0.372
x_{11}	16.31	21.00	0.402
x_{12}	18.00	-	0.442
x_{13}	19.21	-	0.472
y_1	0	0	0
y_2	0.843	0.60	0.034
y_3	1.393	1.22	0.061
y_4	1.893	1.52	0.061

Table 4.3: Frequency and mass ratios of the numerical models.

Quantity	Unit	Locomotive	DMU	Experimental setup
$\eta_{\text{frequency.body}}$	-	0.187	0.244	0.188
$\eta_{\text{frequency.bogie1}}$	-	1.007	2.130	1.006
$\eta_{\text{frequency.bogie2}}$	-	1.008	2.131	1.011
$\eta_{\text{mass.body}}$	-	0.678	0.376	0.646
$\eta_{\text{mass.bogie}}$	-	0.107	0.033	0.101
$\eta_{\text{mass.wheel}}$	-	0.048	0.016	0.045

The bridge is segmented into three sections and phases, as illustrated in fig. 4.4. The entrance phase is incorporated to stabilise the train prior to entering the bridge section, referred to as the traverse phase. Furthermore, the leaving phase is included to facilitate the study of the bridge's freely decaying response. This figure also outlines the phase separation in the dynamic simulations, where the train can be represented as either the bogie, half-train, or train model. The entrance phase begins with the train in the starting position (1) and ends when the first wheel of the train approaches the bridge section (2). Subsequently, the traverse phase extends from this position (2) and ends when the last wheel of the train leaves the bridge section (3). The leaving phase continues until the end of the leaving section (4).

**Figure 4.4:** Bridge model and the phase separation employed in the dynamic analysis.

B21 beam elements, in accordance with the Timoshenko beam theory, are employed for all three sections. The nodes in the entrance and leaving sections are fully con-

strained to represent fixed boundary conditions, whereas the bridge section employs boundary conditions consistent with those of a simply supported beam. In contrast, the train remains unconstrained. The bridge's properties conform to the values listed in table 4.1, which are derived from appendix A. The damping is assigned by implementing Rayleigh damping with $\beta = 0.001$.

For both the locomotive and DMU train configuration, the entrance and leaving sections feature an element edge length of 0.5 (equivalent to 80 elements), while the bridge section employs an element edge length of 0.125 (equivalent to 640 elements). Conversely, the experimental setup employs an element edge length of 0.1 (equivalent to 75 elements) for the entrance and leaving sections, and an element edge length of 0.005 (equivalent to 400 elements) for the bridge section.

A node-to-surface interaction is applied between the train and the bridge, utilising default settings that assume a hard contact model. This choice is made because: 1) the study's aim lies not on determining the most suitable contact treatment, and 2) it aligns with the benchmark model. This contact model implies that the wheels slide rather than roll, which is valid since no friction is defined in the contact model.

4.3 Simulations

The first simulation aims to determine the natural frequencies of the model. This involves introducing a frequency step, with the default settings applied. In this process, either the maximum frequency of interest is specified, or the number of required eigenvalues is defined, which include the rigid body modes.

The modal simulation involves multiple frequency analyses. In this simulation, the train's position is varied from its initial position (1) to its end position (4), with increments of 0.1 m, as depicted in fig. 4.4. This choice of a relatively small step size allows for the accurate capture of variations in the higher fundamental frequencies of the bridge.

Three implicit dynamic steps, corresponding to the phases, are implemented. By default, the Hilber-Hughes-Taylor time integration method is applied, which is an extension of the Newmark β -method. A fixed time increment of 0.001 s is utilised because it provides sufficient accuracy and frequency resolution. An implicit scheme is chosen over an explicit scheme primarily because 1) an explicit scheme suffers from error accumulation, making it more suitable for short-term events such as wave propagation; and 2) an implicit scheme is unconditionally stable, while an explicit scheme is conditionally stable.

For the dynamic simulation, the transient fidelity option has been selected instead of moderate dissipation or quasi-static. The moderate dissipation option addresses energy dissipation, such as in impact or forming analyses, while quasi-static option focuses on unstable behaviour like snap-through phenomena [53].

As mentioned earlier, a ramp has been incorporated into the velocity boundary condition. Specifically, a linear ramp with a 2-second period has been chosen to achieve a constant velocity boundary condition of 10 m/s. This velocity is predicated on monitored data gathered from the Boyne Viaduct and associated train configurations, from which it is deduced that the mean velocity approximates 10 m/s [54].

Additionally, for both the bogie and half-train variants, a length of 40 m has been assigned to both the entrance and leaving sections, while the train variant utilises a length of 50 m. The extended entrance length in the latter case allows the train to reach a constant velocity before entering the bridge section.

4.4 Closing remarks

The goal of this chapter was to provide details regarding the numerical model and simulations. In the process, a sub-question is answered, namely:

- How to realise more realistic numerical train models that incorporate train dynamics, while ensuring a viable solution in terms of computational time, stability, and accuracy?

The pursuit of a more realistic bogie model is realised through the introduction of link connectors, enabling the application of a velocity boundary condition to a single node. These link connectors, when combined with rigid elements and a rigid body, form a coherent model. To ensure the proper functioning of the secondary suspension, the incorporation of a ramp within the velocity boundary condition is incorporated. This, along with maintaining the neutral position after applying the train body mass load to the spring, results in a more realistic train model. Moreover, a viable solution is achieved by employing an implicit dynamic step with a default time integration scheme. This step employs a time increment of 0.001, along with the transient fidelity option.

5 | Results and discussion

This chapter presents the results of both the simulations and experiments, as elaborated in section 3.4 and section 4.3. The aim is to find an answer to the main research question. This is achieved by discussing individual simulations and experiments, relating the two train types, and comparing experimental and numerical results.

5.1 Simulations locomotive

This section is dedicated to simulations regarding the locomotive. Initially, the model is validated through a natural frequency analysis. Subsequently, a stepwise modal analysis is conducted, followed by a dynamic analysis, with both simulations concentrating on the interaction between the train and the bridge.

5.1.1 Natural frequency

The numerically obtained natural frequencies of the train subsystems are presented in table 5.1, where the natural frequency of the bridge is consistent across all train variants. The difference in the bridge's natural frequency is attributed to the use of a Timoshenko beam in the simulation, while an Euler-Bernoulli beam is utilised in the analytical calculation. The differences of 2.52% disappears if the Euler-Bernoulli beam is utilised in the simulations. The mode shapes reveal that, rather than exhibiting an ideal bouncing frequency, the bogie displays a slight pitching motion due to unequal axle spacing. This accounts for the observed differences in the table and these differences disappears upon equalising the axle spacing. Nonetheless relatively small differences, these results suggest that the simulation is closely aligned with the values obtained analytically, indicating that the models are functioning as intended and that subsequent simulations can be performed with these models.

Table 5.1: Natural frequency analysis per train variant.

Variant	Type	Numerical [Hz]	Analytical [Hz]	Difference [-]
Bridge	$f_{1,bridge}$	3.480	3.570	2.52%
Bogie	f_{bogie}	3.289	3.269	0.61%
Half-train	f_{bogie}	3.654	3.546	3.05%
Half-train	f_{body}	0.647	0.651	0.61%
Train	f_{bogie1}	3.648	3.532	3.28%
Train	f_{bogie2}	3.660	3.536	3.51%
Train	f_{body}	0.640	0.656	2.44%

5.1.2 Modal analysis

The stepwise frequency analyses of the bogie variant is depicted in fig. 5.1. During both the entrance and leaving phase, the bogie and bridge behave as separate systems. However, during the traverse phase, a combined system emerges, wherein the resonance frequencies change due to their interaction. This change is attributed to the phase difference between bogie and bridge, as is demonstrated in fig. 5.2. Being in-phase correlates with the first resonance frequency, indicating an added mass by the bogie, while being out-of-phase correlates to the second resonance frequency,

indicating a stiffening effect. Moreover, the pitching frequency exhibits slight variation, likely due to its proximity to the remaining frequencies, thereby facilitating interaction. Finally, the extreme values are denoted by a marker in fig. 5.1. The second and third resonance frequency occur to the right and left of the mid-span, respectively. This is caused by asymmetrical behaviour resulting from unequal axle spacing.

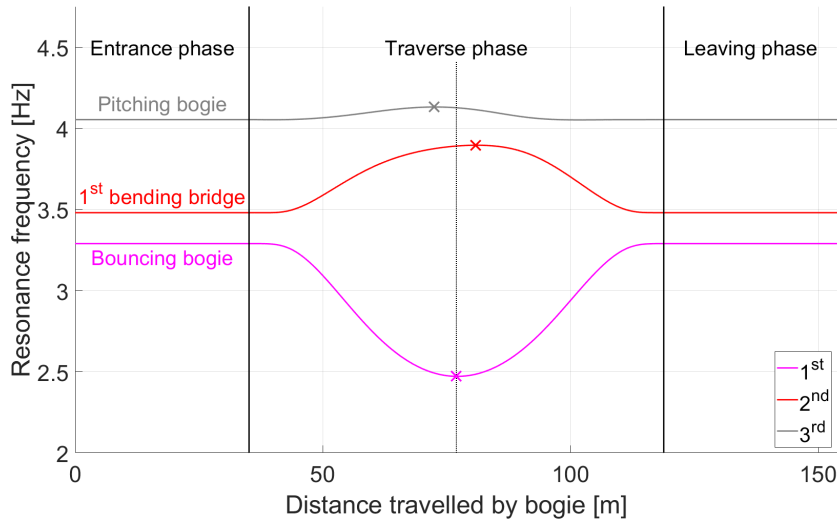


Figure 5.1: Modal analysis of the bogie variant across the bridge.

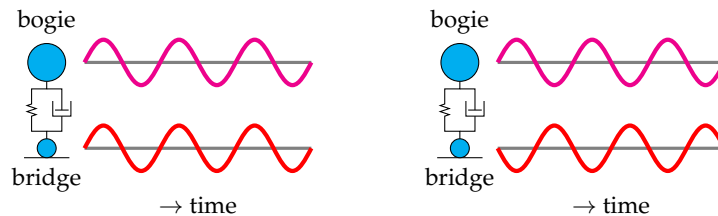


Figure 5.2: Mode shapes retrieved from the stepwise eigenfrequency analyses show that the bogie and the bridge move (a) in-phase or (b) out-of-phase (courtesy R. Loendersloot).

The analysis of the half-train variant is illustrated in fig. 5.3. The introduction of the secondary suspension system (spring stiffness) and body (mass) results in the bouncing frequency of the body, which alters both the bouncing and pitching frequencies of the bogie. Asymmetrical behaviour around the mid-span is mainly observed in the pitching frequency of the bogie, whereas for the bogie variant, the bridge's resonance frequency is also influenced by this behaviour. This suggests that the impact of the additional mass on the resonance frequency of the bridge minimises the effect of unequal axle spacing.

The analysis for the train variant is depicted in fig. 5.4. The extension of the model results in the appearance of additional resonance frequencies. The asymmetrical behaviour becomes less prominent, compared to the other variants, which is likely attributable to a combination of the additional mass and the symmetry of the train with respect to the train body.

From fig. 5.4 two observations are noteworthy: 1) The pitching frequencies of the bogies are dissimilar. The modes demonstrate that, with the first pitching frequency (depicted in dark gray), the bogies rotate in opposing directions, whereas with the second pitching frequency (depicted in light gray), they rotate in the same direction.

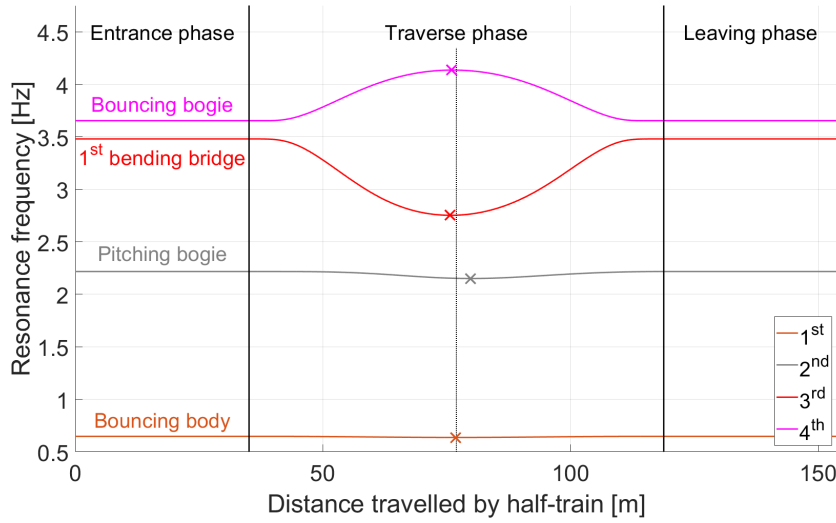


Figure 5.3: Modal analysis of the half-train variant across the bridge.

2) The lowest bouncing frequency of the bogie remains consistent during the traverse phase. In this instance, the modes indicate that only one of the bouncing frequencies of the bogie interacts with the bridge, while the other continues as a resonance frequency of the bogie.

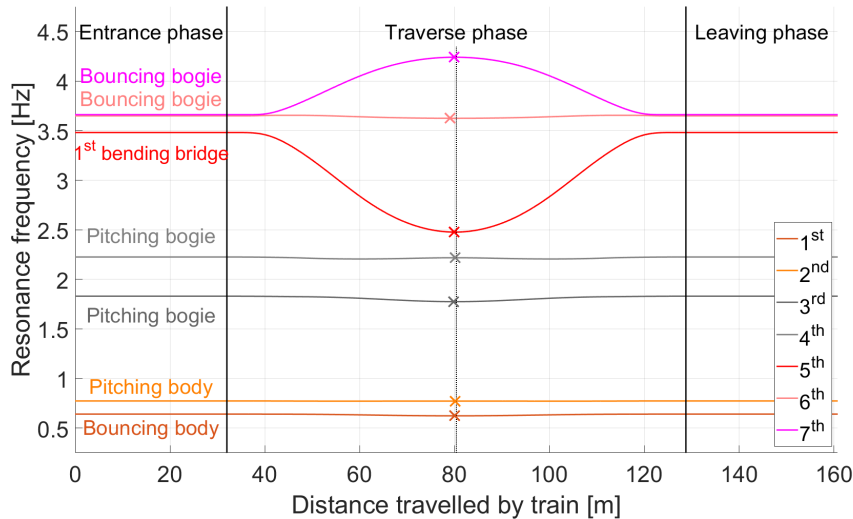


Figure 5.4: Modal analysis of the train variant across the bridge.

These stepwise modal analyses of more complex models demonstrate that the fundamental frequency of the bridge behaves similar as observed in earlier research [18]. By acquiring this understanding of the system’s behaviour at each location, the subsequent subsection expands upon the dynamic analysis and compares it with the modal analysis.

5.1.3 Dynamic analysis

The acceleration response of the bogie variant, traversing with a velocity of 10 m/s, is illustrated in fig. 5.5. The entrance phase is characterised by an absence of vibra-

tions, as the bridge has not yet been excited by the train. In the leaving phase, a free-decaying vibration is noticeable, attributable to the damping properties of the bridge's material and the lack of an input force. The traverse phase contains the vibrations of the integrated system, with three successive spikes observable at the location where the wheels make contact with the measurement node.

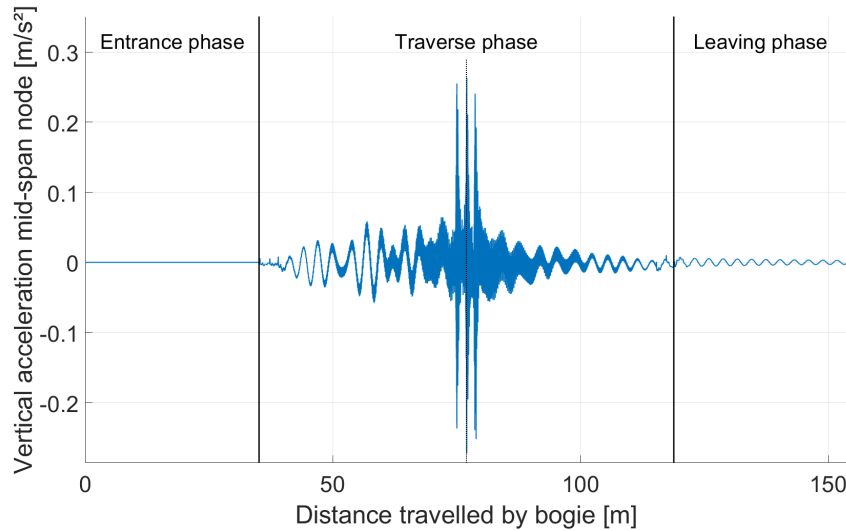


Figure 5.5: Vertical acceleration response of the mid-span node excited by the bogie variant traversing the bridge with a velocity of 10 m/s.

The frequency representation, derived from the response depicted in fig. 5.5, is illustrated in fig. 5.6. The absence of vibrations in the entrance phase also results in a lack of frequency content. In accordance with the modal analysis, the leaving phase contains the bridge's fundamental frequency, due to the free-decaying vibration observed in the response. Although, the first (magenta) and second (red) resonance frequencies are comparable to the frequency content, this content exhibits some waviness or spiky behaviour. These spikes are particularly noticeable around the second resonance frequency, which is close to the bogie's pitching frequency (grey). Furthermore, the second resonance frequency fades during the latter half of the traverse phase. In addition, there is a dispersion of kinetic energy between the first two resonance frequencies. A variation study will be conducted to gain further insight into the behaviour of spikes and energy fading. The influence of spikes on resonance frequency is crucial for Structural Health Methods (SHM).

The amplitude of the bridge and bogie is depicted in fig. 5.7. The entrance and leaving phases reveal that mode 6 is attributed to the bouncing of the bogie (represented by the straight magenta line) and mode 7 to the bridge (represented by the marked red line), due to the other amplitudes being zero. Modes 1 to 5 represent the train's rigid body modes in the simulation. This plot indicates that for mode 7, around 47.3 m and 107.6 m (represented by cyan circles), the amplitude of the bogie is greater than that of the bridge. This suggests that the bogie is more prominently present, which could account for the majority of the kinetic energy in the signal being in the bouncing of the bogie, as can be observed in fig. 5.6.

A distinct frequency representation is achieved by employing an alternative component as input for the WSST function, with the results available in appendix K. Other bridge nodes, such as the quarter and three-quarter nodes, yield similar results as the mid-span node; however, the energy concentration exhibits slight variations. The wheel node also produces a result comparable to that of the mid-span node, although the bridge's fundamental frequency is not visible in the leaving phase. The bogie node presents a more interesting result, with spikes visible in both the traverse

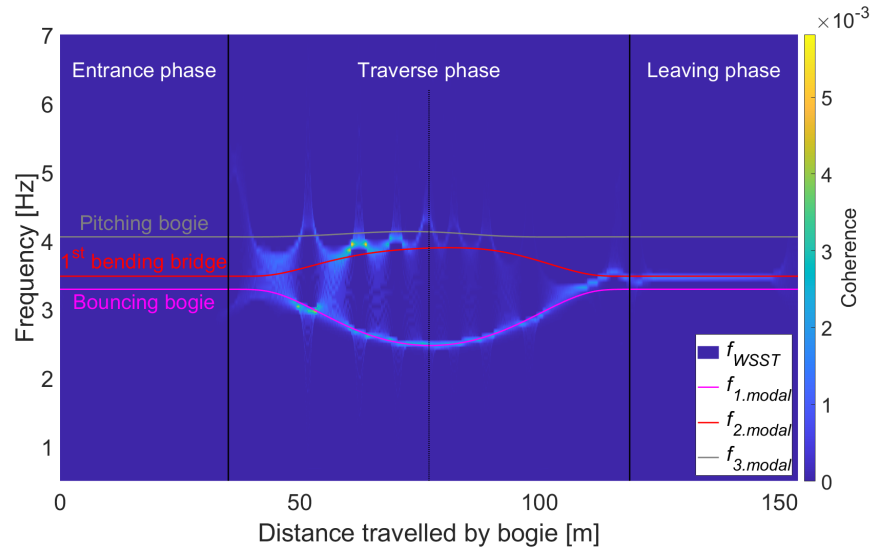


Figure 5.6: A comparison for the bogie variant between the modal analysis, and the dynamic analysis based upon the vertical acceleration of the mid-span node and a velocity of 10 m/s.

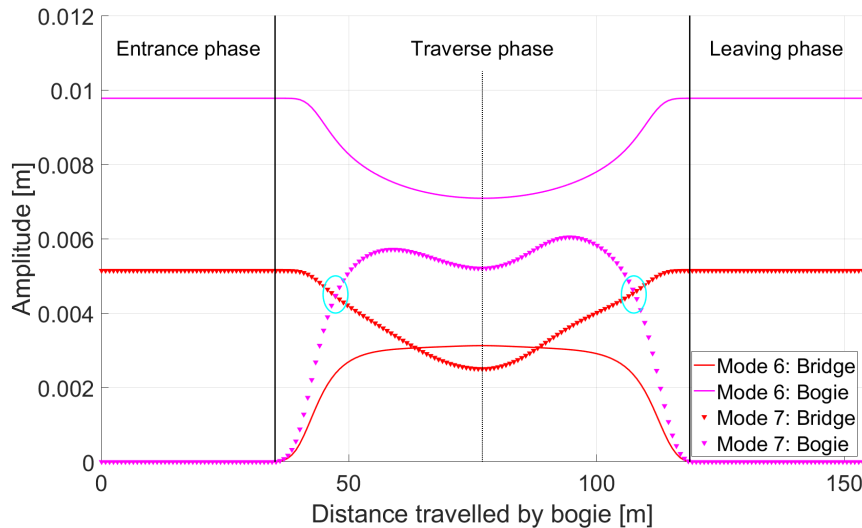


Figure 5.7: Amplitude of modes according the bogie variant.

and entrance phases. This is notable given the limited train-to-bridge interaction in the entrance phase. This will be further explored in a variation study.

The representation for the half-train variant is illustrated in fig. 5.8. The behaviour of the spikes differs from that of the bogie variant, and the resonance frequency of the bridge does not conform to the frequency content, except for some waviness behaviour. This distinct behaviour is not attributed to the proximity to the pitching frequency of the bogie, because 1) simulations with varying inertia terms exhibit similar behaviour, and 2) the train variant (represented in fig. 5.9) does not exhibit this behaviour, despite having an even closer pitching frequency. Finally, the bouncing frequency of the body aligns with the modal analysis.

The frequency representation for the train variant is depicted in fig. 5.9. Both the bouncing of the bogie and the bridge's resonance frequency align with the modal analysis during the traverse phase; however, the frequency of the bridge exhibits waviness behaviour. The precise cause is unknown, but a variation study could

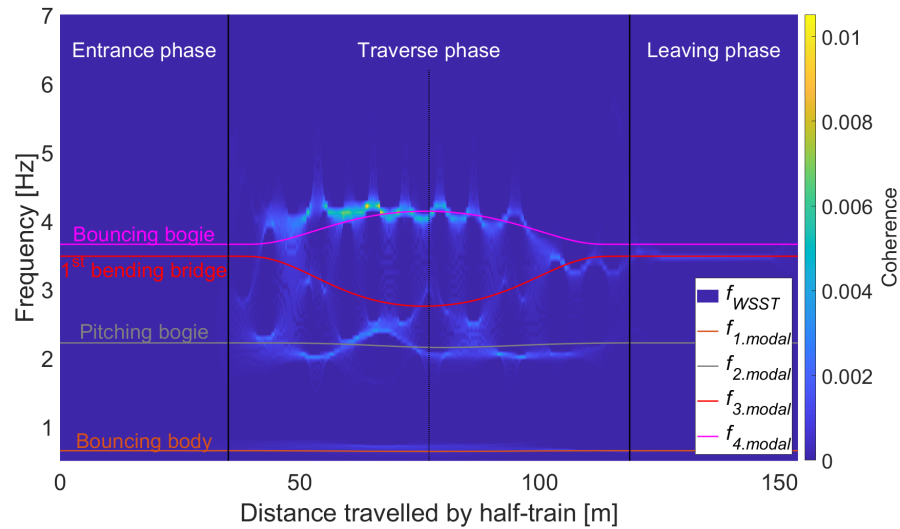


Figure 5.8: A comparison for the half-train variant between the modal analysis, and the dynamic analysis based upon the vertical acceleration of the mid-span node and a velocity of 10 m/s.

enlighten why this occurs. The bogie's bouncing displays similar spikes and kinetic energy fading in comparison to the bogie variant. Furthermore, the lower frequency content is not visible, which could be attributed to these modes not contributing as significantly, as can be verified based on the amplitude ratio between train and bridge for various modes during the traverse phase.

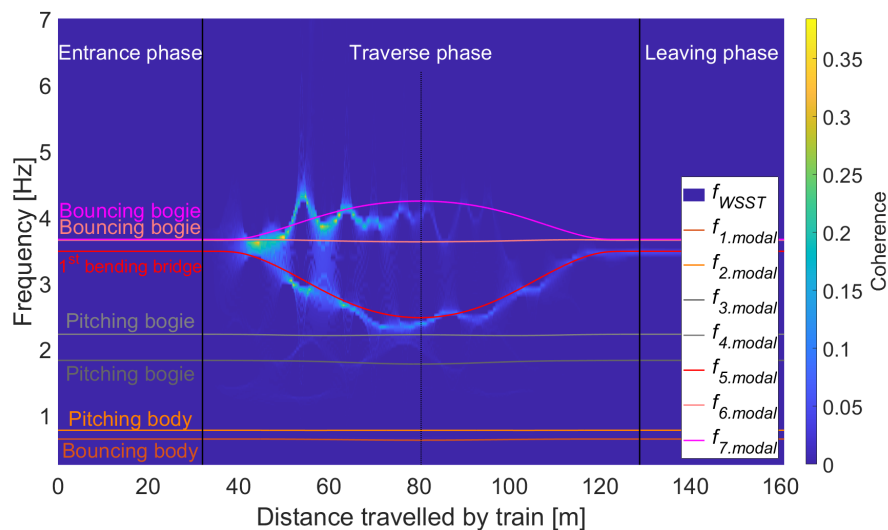


Figure 5.9: A comparison for the train variant between the modal analysis, and the dynamic analysis based upon the vertical acceleration of the mid-span node and a velocity of 10 m/s.

5.2 Variation study of the bogie variant

A variation study has been conducted to gain a deeper understanding of the appearance of spikes and the distribution of kinetic energy. Variation studies have been carried out for: the bogie velocity, damping coefficient, bogie inertia, bogie mass, spring coefficient, and both the bogie mass and spring coefficient simultaneously.

5.2.1 Velocity

The bogie velocity is varied from 1 m/s to 30 m/s in unit intervals. The acceleration response exhibited similar behaviour across the range of velocities, including the absence of vibrations during the entrance phase, free-decaying vibration during the leaving phase, and the presence of three consecutive spikes representing the maximum amplitude as the wheels reached the mid-span node. The maximum amplitude of the response increases with increasing velocity, as the bridge experiences greater excitation at higher velocities. At low velocities, a change in the acceleration response is observed as the wheels enter and leave the bridge, resulting in vertical lines in the frequency content, as can be seen in fig. L.1. However, this behaviour is less prominent at higher velocities, as the bogie is no longer perceived as three individual units but rather as a single unit entering and leaving the bridge.

At relatively low velocities, particularly at velocities of 1 m/s and 2 m/s, the frequency content is limited due to the fact that the system is not excited enough. As the velocity increases, frequencies begin to appear in the traverse phase. At these low velocities, the kinetic energy is primarily distributed into the first resonance frequency, while the second resonance frequency is less prominent. As the velocity increases, the second resonance frequency becomes more prominent.

Spikes have been observed in the frequency content, and the location and frequency of these spikes have been extracted as is represented in fig. 5.10. However, no conclusions can be drawn from the frequency value of the spikes or the difference between the frequency values of consecutive spikes.

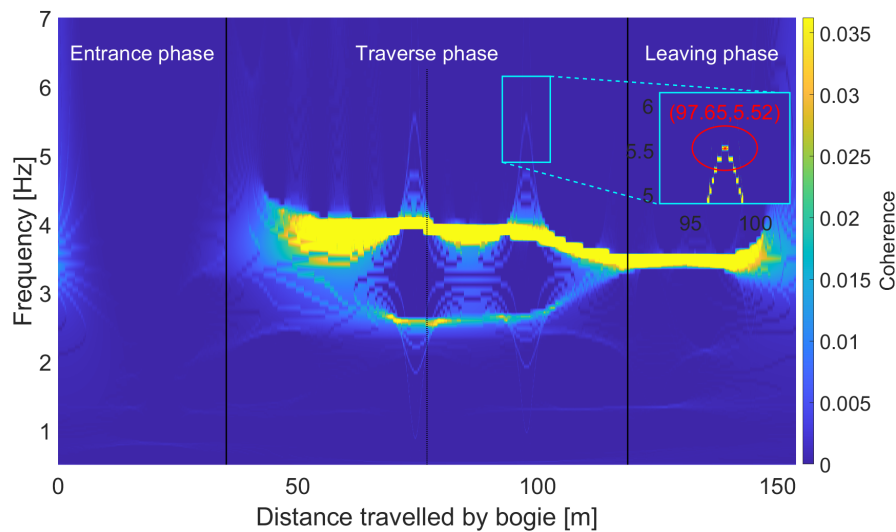


Figure 5.10: The extracting of a spike's location from the result of a dynamic simulation based upon the vertical acceleration of the mid-span node and a velocity of 30 m/s.

The spike positions are obtained from the traverse phase based upon the mid-span node, and the entrance phase based upon the bogie node, as illustrated in fig. 5.11. At relatively low velocities, the spikes are inconsistently throughout the entire traverse phase, because the system is not sufficiently excited, excluding these results. If the velocity is relatively high, the entrance length is too short to have at least two spikes making them unusable for processing. Nevertheless both subfigures show an inverse correlation between the number of spikes and the velocity. By increasing velocity, it is observed that the spikes move from left to right through the phases. For the traverse phase the spikes disappear in the direction of the leaving phase, as shown in appendix L, and new spikes appear from the entrance phase. The simulation with a velocity of 14 m/s, in fig. 5.11a, is in the middle between the appearance and

disappearance of a spike, resulting in a back-and-forth pattern.

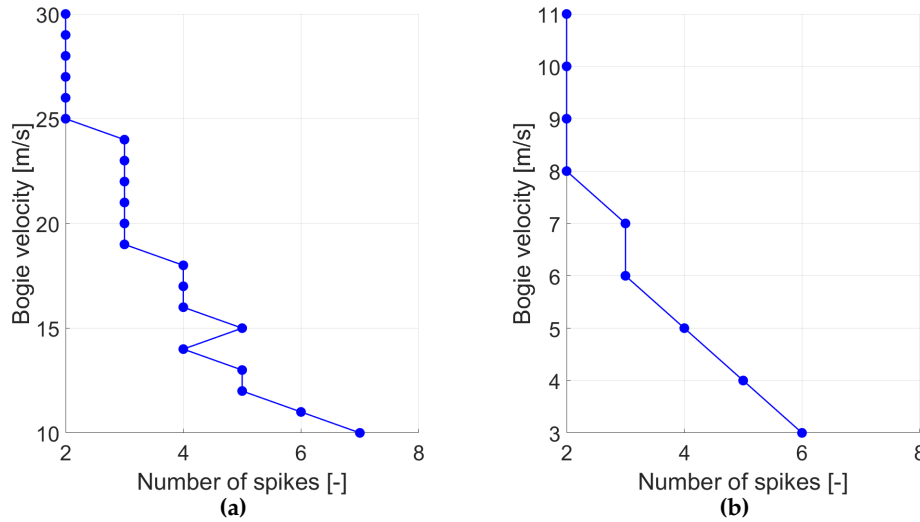


Figure 5.11: Number of spikes retrieved from the vertical acceleration response of (a) the traverse phase of the the mid-span node or (b) the entrance phase of the bogie node.

The location of the spikes is illustrated in fig. 5.12, and the difference between the location of consecutive spikes is depicted in fig. 5.13, where blue lines indicate suggested patterns. The first pattern intensifies with an increase in velocity, as shown in fig. 5.12a, implying that the bridge's mid-span forms an asymptote, while subsequent patterns become less steep. This behaviour does not correlate with unequal axle spacing, as further simulations employing equidistant axle spacing continue to display similar behaviour. Furthermore, as depicted in fig. 5.13a, this behaviour does not demonstrate a constant difference, although a certain pattern is visible.

Linear patterns appear in the spikes of the entrance phase, as illustrated in fig. 5.12b. The difference between consecutive spikes follows a linear trend as illustrated in fig. 5.13b. This line corresponds with the velocity over the edge length, thereby suggesting that spikes are formed based on these quantities. During the traverse phase, an increased number of spikes is observed than if this pattern is continued. Some spikes adhere to the previously identified pattern, while others may be attributed to either the bogie-to-bridge interaction or unequal edge lengths in the entrance and traverse sections. Additionally, axle spacing might be a factor, as some spikes correspond to velocity over axle spacing.

5.2.2 Remaining quantities

A similar variation study is conducted by varying the damping coefficient, bogie inertia, bogie mass, spring coefficient, and both the bogie mass and spring coefficient simultaneously. In general, these studies reveal that the distribution of kinetic energy between resonance frequencies change as the quantities are varied, but no clear relationship has been found. This is also true for the number of spikes and their position in the traverse phase, for which no clear relationship has been found. Furthermore, when two resonance frequencies are close to each other, the kinetic energy is distributed between them. Additional observations are as follows:

- **Damping:** The response ceases to change by a considerably high damping coefficient, suggesting that the suspension system operates as filter. This behaviour starts before reaching the critical damping coefficient.

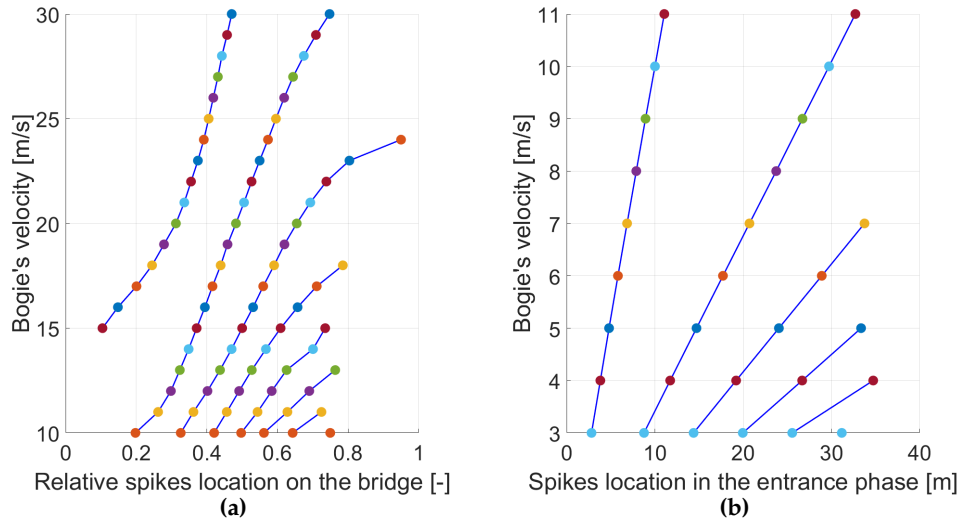


Figure 5.12: Spike locations retrieved from the vertical acceleration response of (a) the traverse phase of the the mid-span node or (b) the entrance phase of the bogie node.

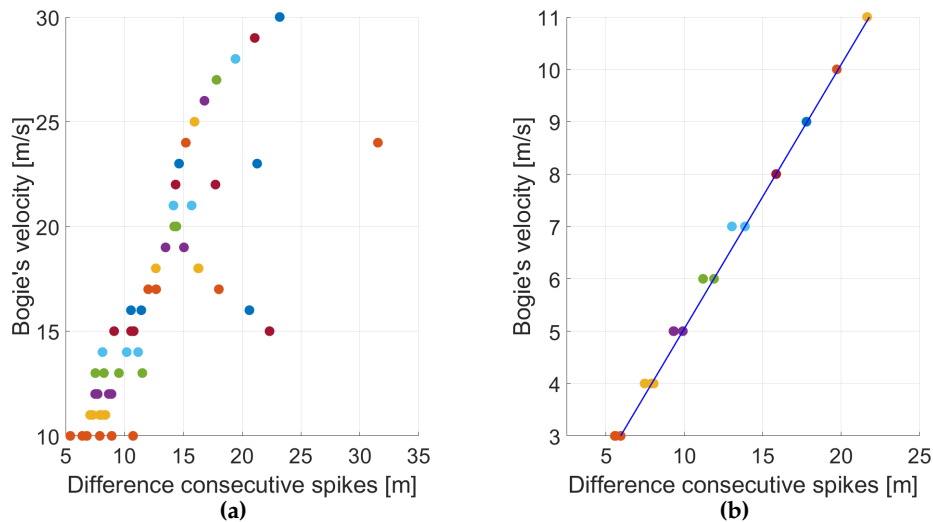


Figure 5.13: Difference between consecutive spikes retrieved from the vertical acceleration response of (a) the traverse phase of the the mid-span node or (b) the entrance phase of the bogie node.

- **Inertia:** A relatively high inertia term, resulting in a low pitching frequency, ensures a decrease in the resonance frequency and a spread in the frequency content, leading to inconsistent results.
- **Mass:** A decrease in resonance frequency is caused by relatively high mass. However, by a relatively low mass, the bridge's resonance frequency is prominent in both the traverse and leaving phase.
- **Stiffness:** A relatively high stiffness ensures an increase in the resonance frequency also. The resonance frequency corresponding with the bridge in both the traverse and leaving phase fades.
- **Mass and stiffness:** Increasing both quantities yields in a larger difference between both resonance frequencies.

The damping acting as a filter is logical, as it filters vibrations, reducing available information. The inconsistency in inertia results remains unexplained, as the pitching frequency is absent from the frequency content. However, as previously noted, this might be associated with axle spacing. Mass and stiffness effects align with the general frequency equation. Prominent results and fading resemble earlier mentioned mode impacts and can be connected. Varying both mass and stiffness maintains the frequency but increases bridge excitation, making an expected notable difference.

5.3 Simulations DMU

The DMU train differs from the locomotive train in terms of mass and spring stiffness, as illustrated in table 4.1. These quantities yield in a difference in mass and frequency ratio, as shown in table 4.3. Moreover, the damping coefficient of the DMU train is considerably higher than that of the locomotive, and the DMU train is symmetrical in terms of axle spacing.

The result of the dynamic simulation for the bogie variant is illustrated in fig. 5.14. This reveals that only a single resonance frequency is visible, where the modal analysis correlates this frequency with the bridge's natural frequency. It is significant to note that the recurring spikes are absent in this frequency. Spikes are only visible in the bridge's resonance frequency at the location of the wheels entering and leaving the bridge section, as previously indicated in section 5.1. Furthermore, limited frequency content is near the bogie's bouncing frequency, as highlighted with the cyan circle. The pitching frequency is 10.857 Hz and falls, for all results, outside the bound of the plot and therefore not visible. Nevertheless, this train is deemed suitable for DI, as the method for DI relies on the bridge's fundamental frequency, which is clearly visible in these results.

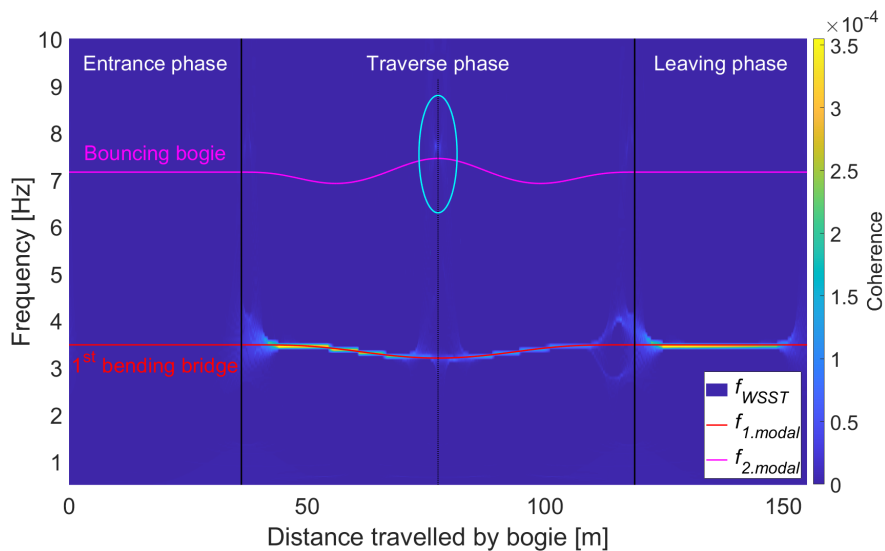


Figure 5.14: A comparison for the bogie variant between the modal analysis, and the dynamic analysis based upon the vertical acceleration of the mid-span node and a velocity of 10 m/s.

To improve the results of the DMU train and account for the absence of the bogie frequency, quantities such as velocity, mass and spring stiffness are independently varied. However, these variations yield results that are either similar to or worse than those obtained using the original values. By equating the damping coefficient with that of the locomotive, the second resonance frequency appears, as shown in fig. 5.15. This indicates that the high damping coefficient acts as a filter for the bogie's frequencies. Moreover, the result demonstrates that the bouncing of the bogie is

most prominent during the first half of the traverse phase, which is similar to the locomotive. A waviness pattern is observed around this frequency, as highlighted. Nevertheless, the frequency closely aligns with the modal analysis, in contrast with the locomotive where the spikes cause the frequency to deflect from this analysis.

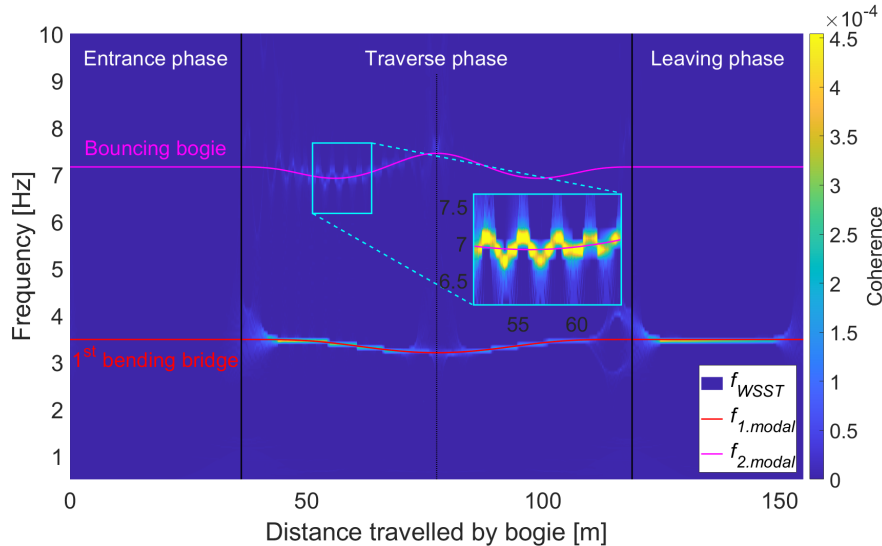


Figure 5.15: A comparison for the bogie variant between the modal analysis, and the dynamic analysis based upon the vertical acceleration of the mid-span node, a velocity of 10 m/s and by equating the damping coefficient to the locomotive.

To improve the response during the latter half of the traverse phase, both the mass ratio and damping coefficient are equalised with those of the locomotive. By simultaneously adjusting the spring coefficient to maintain the same frequency ratio, this resulted in fig. 5.16. This result indicates that the second frequency lasts throughout the traverse phase due to increased train-bridge interaction resulting from higher mass, leading to sufficient bridge excitation. The waviness behaviour is less prominent in the bouncing of the bogie when compared to fig. 5.15, although some spikes are present at the mid-span of the bridge, as highlighted. By introducing unequal axle spacing these spikes become smoother, as can be seen in fig. M.1. Furthermore, unlike the locomotive, the bridge frequency does not exhibit any spikes.

By establishing an equivalence between the mass ratio, frequency ratio, and damping coefficient with those of the locomotive, the results depicted in fig. 5.17 are obtained. This dynamic analysis, which follows the modal analysis, exhibits spikes in both resonance frequencies, in contrast to fig. 5.16, where spikes are only present in the bogie's bouncing frequency. These spikes are similar to those observed for the locomotive in fig. 5.6. This result suggests that when the frequency ratio approaches unity, spikes and kinetic energy smearing appear for both resonance frequencies.

The simulations for the half-train and train variants are depicted in appendix M. The half-train variant only exhibits the bridge's fundamental frequency when the original values are implemented. On the other hand, the train variant reveals multiple resonance frequencies. However, these frequencies become faded in the latter half of the traverse phase, rendering it unsuitable for DI.

5.4 Experiments

This section is dedicated to the experiments conducted using the experimental setup. The initial step entails determining the natural frequencies of the system and evalu-

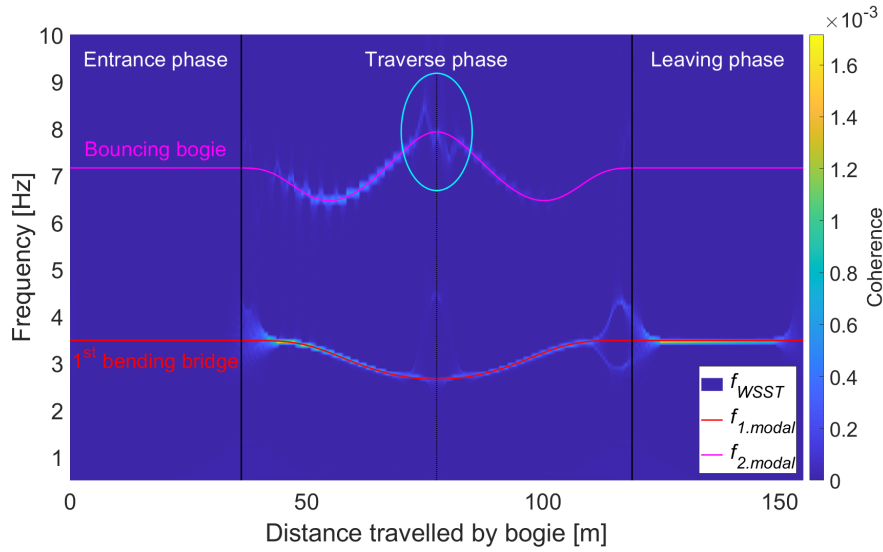


Figure 5.16: A comparison for the bogie variant between the modal analysis, and the dynamic analysis based upon the vertical acceleration of the mid-span node, a velocity of 10 m/s, and by equating the damping coefficient and mass ratio to the locomotive.

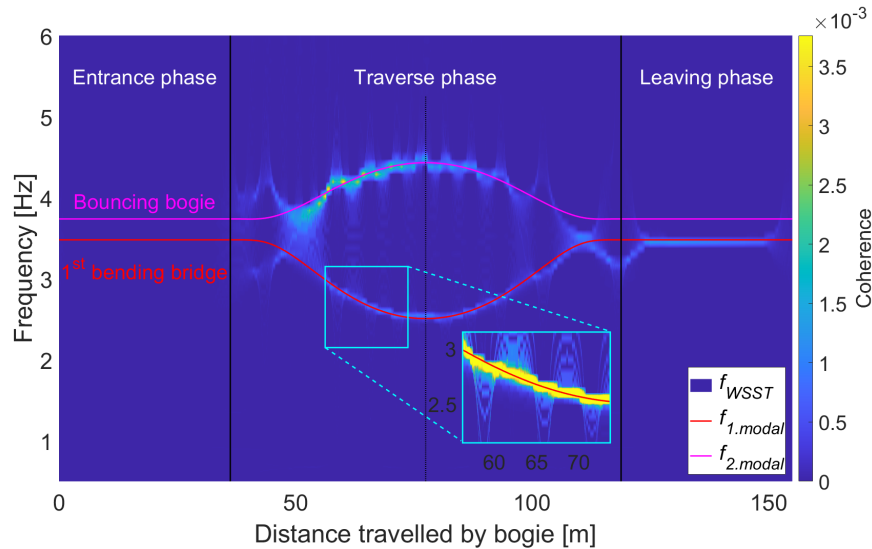


Figure 5.17: A comparison for the bogie variant between the modal analysis, and the dynamic analysis based upon the vertical acceleration of the mid-span node, a velocity of 10 m/s, and by equating the damping coefficient, mass ratio and frequency to the locomotive.

ating the reliability of the obtained results. Subsequently, a stepwise modal analysis is executed to investigate the interaction between the bogie and the bridge at various bridge positions. Finally, a dynamic experiment is conducted, aiming to produce results consistent with those obtained in the earlier simulations.

5.4.1 Natural frequency

The experimentally determined natural frequencies that correspond best with the system are illustrated in table 5.2. The body exhibits a low difference between the experimental and analytical values. This can be attributed to the fact that a thick strip on top of the train minimises the local geometric bouncing after impact, unintended

double hits, and the smearing of a hit.

Meanwhile, these factors, which contribute to the local geometric bouncing, are present by experiments conducted on the bogie, yielding a significant difference in frequency. These factors arise from the bogie's low mass and the employment of thin plates. Conversely, the results could be improved if a shaker were to be employed instead of the modal hammer. The shaker has the capability to selectively excite a specific frequency range, thereby improving both the reliability and validity of the results. The main disadvantage opposing the use of the shaker lies in its requirement for space, which was not available during the course of the experiments. Furthermore, the presence of moving components plays an additional role in the observed differences. The animation in FEMtools illustrates that the pitching motion also displays substantial bouncing, introducing a notable Modal Assurance Criterion (MAC) alias and resulting difference.

Table 5.2: Natural frequencies per train variant obtained experimentally.

Type	Experimental	Analytical	Difference	MAC alias
$f_{\text{bouncing.body}}$	25.85 Hz	28.74 Hz	10.06%	0.9%
$f_{\text{pitching.body}}$	42.13 Hz	45.53 Hz	7.47%	0.9%
$f_{\text{pitching.bogie1}}$	43.69 Hz	89.05 Hz	50.94%	57.5%
$f_{\text{bouncing.bogie1}}$	124.80 Hz	134.02 Hz	6.88%	57.5%
$f_{\text{pitching.bogie2}}$	43.67 Hz	89.05 Hz	50.96%	54.3%
$f_{\text{bouncing.bogie2}}$	126.45 Hz	134.02 Hz	5.65%	54.3%
$f_{\text{bending1.bridge}}$	187.69 Hz	143.73 Hz	30.6%	0.9%
$f_{\text{bending2.bridge}}$	681.37 Hz	574.92 Hz	18.5%	0.9%

The bridge's fundamental frequencies exhibit an increased error, which can be attributed to various factors including the bridge's stiffness, the bridge's mass, and the applied boundary conditions. The intended boundary conditions for the design are similar to those of a simply supported beam. However, alternatively, the boundary condition can be fixed at either end, resulting in a more strict boundary conditions and significantly higher frequencies compared to a simply supported beam.

Furthermore, the boundary conditions regarding to the entrance and leaving sections, denoted as supports in 3.3, are intended to function as fixed boundary conditions, thereby restraining any motion. Nevertheless, due to insufficient fixating of these components, motion can manifest, resulting in a difference in frequency. An attempt to address this is made through a simplified experiment wherein the support is firmly clamped. The obtained results exhibit a comparable bridge's fundamental frequency. Consequently, it remains uncertain whether this observed difference is attributable to the clamping procedure or if it accounts from inaccuracies inherent in the experimental methodology.

To reduce the difference between experimental and numerical values, various approaches can be employed. Firstly, reducing the bridge's stiffness can be achieved by introducing structural damage across the bridge section. This damage can be induced by incorporating disconnections or tears in the plates, resulting in reduced stiffness while maintaining the same mass.

Secondly, increasing the bridge's mass can be achieved by adding distributed hanging weights along the entire bridge length. These weights ensure that the bridge's stiffness remains constant, albeit with a modified mass ratio. To offset the change in mass ratio, additional mass can be added to the train and springs with higher coefficients, ensuring the bogie's natural bouncing frequency remains unchanged.

Furthermore, it is possible to loosen the boundary condition at the junction between the entrance and bridge sections. Originally, the bridge spans continuously over this section, but the proposed solution suggests interrupting the upper side of the

bridge at the junction. This alteration results in a reduction of stiffness; however, implementing this solution requires redesigning.

Finally, both the mass and spring stiffness of the train can be adjusted to increase the natural bouncing frequency and align the frequency ratio correctly. While this adjustment would yield the desired ratios, it also introduces a distortion in the model concerning the similarity analysis in terms of the mass ratio.

Upon evaluating all potential solutions, it becomes apparent that modifying the bridge's mass would attain the correct frequency ratio and in order to maintain the desired mass ratio the train's mass is adjusted. This combination is chosen so the similarity between the actual case is maintained in terms of frequency ratio. Modifying the bridge's stiffness or boundary conditions becomes significantly more complex, rendering them less desirable options.

Despite the differences between the experimental results and those calculated analytically, the obtained natural frequencies are reasonable close to the theoretical values. This indicates that the experimental setup is indeed similar to the design in the numerical environment, and therefore, the setup is deemed sufficient for conducting subsequent experiments.

5.4.2 Modal analysis

In the preceding section, the natural frequencies that best align with the mode shapes are presented, as displayed in table 5.2. It is noteworthy that, rather than a single frequency, there exists a range of potential frequencies. This implies that frequencies in the vicinity of those represented in table 5.2 also closely resemble the mode shape, forming a range. This range is employed in the modal analysis, as it provides a more comprehensive insight into the integrated system.

The stepwise frequency analyses of the scaled bogie variant is depicted in fig. 5.18. Throughout all phases, the upper limit remains constant, whereas the lower limit decreases during the traverse phase. The behaviour of the lower limit aligns with expectations, albeit the range remains relatively wide. As discussed in the preceding subsection, employing a shaker instead of the modal hammer can lead to more precise determination of the natural frequencies, thereby reducing the range.

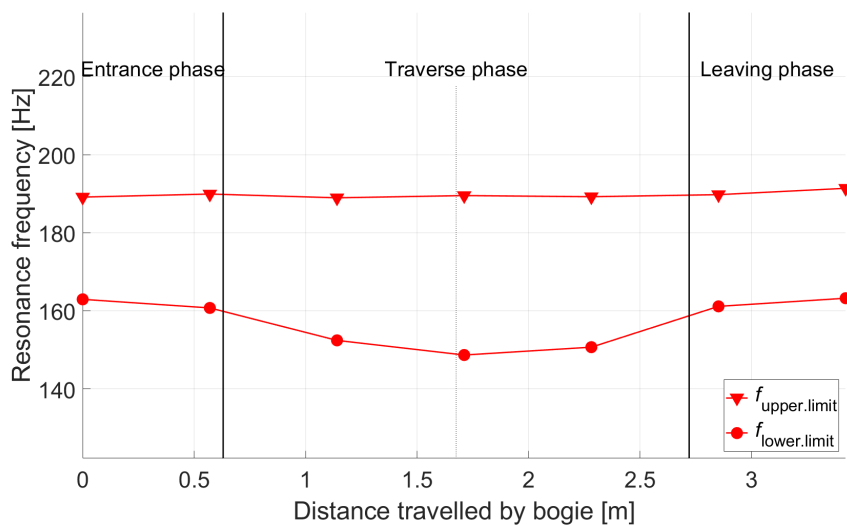


Figure 5.18: Modal analysis of the bogie variant across the bridge.

The results for both the half-train variant and the train variant exhibit similarities to those of the bogie variant, and they are listed in appendix N. The minimum reso-

nance frequency of the bridge during the traverse phase differs among these variants, similar to the observations in the locomotive. It is worth highlighting that a similar frequency range, as depicted in fig. 5.18, is consistently observed across all these variants, suggesting that the method may not be adequate for accurately determining the natural frequency.

5.4.3 Dynamic analysis

The frequency representation of the bogie variant is depicted in 5.19. This result reveals prominent frequency components within the range of 140-200 Hz. However, it is important to note that the results exhibit a considerable level of noise, making the extraction of a clear resonance frequency challenging. Furthermore, during the leaving phase, the bridge's fundamental frequency remains concealed, with only the presence of waviness behaviour in the frequency content. Notably, these results deviate from the results of simulations conducted using actual quantities, and attempts to enhance the results through data processing techniques such as denoising, smoothing, or filtering have not yielded improvements.

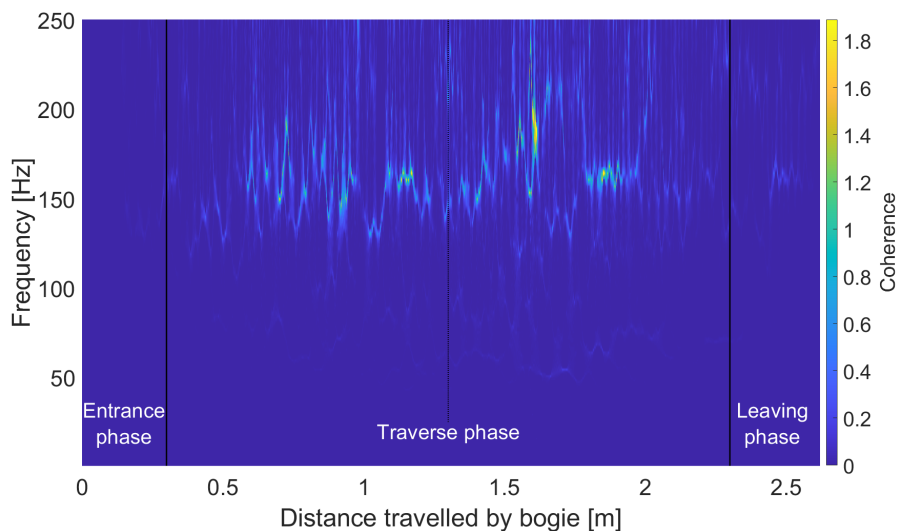


Figure 5.19: Dynamic analysis of the bogie variant based upon experimental data from the vertical acceleration of the mid-span node.

The results for the half-train variant exhibit similar behaviour to that of the bogie variant, whereas the train variant displays a notably higher degree of noise represented as vertical frequency content. The results for both variants can be found in N. To explain both the observable results and, notably, the concealed results, simulations involving the scaled prototype are conducted in the subsequent section. This aims to enhance the understanding of the system and provide explanations for the results that have been acquired.

5.5 Simulations experimental setup

This section contains both the modal analysis and the dynamic analysis of the scaled prototype. The modal analysis comprises multiple simulations aimed at replicating behaviour observed experimentally, whereas the dynamic simulation seeks to explain the experimental results.

5.5.1 Modal analysis

The preceding section has revealed that a range of frequencies closely resembles a mode shape. Consequently, multiple simulations have been conducted by varying bridge's fundamental frequency. This variation is relevant because the bridge's resonance frequencies (during the traverse phase) are influenced by its fundamental frequency. So, a broader frequency range enables the establishment of correlations between experimental and numerical findings. Simulations have been executed at three distinct bridge's fundamental frequencies: 145 Hz (original), 162.5 Hz (lower limit in the experimental results), and 189 Hz (upper limit in the experimental results). The value of the bridge's fundamental frequency serves as a distinguishing parameter for these simulations, as illustrated in 5.20. It is noteworthy that the bogie's bouncing frequency, in accordance with the original values, is 135 Hz, while experimental results yields a frequency of approximately 125 Hz. This latter value has been incorporated into the simulations to ensure an accurate representation. The bogie's pitching frequency has been omitted due to its lack of relevance.

Results obtained at a bridge fundamental frequency of 145 Hz (represented with solid lines in 5.20) indicate behaviour similar to that of the locomotive train configuration in the traverse phase. Nonetheless, these values and behaviour do not align with experimental findings, implying that the bridge's fundamental frequency is not 145 Hz. By increasing this frequency to 162.5 Hz, the bridge's resonance frequency remains relatively constant across all phases, aligning more closely with the experimental results. Nevertheless, experimental results show a decrease in frequency at this particular frequency, contrary to the nearly constant trend observed in the simulations. Further increasing the frequency to 189 Hz leads to a decrease in the bridge's resonance frequency. Conversely, experimental results show a constant frequency throughout all phases at this frequency. These results suggest that the bridge's fundamental frequency likely falls within this range, indicating either a continuous or decreasing trend in behaviour. The modes reveal that with a lower frequency ratio, corresponding to a higher bridge's fundamental frequency, there is reduced interaction. This yields in that the mode shapes remaining similar to those observed in the entrance phase. The bogie's resonance frequency decreases across all simulations; however, a lower frequency ratio corresponds to reduced interaction.

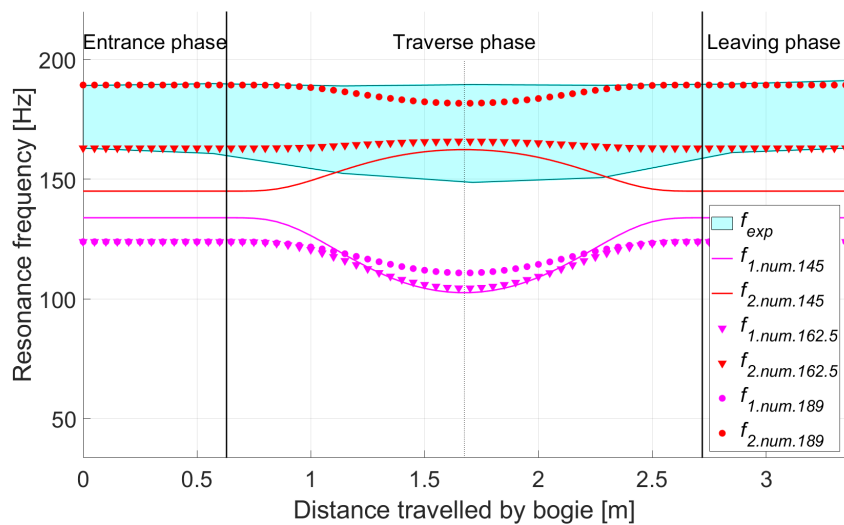


Figure 5.20: A comparison for the bogie variant between experimental results and numerical results of the modal analysis.

Both the half-train and train variant exhibit similar behaviour to that of the bogie

variant, as illustrated in appendix O. The difference in resonance frequencies can be attributed to the introduction of the body mass and secondary suspension, influencing the train-to-bridge interaction. In all cases, the range of potential frequencies is too wide to accurately determine the natural frequency of the experimental results.

5.5.2 Dynamic analysis

By incorporating the quantities listed in table 4.1, a single horizontal line emerges in the frequency content. This line corresponds to the driving frequency, determined by dividing the velocity by the edge length. Consequently, excluding this numerically generated frequency renders the simulation non-representative of the system's behaviour. This explains the absence of observable results in the experiments.

Upon reevaluation of the input file, it is observed that the gravitational force and material damping are not scaled in accordance with the procedure outlined in chapter 2. The initial reason for neglecting gravity was that natural frequencies are deemed unaffected by its presence. However, in a dynamic simulation, gravity is intertwined with the impact of the train on the bridge. Consequently, without adjusting this force, the bridge experiences a force roughly 40 times smaller than the train's mass, resulting in insufficient excitation of the bridge. This behaviour mirrors what is observed during the variation study involving a lower bogie mass.

Higher damping leads to an absence of vibrations in the leaving phase, as well as a faded frequency content during the traverse phase, as previously noted in the variation study. Scaling both the gravitational force and damping coefficient by a factor of 40 yields the frequency representation shown in fig. 5.21. This result closely resembles the earlier findings for the locomotive. Nonetheless, differences arise in the energy distribution, attributed to the arbitrary selection of material damping. Therefore, this aspect should be investigated in future work.

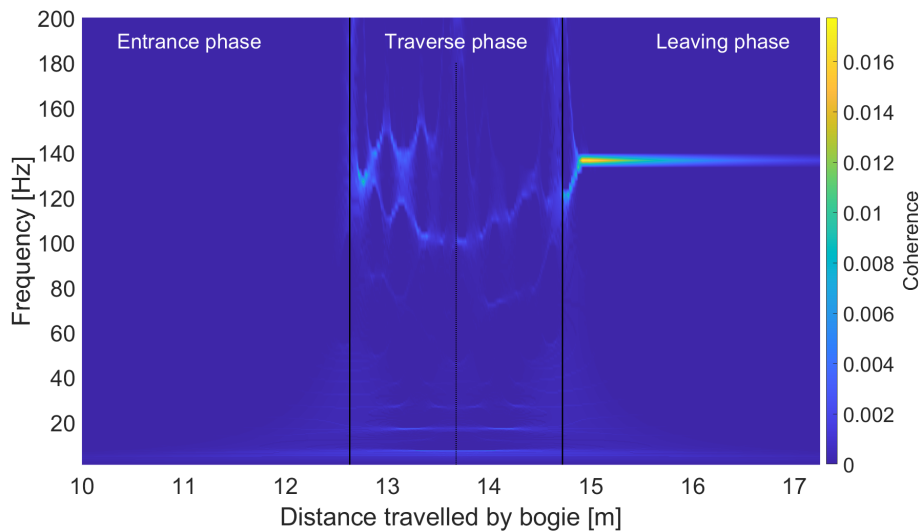


Figure 5.21: Dynamic analysis of the bogie variant based upon the vertical acceleration response of the mid-span node with a gravitational constant of 396.177 m/s^2 and a material damping coefficient (β) of 0.000025 .

As adjusting the gravitational force proves impractical within the confines of the experimental setup, an alternative approach involves modifying the bogie's mass in combination with the spring stiffness. This approach remains feasible because the gravitational force and the bogie's mass collectively influence the impact of the bogie on the bridge, while the spring stiffness ensures the desired frequency ratio. A

simulation is conducted wherein both the mass and stiffness are increased by a factor of 40, and Earth's gravitational force was applied. The result is depicted in 5.22. This simulation indicates the presence of both frequencies. However, it is important to note that the arbitrary choice of the damping ensures the faded frequencies. Nevertheless, this demonstrates that by adapting the bogie's mass and stiffness, it is possible to obtain viable results for the experiments.

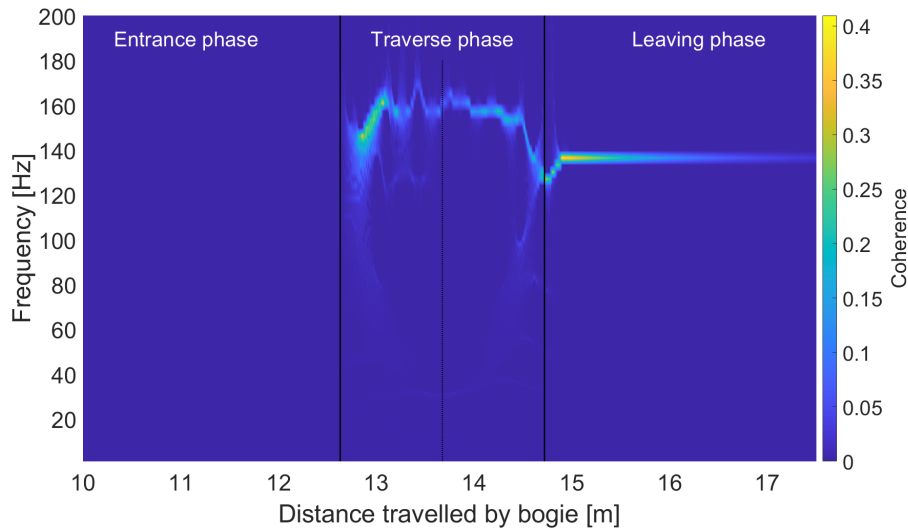


Figure 5.22: Dynamic analysis of the bogie variant based upon the vertical acceleration response of the mid-span node with the bogie mass and the spring stiffness multiplied by 40.

5.6 Closing remarks

The goal of this chapter was to present and discuss the results of both the simulations and experiments. In the process, a sub-question is answered, namely:

- Which train configuration, concerning the Boyne Viaduct, is most suitable for capturing and validating train dynamics?

Numerical simulations indicate that the locomotive train configuration reveals both the bridge's fundamental frequency and the bogie's bouncing frequency. Conversely, the DMU train configuration only displays the latter frequency due to its reduced train-bridge interaction (low mass) and higher damping coefficient. Additionally, the DMU train lacks spikes in its frequency content, while the locomotive train shows such spikes, potentially suggesting numerically generated effects.

The DMU train reveals the bridge's fundamental frequency. However, it is important to note that the difference in this frequency during the traverse phase is less noticeable for the DMU train. This is attributed to its reduced train-bridge interaction resulting from low mass, leading to insufficient bridge excitation. Consequently, this makes the DMU train less suitable for Structural Health Monitoring (SHM).

Finally, experimental validation has not yet been completed, where enhancements to the validation, such as increasing bridge and train masses and varying spring coefficients, are proposed. The current method of determining natural frequencies using the roving hammer technique was found inaccurate. Nonetheless, dynamic simulations align with modal analysis and exhibit expected behaviour. The modal analyses indicate that uneven axle spacing leads to asymmetrical behaviour. Additionally, instantaneous modes were found to offer insights into (kinetic) energy distribution.

6 | Conclusions

This chapter presents the answer to the main research question, followed by a series of more detailed conclusions regarding dynamic modelling, spikes in the frequency content and DMU train configuration.

The main research question of this study is:

- **How to realise an experimental setup that is capable of capturing and validating numerically calculated train dynamics?**

The research outlined in this thesis has provided an answer to this question, which can be partitioned into two distinct facets, specifically: 1) the realisation of the experimental setup and 2) the validation of experimental results against numerical results.

1. The research aimed to develop an experimental setup capable of capturing numerically calculated train dynamics. This realisation involves scaling down the Boyne Viaduct to a laboratory-scale prototype using the similarity analysis. This method is based on complete similarity, however, a relaxed model, allowing for deviations in quantities like damping coefficient and inertia terms, is found to be sufficient. This has been proven by comparing the frequency and mass ratios between train and bridge, which exhibit similar behaviour when a relaxed model is employed, as long as these ratios remain alike. In the end, this led to an experimental setup comprising the train, the bridge, the support and the motor system.
2. The research aimed to validate experimental findings against numerical results. However, it can be concluded that this validation has not yet been successfully accomplished. Although modal analysis exhibited behaviour similar to that observed in simulations, the results suggest a need for methodological adjustments. Specifically, it is recommended to employ a shaker system to more accurately determine the natural frequencies of the system.

Additionally, the experimental determination of the bridge's fundamental frequency revealed a higher value than initially anticipated. To align the frequency components and maintain similarity, the introduction of distributed hanging weights along the entire length of the bridge is proposed. Furthermore, adjustments to the train's mass and stiffness, approximately by a factor of 40, are recommended to compensate for gravitational scaling effects.

Furthermore, specific conclusions drawn from the simulations are grouped among dynamic modelling, spikes in the frequency content and the DMU train configuration are listed as follows:

- Dynamic modelling
 - The numerical model functions as intended due to the lack of vibrations during the entrance phase, resulting in the absence of frequency content, and a free-decaying vibration during the leaving phase, aligning with the bridge's fundamental frequency.
 - The numerical model captures the interaction between train and bridge during the traverse phase in the processed data, resulting in the Instantaneous Frequencies (IFs).
 - The results of the dynamic analysis align with those of the modal analysis, with the exception of the spikes in the frequency content.

- For various modes, the amplitude ratio between train and bridge varies during the traverse phase, indicating a correlation with the distribution of kinetic energy between the train and the bridge at this phase.
- Modal analysis of the locomotive train configuration reveals asymmetrical behaviour around the mid-span node, attributed to unequal axle spacing.
- Although more advanced models like the half-train and train models have the potential to identify frequency content, these models yield less favorable results in the WSST plot.
- Spikes in the frequency content
 - The number of the spikes exhibits an inverse correlation with the velocity in both the entrance and traverse phases.
 - The spike position is linked to the velocity; as the velocity increases, the spikes appear further along the bridge.
 - Spike position is connected to the element edge length, which corresponds to the time it takes for the train to pass an element.
 - Spikes emerge in the frequency content when the frequency ratio between train and bridge approaches unity.
- DMU train configuration
 - Sufficient train-bridge interaction, resulting from high mass, leads to sufficient bridge excitation essential for obtaining frequency content.
 - A relatively high damping coefficient ensures a fading effect in the frequency content, particularly in the latter half of the traverse phase, rendering the frequency content less visible.
 - The DMU train configuration only reveals the bridge's fundamental frequency due to higher damping acting as a filter, coupled with lower train-bridge interaction resulting from lower mass.

7 | Recommendations

A framework for experimental validation, encompassing the experimental setup and methodology, has been established in combination with numerical simulations to advance model development and gain a deeper understanding in this field. Several subjects for future research are identified, with recommendations clustered into three categories: 1) experimental validation, 2) future experimental work and 3) numerical simulations.

Experimental validation

- To enhance the accuracy of determining the system's natural frequencies, it is advisable to use a shaker since it provides consistent results and minimises local geometric bouncing.
- Adjust the bridge's mass by adding distributed hanging weights along its entire length to align the bridge's fundamental frequency of the experimental setup with the frequency derived from similarity analysis.
- In dynamic experiments, scale the train's mass and spring stiffness by a factor of approximately 40 to account for the scaling of gravitational forces. It is recommended to simulate these newly determined quantities to validate the viability of the results before implementing these changes.

Future experimental work

- To assess the feasibility of Damage Identification (DI) within the experimental setup, it is essential to introduce damage, such as removing bolts or replacing intact components with plates containing tears, imitating stiffness loss.

Numerical simulations

- Dynamic modelling
 - Extend the application of instantaneous modes for both the train and bridge in more simulations, thereby exploring the distribution of kinetic energy between the train and bridge within the results.
 - Incorporate multiple train carriages into the model and explore their impact on resonance caused by recurring distances within the train configuration. This would improve the simulations compared to real-world applications and determine the feasibility of DI.
 - Considering the significant influence of (material) damping on the frequency content of the results, it is essential to conduct a thorough analysis of the effect of material damping and ensure its accurate implementation.
- Spikes in the frequency content
 - To confirm that the spikes are numerically generated within the model and linked to the element edge length, it is necessary to vary either the entrance length or the element edge length in the entrance section.
 - Equalising the element edge length across all sections is essential to examine whether the variance in the position of consecutive spikes during the traverse phase follows a pattern.

- Investigating the axle spacing is required to validate the observed correlation between spikes in the traverse phase and axle spacing.
- Varying the frequency ratio between train and bridge beyond unity is vital to assess if this ratio influences the appearance of these spikes in the bridge's resonance frequency.

References

- [1] W. Zhai, Z. Han, Z. Chen, L. Ling, and S. Zhu. Train–track–bridge dynamic interaction: a state-of-the-art review. *Vehicle System Dynamics*, 57(7):984–1027, 2019. doi:10.1080/00423114.2019.1605085.
- [2] P. A. Montenegro, H. Carvalho, D. Ribeiro, R. Calçada, M. Tokunaga, M. Tanabe, and W. M. Zhai. Assessment of train running safety on bridges: A literature review. *Engineering Structures*, 241:e112425, 2021. doi:10.1016/j.engstruct.2021.112425.
- [3] T. Arvidsson and R. Karoumi. Train–bridge interaction – a review and discussion of key model parameters. *International Journal of Rail Transportation*, 2(3): 147–186, 2014. doi:10.1080/23248378.2014.897790.
- [4] K. Wang, H. Xia, M. Xu, and W. Guo. Dynamic analysis of train-bridge interaction system with flexible car-body. *Journal of Mechanical Science and Technology*, 29(9):3571–3580, 2015. doi:10.1007/s12206-015-0801-y.
- [5] L. Ling, X. B. Xiao, and X. S. Jin. Development of a simulation model for dynamic derailment analysis of high-speed trains. *Acta Mechanica Sinica/Lixue Xuebao*, 30(6):860–875, 2014. doi:10.1007/s10409-014-0111-0.
- [6] P. Lou. A vehicle-track-bridge interaction element considering vehicle’s pitching effect. *Finite Elements in Analysis and Design*, 41(4):397–427, 2005. doi:10.1016/j.finel.2004.07.004.
- [7] Y. S. Cheng, F. T. K. Au, and Y. K. Cheung. Vibration of railway bridges under a moving train by using bridge-track-vehicle element. *Engineering Structures*, 23(12):1597–1606, 2001. doi:10.1016/s0141-0296(01)00058-x.
- [8] Y. B. Yang, J. D. Yau, and Y. S. Wu. *Vehicle–bridge interaction dynamics*. World Scientific Publishing Co. Pte. Ltd, Singapore, 2004.
- [9] C. Rigueiro, C. Rebelo, and L. Simões da Silva. Influence of ballast models in the dynamic response of railway viaducts. *Journal of Sound and Vibration*, 329(15):3030–3040, 2010. doi:10.1016/j.jsv.2010.02.002.
- [10] V. N. Dinh, K. D. Kim, and P. Warnitchai. Dynamic analysis of three-dimensional bridge-high-speed train interactions using a wheel-rail contact model. *Engineering Structures*, 31(12):3090–3106, 2009. doi:10.1016/j.engstruct.2009.08.015.
- [11] M. Majka and M. Hartnett. Dynamic response of bridges to moving trains: A study on effects of random track irregularities and bridge skewness. *Computers and Structures*, 87(19-20):1233–1252, 2009. doi:10.1016/j.compstruc.2008.12.004.
- [12] T. Arvidsson, A. Andersson, and R. Karoumi. Train running safety on non-ballasted bridges. *International Journal of Rail Transportation*, 7(1):1–22, 2019. doi:10.1080/23248378.2018.1503975.
- [13] A. Rytter. *Vibration Based Inspection of Civil Engineering Structures*. Dept. of Building Technology and Structural Engineering. PhD dissertation, University of Aalborg, Aalborg, Denmark, 1993.
- [14] N. Mostafa, D. Di Maio, R. Loendersloot, and T. Tinga. Railway bridge damage detection based on extraction of instantaneous frequency by wavelet synchrosqueezed transform. *Advances in Bridge Engineering*, 3(12), 2022. doi:10.1186/s43251-022-00063-0.

- [15] Y. B. Yang and J. P. Yang. State-of-the-art review on modal identification and damage detection of bridges by moving test vehicles. *International Journal of Structural Stability and Dynamics*, 18(2):e1850025, 2018. doi:10.1142/S0219455418500256.
- [16] Y. B. Yang, C. W. Lin, and J. D. Yau. Extracting bridge frequencies from the dynamic response of a passing vehicle. *Journal of Sound and Vibration*, 272(3):471–493, 2004. doi:10.1016/S0022-460X(03)00378-X.
- [17] A. Khorram, F. Bakhtiari-Nejad, and M. Rezaeian. Comparison studies between two wavelet based crack detection methods of a beam subjected to a moving load. *International Journal of Engineering Science*, 51:204–215, 2012. doi:10.1016/j.ijengsci.2011.10.001.
- [18] N. Mostafa, D. Di Maio, R. Loendersloot, and T. Tinga. Extracting the time-dependent resonances of a vehicle–bridge interacting system by wavelet synchrosqueezed transform. *Structural Control and Health Monitoring*, 28(12):e2833, 2021. doi:10.1002/stc.2833.
- [19] J. J. Moughty and J. R. Casas. A state of the art review of modal-based damage detection in bridges: Development, challenges, and solutions. *Applied Sciences*, 7(5):1–24, 2017. doi:10.3390/app7050510.
- [20] P. Cornwell, C. R. Farrar, S. W. Doebling, and H. Sohn. Environmental variability of modal properties. *Experimental Techniques*, 23(6):45–48, 1999. doi:10.1111/j.1747-1567.1999.tb01320.x.
- [21] Y. Xia, H. Hao, G. Zanardo, and A. Deeks. Long term vibration monitoring of an rc slab: Temperature and humidity effect. *Engineering Structures*, 28(3):441–452, 2006. doi:10.1016/j.engstruct.2005.09.001.
- [22] Y. L. Xu, B. Chen, C. L. Ng, K. Y. Wong, and W. Y. Chan. Monitoring temperature effect on a long suspension bridge. *Structural Control and Health Monitoring*, 17(6):632–653, 2010. doi:10.1002/stc.340.
- [23] J. Chen. Application of empirical mode decomposition in structural health monitoring: Some experience. *Advances in Adaptive Data Analysis*, 1(4):601–621, 2009. doi:10.1142/S1793536909000321.
- [24] D. Hester and A. González. A wavelet-based damage detection algorithm based on bridge acceleration response to a vehicle. *Mechanical Systems and Signal Processing*, 28:145–166, 2012. doi:10.1016/j.ymsp.2011.06.007.
- [25] A. González and D. Hester. An investigation into the acceleration response of a damaged beam-type structure to a moving force. *Journal of Sound and Vibration*, 332(13):3201–3217, 2013. doi:10.1016/j.jsv.2013.01.024.
- [26] Z. Yu, H. Xia, J. M. Goicolea, and C. Xia. Bridge damage identification from moving load induced deflection based on wavelet transform and lipschitz exponent. *International Journal of Structural Stability and Dynamics*, 16(5):e1550003, 2016. doi:10.1142/S0219455415500030.
- [27] W. Zhang, J. Li, H. Hao, and H. Ma. Damage detection in bridge structures under moving loads with phase trajectory change of multi-type vibration measurements. *Mechanical Systems and Signal Processing*, 87:410–425, 2016. doi:10.1016/j.ymsp.2016.10.035.
- [28] M. I. Friswell. Damage identification using inverse methods. *Philosophical Transactions of the Royal Society A: Mathematical, Physical and Engineering Sciences*, 365(1851):393–410, 2007. doi:10.1098/rsta.2006.1930.

- [29] L. Sun, Z. Shang, Y. Xia, S. Bhowmick, and S. Nagarajaiah. Review of bridge structural health monitoring aided by big data and artificial intelligence: From condition assessment to damage detection. *Journal of Structural Engineering (United States)*, 146(5), 2020. doi:10.1061/(ASCE)ST.1943-541X.0002535.
- [30] Q. L. Cai, Z. W. Chen, S. Zhu, and L. Y. Mo. On damage detection of beam structures using multiple types of influence lines. *Structures*, 42:449–465, 2022. doi:10.1016/j.istruc.2022.06.022.
- [31] M. Link and M. Weiland. Damage identification by multi-model updating in the modal and in the time domain. *Mechanical Systems and Signal Processing*, 23(6):1734–1746, 2009. doi:10.1016/j.ymsp.2008.11.009.
- [32] Z. Chen, S. Weng, H. Yu, J. Li, H. Zhu, Y. Yan, and L. Wu. Bayesian-based method for the simultaneous identification of structural damage and moving force. *Mechanical Systems and Signal Processing*, 185:e109742, 2023. doi:10.1016/j.ymsp.2022.109742.
- [33] K. Liu, G. De Roeck, and G. Lombaert. The effect of dynamic train-bridge interaction on the bridge response during a train passage. *Journal of Sound and Vibration*, 325(1-2):240–251, 2009. doi:10.1016/j.jsv.2009.03.021.
- [34] M. Majka and M. Hartnett. Effects of speed, load and damping on the dynamic response of railway bridges and vehicles. *Computers and Structures*, 86(6):556–572, 2008. doi:10.1016/j.compstruc.2007.05.002.
- [35] D. Cantero, T. Arvidsson, E. O'Brien, and R. Karoumi. Train-track-bridge modelling and review of parameters. *Structure and Infrastructure Engineering*, 12(9):1051–1064, 2016. doi:10.1080/15732479.2015.1076854.
- [36] D. Thompson. *Railway Noise and Vibration: Mechanisms, Modelling and Means of Control*. Elsevier, 2009.
- [37] F. Huseynov, C. Kim, E. J. O'Brien, J. M. W. Brownjohn, D. Hester, and K. C. Chang. Bridge damage detection using rotation measurements – experimental validation. *Mechanical Systems and Signal Processing*, 135:e106380, 2020. doi:10.1016/j.ymsp.2019.106380.
- [38] Y. Zhang, H. Zhao, and S. T. Lie. Estimation of mode shapes of beam-like structures by a moving lumped mass. *Engineering Structures*, 180:654–668, 2019. doi:10.1016/j.engstruct.2018.11.074.
- [39] Z. W. Chen, Q. L. Cai, and S. Zhu. Damage quantification of beam structures using deflection influence lines. *Structural Control and Health Monitoring*, 25(11):e2242, 2018. doi:10.1002/stc.2242.
- [40] N. B. Wang, L. X. He, W. X. Ren, and T. L. Huang. Extraction of influence line through a fitting method from bridge dynamic response induced by a passing vehicle. *Engineering Structures*, 151:648–664, 2017. doi:10.1016/j.engstruct.2017.06.067.
- [41] P. J. McGetrick and C. W. Kim. A parametric study of a drive by bridge inspection system based on the morlet wavelet. *Key Engineering Materials*, 569-570:262–269, 2013. doi:10.4028/www.scientific.net/KEM.569-570.262.
- [42] Y. Zhang, S. T. Lie, and Z. Xiang. Damage detection method based on operating deflection shape curvature extracted from dynamic response of a passing vehicle. *Mechanical Systems and Signal Processing*, 35(1-2):238–254, 2013. doi:10.1016/j.ymsp.2012.10.002.

- [43] F. Cerda, J. Garrett, J. Bielak, J. Barrera, Z. Zhuang, S. Chen, M. McCann, J. Kovačević, and P. Rizzo. Indirect structural health monitoring in bridges: Scale experiments. In *Bridge Maintenance, Safety, Management, Resilience and Sustainability - Proceedings of the Sixth International Conference on Bridge Maintenance, Safety and Management*, pages 346–353, 2012.
- [44] V. Pakrashi, A. O’Connor, and B. Basu. A bridge-vehicle interaction based experimental investigation of damage evolution. *Structural Health Monitoring*, 9(4):285–296, 2010. doi:10.1177/1475921709352147.
- [45] S. Marchesiello, S. Bedaoui, L. Garibaldi, and P. Argoul. Time-dependent identification of a bridge-like structure with crossing loads. *Mechanical Systems and Signal Processing*, 23(6):2019–2028, 2009. doi:10.1016/j.ymssp.2009.01.010.
- [46] X. Q. Zhu and S. S. Law. Wavelet-based crack identification of bridge beam from operational deflection time history. *International Journal of Solids and Structures*, 43(7-8):2299–2317, 2006. doi:10.1016/j.ijsolstr.2005.07.024.
- [47] I. Oskam, P. Souren, I. Berg, K. Cowan, and L. Hoiting. *Ontwerpen van technische innovaties: door onderzoek, creatief denken en samenwerken*. Noordhoff Uitgevers, 2 edition, 2017.
- [48] A. Jha. *Dynamic Testing of Structures Using Scale Models*. Dept. of Mechanical and Industrial Engineering. MSc thesis, Concordia University, Montreal, Quebec, Canada, 2005.
- [49] K. Luo and X. Lei. A study of modeling experiments of the vibration behavior of elevated railway box girder. *Journal of Vibration and Control*, 25(5):963–1130, 2019. doi:10.1016/j.engstruct.2019.109539.
- [50] E. Buckingham. On physically similar systems; illustrations of the use of dimensional equations. *Physical Review*, 4(4):354–376, 1914. doi:10.1103/PhysRev.4.345.
- [51] C. Bowe. *Dynamic Interaction of Trains and Railway Bridges Using Wheel Rail Contact Method*. Dept. of Civil Engineering. PhD dissertation, University of Galway, Galway, Ireland, 2009.
- [52] Y. Lu, L. Mao, and P. Woodward. Frequency characteristics of railway bridge response to moving trains with consideration of train mass. *Engineering Structures*, 42:9–22, 2012. doi:10.1016/j.engstruct.2012.04.007.
- [53] Dassault Systèmes. *Abaqus 6.11 Analysis User’s Manual Volume II: Analysis*. Dassault Systèmes Simulia Corp., United States, 2011.
- [54] L. Connolly, L. Prendergast, N. Mostafa, and R. Loendersloot. Report on assessment of bridges. Technical Report D2.2 EU H2020 DESTinationRail, Project Reference: 636285, H2020-MG 2014-2015, 2017.
- [55] EN 1991-2:2003. *Eurocode 1: Actions on structures - Part 2: Traffic loads on bridges*, Brussels, 2003. EN, CEN.
- [56] J. M. Biggs. *Introduction to Structural Dynamics*. McGraw-Hill, New York, 1964.

Appendices

[Appendix A Boyne Viaduct](#)

[Appendix B Train configurations](#)

[Appendix C Similarity analysis](#)

[Appendix D Equations of motion: train-bridge problem](#)

[Appendix E Development of the experimental setup](#)

[Appendix F Concepts and assessment](#)

[Appendix G Design details](#)

[Appendix H Validation experimental setup](#)

[Appendix I Settings experiments](#)

[Appendix J Numerical model development](#)

[Appendix K Simulations locomotive](#)

[Appendix L Variation study: Velocity](#)

[Appendix M Simulations DMU](#)

[Appendix N Experimental results](#)

[Appendix O Simulations experimental setup](#)

A | Boyne Viaduct

In the early 1930s, the Boyne Viaduct was constructed in Drogheda, County Louth, Ireland. A representation of this Viaduct can be seen in fig. A.1, while a schematic representation is provided in fig. A.2.



Figure A.1: Boyne Viaduct in Drogheda, County Louth, Ireland [54].

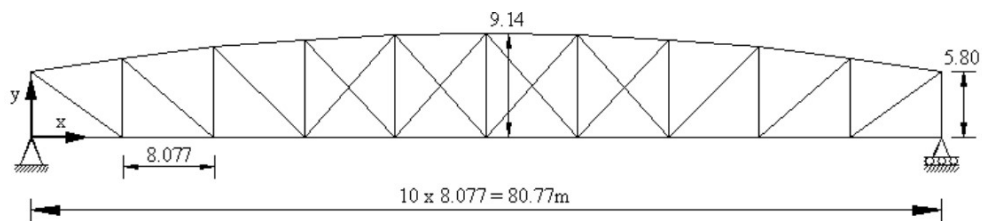


Figure A.2: Schematic representation of the Boyne Viaduct [51].

The quantities related to the Boyne Viaduct are presented in table A.1. Bowe [51] developed a model for the Boyne Viaduct, and based on this model, various calculations were performed to determine its quantities. A static analysis was conducted to compute the mass per unit length, which was then used to calculate the area moment of inertia. This area moment of inertia is derived from the static deflection of the Viaduct, resulting in an averaged value along its entire length. Subsequently, the averaged cross-sectional area is determined by considering its mass per unit length and the density of the Viaduct's material.

The natural frequencies exhibit a range, with their values depending on the calculation method employed. The minimum value is obtained through a 3D simulation, while the maximum value is determined analytically, assuming the Viaduct behaves as a simply supported beam. These natural frequencies fall within the limits specified by Eurocode EN 991-2 [55], with a lower bound of 1.752 Hz and an upper bound of 3.548 Hz. For more comprehensive information on dimensions, properties, as well as static and modal analysis, readers can refer to Bowe [51].

Table A.1: *Properties of the Boyne Viaduct [51].*

E_{bridge} N/m²	I_{bridge} m⁴	L_{bridge} m	ρ_{bridge} kg/m³	A_{bridge} m²	M_{bridge} kg	$f_{1,\text{bridge}}$ ¹ Hz
$205 \cdot 10^9$	1.220	80.77	7850	0.15	95107.03	3.12-3.51

¹ Natural frequency in the vertical direction.

B | Train configurations

This appendix presents information on two distinct train configurations traversing the Boyne Viaduct: 1) a locomotive class 201 with six axles, and 2) a diesel multiple unit (DMU) carriage train with four axles. This appendix also includes the matrix definitions for both configurations.

A detailed 2D representation of the train configurations are depicted in fig. B.1.

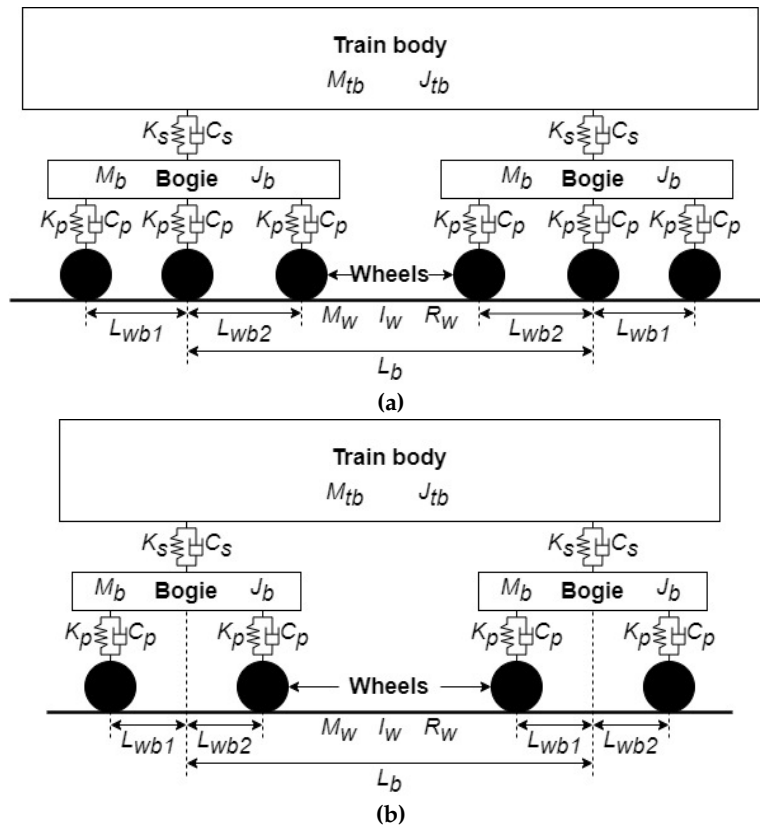


Figure B.1: Schematic representation of (a) the 201 Class locomotive or (b) the diesel multiple unit (DMU) carriage train.

The matrix definitions for the train configurations are derived from the equations of motion provided in appendix D. The mass matrix for both configurations is defined as follows:

$$M = \text{diag} [M_{tb} \quad J_{tb} \quad M_b \quad J_b \quad M_b \quad J_b] \quad (\text{B.1})$$

C | Similarity analysis

This appendix provides details regarding the implementation of the similarity analysis for scaling the Boyne Viaduct to a laboratory-scale prototype. This appendix includes details related to the use of a relaxed model.

C.1 Implementation of the complete similarity

The theoretical basis for the similarity analysis is outlined in section 2.2, where a simplified problem is tackled. The experimental setup follows a four-step process, outlined as follows:

Step 1: Identify the physical system to be analysed

The problem is depicted in fig. 3.2, which depicts the train variant. The additional two variants (referred to as the bogie variant and half-train variant, as depicted in fig. 1.2) serve as simplified representations of these versions. Consequently, a reduced set of quantities is employed for these variants. Thus, the most elaborate version is utilised for the similarity analysis to encompass all relevant quantities. The equations of motion for both the bridge and the train are detailed in appendix D.

Step 2: Identify n relevant independent quantities and their k basic dimensions

The aim of this thesis is to experimentally validate Instantaneous Frequencies (IFs) against numerical counterparts. Since IFs are independent of gravity, gravity is not considered a relevant physical quantity. There are 20 physical quantities ($n = 20$) and three fundamental dimensions ($k = 3$), as indicated in table C.1. Consequently, there are $i = 20 - 3 = 17$ dimensionless products.

Irrelevant physical quantities like shear modulus, Poisson's ratio, and other material properties are omitted from this table. These quantities are also omitted from the equations of motion due to the assumptions and limitations in their derivation process. These decisions are based on the understanding that these quantities have minimal impact on the final results and are hence disregarded. For instance, although material damping should be included in the analysis, it is often omitted due to its negligible influence on the results, supported by previous research [56]. This selective consideration of only those quantities present in the equation(s) of motion is known as the characteristic equation approach [48].

It is important to highlight that certain physical quantities share similar characteristics, creating dependencies. For instance, both the mass of the bogies and the mass of the wheels share the same fundamental dimension. Consequently, these quantities are scaled in a similar manner, leading to comparable dimensionless products. Repetitive physical quantities can be omitted to reduce the number of dimensionless products. This omission does not impact the results but serves as an effective method to reduce workload. In this simplification method, both the length of the bridge and a single length for the train are considered. This approach allows the bridge's length to be utilised for scaling in dimensionless analysis, while a single length for the train is employed to scale these quantities. Consequently, the total number of physical quantities can be reduced to 10 ($n = 10$), yielding $i = 10 - 3 = 7$ dimensionless products.

Step 3: Choose n dimensionally independent quantities to derive i dimensionless products

Initially, the quantities E_{bridge} , ρ_{bridge} , and L_{bridge} are arbitrarily selected for the first dimensionless product, primarily due to their shared dimensions. Alternative combinations are also viable, provided they satisfy the criteria of a non-zero determinant, non-repeating quantities, inclusion of all fundamental dimensions at least once, and

Table C.1: Physical quantities and their fundamental dimensions occurring in the experimental setup.

Physical quantity	Symbol	Unit	Dimension ¹
Young's modulus of Elasticity bridge	E_{bridge}	Nm^{-2}	$ML^{-1}T^{-2}$
Area moment of inertia bridge	I_{bridge}	m^4	L^4
Length bridge	L_{bridge}	m	L
Density of the bridge material	ρ_{bridge}	kgm^{-3}	ML^{-3}
Cross-sectional area bridge	A_{bridge}	m^2	L^2
The train's body mass	M_{tb}	kg	M
The train's body mass moment of inertia	J_{tb}	kgm^2	ML^2
The bogie's mass	M_{b}	kg	M
The bogie's mass moment of inertia	J_{b}	kgm^2	ML^2
The wheel's mass	M_{w}	kg	M
The wheel's mass moment of inertia	J_{w}	kgm^2	ML^2
Damping of primary suspension	C_{p}	Nsm^{-1}	MT^{-1}
Stiffness of primary suspension	K_{p}	Nm^{-1}	MT^{-2}
Damping of secondary suspension	C_{s}	Nsm^{-1}	MT^{-1}
Stiffness of secondary suspension	K_{s}	Nm^{-1}	MT^{-2}
The wheel's radius	R_{w}	m	L
Distance: wheel 1 and wheel 2	L_{wb1}	m	L
Distance: wheel 2 and wheel 3	L_{wb2}	m	L
Distance: the secondary suspensions	L_{b}	m	L
The train's position along the bridge	x_{train}	m	L

¹ M : Mass, L : Length, T : Time

independence of the chosen quantities. A non-zero determinant is confirmed, as shown in eq. (2.1).

Having established the suitability of these three quantities (E_{bridge} , ρ_{bridge} and L_{bridge}), the dimensionless analysis can be performed on the remaining physical quantities. To obtain the dimensionless products, a matrix-vector formulation is created and subsequently solved. The same procedure as described in section 2.2 is applied to determine the remaining quantities, resulting in the seven dimensionless parameters outlined in table C.2.

Table C.2: Dimensionless products for the train-bridge problem.

Dimensionless products		
$\Pi_1 = I_{\text{bridge}} \cdot \frac{1}{L_{\text{bridge}}^4}$	$\Pi_2 = A_{\text{bridge}} \cdot \frac{1}{L_{\text{bridge}}^2}$	$\Pi_3 = M_i \cdot \frac{1}{\rho_{\text{bridge}} L_{\text{bridge}}^3}$
$\Pi_4 = C_j \cdot \frac{1}{\sqrt{E_{\text{bridge}} \rho_{\text{bridge}} L_{\text{bridge}}^2}}$	$\Pi_5 = K_j \cdot \frac{1}{E_{\text{bridge}} \rho_{\text{bridge}}}$	$\Pi_6 = J_i \cdot \frac{1}{\rho_{\text{bridge}} L_{\text{bridge}}^5}$
$\Pi_7 = L_k \cdot \frac{1}{L_{\text{bridge}}}$		

i refers to tb, b or w

j refers to p or s

k refers to b, wb1, wb2 or r

Step 4: Solve the i remaining prototype quantities based on i dimensionless products, n model quantities and k prototype quantities (self-selected)

Three self-selected prototype quantities are required for the similarity analysis, where E_{bridge} , ρ_{bridge} , and L_{bridge} have been carefully chosen. The selection of steel for the prototype material in the experimental setup is based on its availability in the required thickness, good processability, and low cost. Further details about this choice

are elaborated in appendix G.1. It is important to note that the elastic modulus and density of a material are linked properties; thus, these values cannot be arbitrarily chosen to represent an available material.

The length of the bridge (L_{bridge}) is determined by the placement of the experimental setup in the Dynamics Lab at the University of Twente. The overall setup length, comprising entrance, center, and leaving sections, is dependent upon the available space in the Dynamics Lab. For the similarity analysis, only the length of the central part is considered, with the entrance and leaving lengths being combined with this central length. The choice of the central part's length holds significance, as it impacts other length scales within the problem, such as the wheelbase length. Assuming a very small central part would present challenges in designing the suspension system for the bogie. Conversely, an excessively long central part would be incompatible with the space available. It is assumed that a central part length of 2 m for the bridge, resulting in a minimum wheelbase of 40 mm, will provide adequate space for designing the suspension system while fitting within the lab's constraints.

The input for the similarity analysis includes all model quantities, as stated by Bowe [51], the dimensionless products listed in table C.2, and three self-selected prototype quantities. The results of the similarity analysis, depicted in table C.3 and highlighted in gray, consist of the prototype quantities, excluding the self-selected ones. The design of the experimental setup is based on these prototype quantities.

Table C.3: Input and output values, denoted by gray-filled cells, of the similarity analysis with prototype values corresponding to the experimental setup.

Quantity	Unit	Dimension ¹	Model	Prototype
E_{bridge}	Nm ⁻²	$ML^{-1}T^{-2}$	$2.050 \cdot 10^{11}$	$2.050 \cdot 10^{11}$
I_{bridge}	m ⁴	L^4	1.220	$4.586 \cdot 10^{-7}$
L_{bridge}	m	L	$8.077 \cdot 10^1$	2.000
ρ_{bridge}	kgm ⁻³	ML^{-3}	$7.850 \cdot 10^3$	$7.850 \cdot 10^3$
A_{bridge}	m ²	L^2	$1.500 \cdot 10^{-1}$	$9.197 \cdot 10^{-5}$
M_{tb}	kg	M	$6.448 \cdot 10^4$	$9.780 \cdot 10^{-1}$
J_{tb}	kgm ²	ML^2	$2.002 \cdot 10^6$	$1.864 \cdot 10^{-2}$
M_{b}	kg	M	$1.018 \cdot 10^4$	$1.546 \cdot 10^{-1}$
J_{b}	kgm ²	ML^2	$1.155 \cdot 10^4$	$1.075 \cdot 10^{-4}$
M_{w}	kg	M	$4.520 \cdot 10^3$	$6.862 \cdot 10^{-2}$
J_{w}	kgm ²	ML^2	$4.520 \cdot 10^3$	$4.208 \cdot 10^{-5}$
C_{p}	Nsm ⁻¹	MT^{-1}	$4.000 \cdot 10^3$	2.453
K_{p}	Nm ⁻¹	MT^{-2}	$1.470 \cdot 10^6$	$3.640 \cdot 10^4$
C_{s}	Nsm ⁻¹	MT^{-1}	$2.0000 \cdot 10^4$	$1.226 \cdot 10^1$
K_{s}	Nm ⁻¹	MT^{-2}	$6.300 \cdot 10^5$	$1.560 \cdot 10^4$
R_{w}	m	L	$5.080 \cdot 10^{-1}$	$1.258 \cdot 10^{-2}$
L_{wb1}	m	L	1.689	$4.182 \cdot 10^{-2}$
L_{wb2}	m	L	2.019	$5.000 \cdot 10^{-2}$
L_{b}	m	L	$1.341 \cdot 10^1$	$3.320 \cdot 10^{-1}$

¹ M: Mass, L: Length, T: Time

C.2 Relaxation of the similarity analysis

The implementation outlined in the preceding section refers to a state of complete similarity between the prototype and model. Although, complete similarity is not mandatory for obtaining a valid result; hence, a relaxed model suffices.

To simplify the system, it is often assumed that damping within a system can be ne-

glected due to its minimal impact on the natural frequency. However, capturing this influence in a multiple degree of freedom system, such as a train, is more complex. To address this, a variation study is conducted, exploring the effect of damping coefficients. In this study, the system's natural frequency is calculated while varying the damping coefficient from zero to the value determined through the similarity analysis in table C.3. Both primary and secondary suspensions are varied simultaneously as they are likely to be made from the same material. The matrix definitions provided in appendix B are utilised in these calculations. The MATLAB software is employed for this variation study, using the maximum damping values from the similarity analysis since it is unlikely that a damper with a higher coefficient would be used in practical applications.

The results of this study, depicted in fig. C.1, indicate a significant decrease in natural frequency in general. However, the vertical axis shows that the change in natural frequency is relatively small. Specifically, the difference between damped and undamped natural frequencies for the body is 0.2%, and for the bogie, it is 0.26%. These percentages are minimal, suggesting that even a slight variation in damping coefficient results in only minor changes in natural frequency. Therefore, a relaxed model concerning the damping coefficient is adequate.

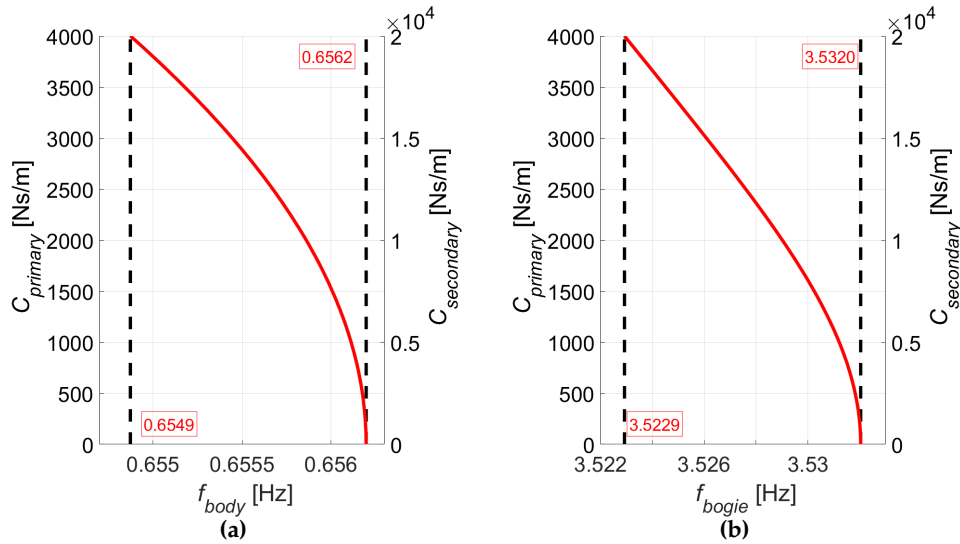


Figure C.1: Effect of varying the primary and secondary damping coefficients on the frequency component of (a) the body or (b) the bogie.

A comparable variation study is conducted using Abaqus to examine the impact of inertia terms on the bouncing natural frequency. Abaqus is employed for visualising the modes, such as the bouncing motion of both the train body and the bogie. During this study, the inertia terms for both the train body and the bogie are simultaneously adjusted, and the results indicate that the frequencies remain consistent. Consequently, it is evident that deviating from the initially obtained inertia terms can accelerate the design phase while still producing valid results.

D | Equations of motion: train-bridge problem

This appendix provides the equations of motion that govern the train-bridge problem. These equations are categorised into those concerning the bridge and train, including their interaction. A representation of the problem is depicted in fig. D.1, encompassing all relevant quantities within the problem.

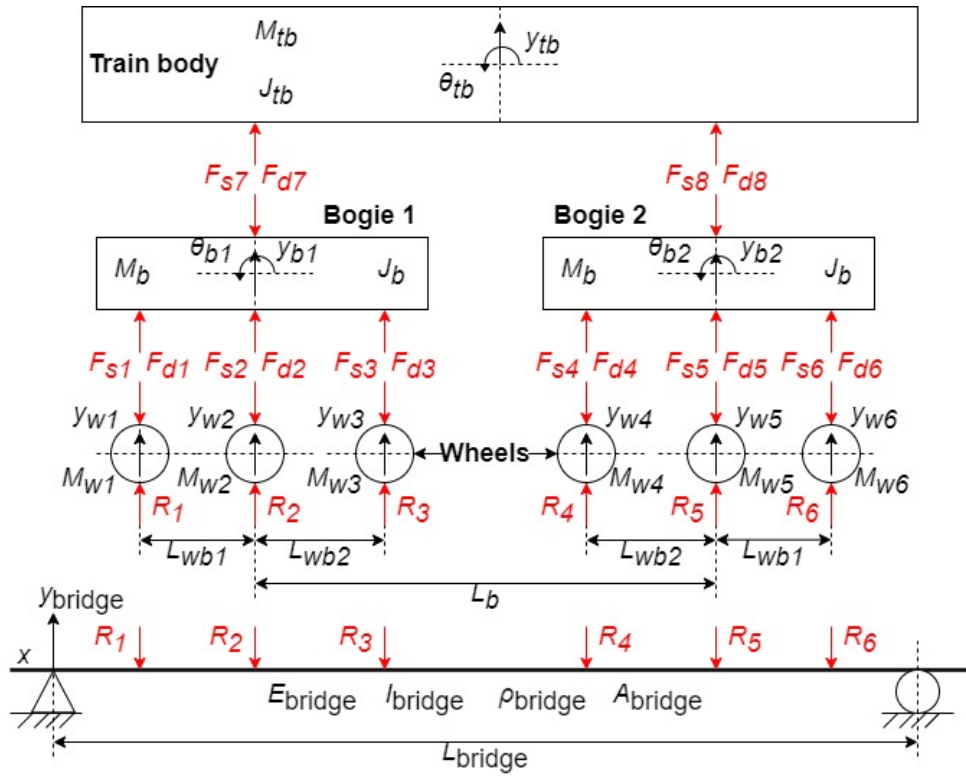


Figure D.1: Representation for obtaining the equations of motion for the problem.

The bridge's equation of motion in traverse direction, neglecting damping as discussed in appendix C, is expressed as follows:

$$\rho A \frac{\partial^2 y_{bridge}(x, t)}{\partial t^2} + EI \frac{\partial^4 y_{bridge}(x, t)}{\partial x^4} = - \sum_{i=1}^6 R_i(t) \delta(x - x_{train}) \quad (D.1)$$

This equation is predicated on the assumption that the beam is simply supported with pinned and roller support. Here, R represents the reaction force between the bridge and wheel. Additionally, the train's location is denoted by x_{train} , which is typically represented as $v_{train}t$.

The spring forces, as depicted in fig. D.1, are expressed by

$$F_{s1} = K_p(y_{w1} - y_{b1} + \theta_{b1}L_{wb1}) \quad (D.2a)$$

$$F_{s2} = K_p(y_{w2} - y_{b1}) \quad (D.2b)$$

$$F_{s3} = K_p(y_{w3} - y_{b1} - \theta_{b1}L_{wb2}) \quad (D.2c)$$

$$F_{s4} = K_p(y_{w4} - y_{b2} + \theta_{b2}L_{wb2}) \quad (D.2d)$$

$$F_{s5} = K_p(y_{w5} - y_{b2}) \quad (D.2e)$$

$$F_{s6} = K_p(y_{w6} - y_{b2} - \theta_{b2}L_{wb1}) \quad (D.2f)$$

$$F_{s7} = K_s(y_{b1} - y_{tb} + \frac{1}{2}\theta_{tb}L_b) \quad (D.2g)$$

$$F_{s8} = K_s(y_{b2} - y_{tb} - \frac{1}{2}\theta_{tb}L_b) \quad (D.2h)$$

The damping forces, as depicted in fig. D.1, are expressed by

$$F_{d1} = C_p(\dot{y}_{w1} - \dot{y}_{b1} + \dot{\theta}_{b1}L_{wb1}) \quad (D.3a)$$

$$F_{d2} = C_p(\dot{y}_{w2} - \dot{y}_{b1}) \quad (D.3b)$$

$$F_{d3} = C_p(\dot{y}_{w3} - \dot{y}_{b1} - \dot{\theta}_{b1}L_{wb2}) \quad (D.3c)$$

$$F_{d4} = C_p(\dot{y}_{w4} - \dot{y}_{b2} + \dot{\theta}_{b2}L_{wb2}) \quad (D.3d)$$

$$F_{d5} = C_p(\dot{y}_{w5} - \dot{y}_{b2}) \quad (D.3e)$$

$$F_{d6} = C_p(\dot{y}_{w6} - \dot{y}_{bogie2} - \dot{\theta}_{b2}L_{wb1}) \quad (D.3f)$$

$$F_{d7} = C_s(\dot{y}_{b1} - \dot{y}_{tb} + \frac{1}{2}\dot{\theta}_{tb}L_b) \quad (D.3g)$$

$$F_{d8} = C_s(\dot{y}_{b2} - \dot{y}_{tb} - \frac{1}{2}\dot{\theta}_{tb}L_b) \quad (D.3h)$$

The train's equations of motion are given by

$$M_{tb}\ddot{y}_{tb} = F_{s7} + F_{s8} + F_{d7} + F_{d8} - M_{tb}g \quad (D.4a)$$

$$J_{tb}\ddot{\theta}_{tb} = \frac{1}{2}L_b(F_{s8} + F_{d8}) - \frac{1}{2}L_b(F_{s7} + F_{d7}) \quad (D.4b)$$

$$M_{b1}\ddot{y}_{b1} = F_{s1} + F_{s2} + F_{s3} - F_{s7} + F_{d1} + F_{d2} + F_{d3} - F_{d7} - M_{b1}g \quad (D.4c)$$

$$J_{b1}\ddot{\theta}_{b1} = \frac{1}{2}L_{wb2}(F_{s3} + F_{d3}) - \frac{1}{2}L_{wb1}(F_{s1} + F_{d1}) \quad (D.4d)$$

$$M_{b2}\ddot{y}_{b2} = F_{s4} + F_{s5} + F_{s6} - F_{s8} + F_{d4} + F_{d5} + F_{d6} - F_{d8} - M_{b2}g \quad (D.4e)$$

$$J_{b2}\ddot{\theta}_{b2} = \frac{1}{2}L_{wb1}(F_{s6} + F_{d6}) - \frac{1}{2}L_{wb2}(F_{s4} + F_{d4}) \quad (D.4f)$$

$$M_{w1}\ddot{y}_{w1} = R_1 - F_{s1} - F_{d1} - M_{w1}g \quad (D.4g)$$

$$M_{w2}\ddot{y}_{w2} = R_2 - F_{s2} - F_{d2} - M_{w2}g \quad (D.4h)$$

$$M_{w3}\ddot{y}_{w3} = R_3 - F_{s3} - F_{d3} - M_{w3}g \quad (D.4i)$$

$$M_{w4}\ddot{y}_{w4} = R_4 - F_{s4} - F_{d4} - M_{w4}g \quad (D.4j)$$

$$M_{w5}\ddot{y}_{w5} = R_5 - F_{s5} - F_{d5} - M_{w5}g \quad (D.4k)$$

$$M_{w6}\ddot{y}_{w6} = R_6 - F_{s6} - F_{d6} - M_{w6}g \quad (D.4l)$$

$$(D.4m)$$

where the first two equations represent the vertical bouncing and pitching (in-plane rotation) of the train body. The third and fourth equations denote the vertical bouncing and pitching motion of the first bogie. The fifth and sixth equations correspond to the vertical bouncing and pitching motion of the second bogie. The remaining six equations illustrate the bouncing motion of the six wheels.

E | Development of the experimental setup

This appendix provides additional information concerning the development of the experimental setup, where this development is inspired by Oskam et al. [47]. This appendix encompasses the function analysis, design requirements and success criteria for the experimental design.

E.1 Function analysis

The main function and sub functions of the setup have been identified and are depicted in fig. E.1. A similar component exhibits similar functionality between parts. For example, both the primary and secondary suspension systems mimic dynamic behavior. A module is a combination of functions integrated into a single component. For example, the rails serve the purpose of guiding the train, transmitting forces, and stabilising the train, thus integrating multiple functions into a single module. In summary, the experimental setup must fulfil four sub functions: 1) mimicking of dynamic behaviour (suspension), 2) guidance, 3) movement of the train, and 4) fixation.

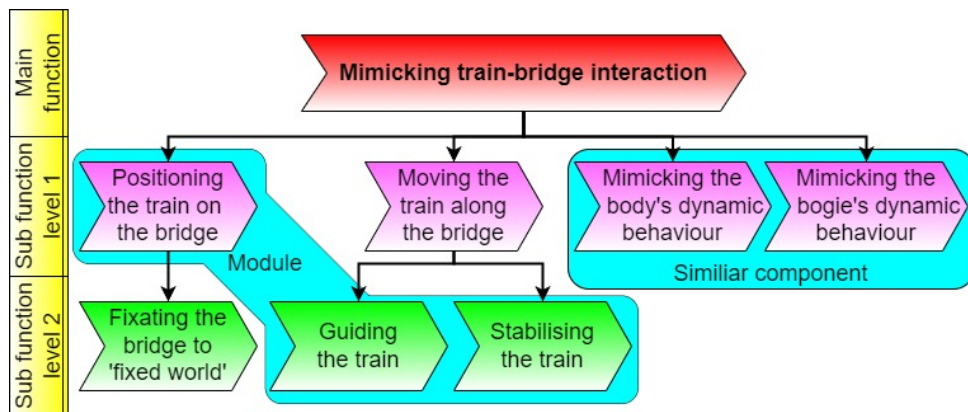


Figure E.1: Function tree regarding the design of the experimental setup.

E.2 Design requirements

The design requirements, also referred to as functional requirements, have been formulated based on chapter 1 and the function analysis. The most important design requirements are listed in table E.1, categorised into groups to improve clarity and comprehensibility.

E.3 Success criteria

The success criteria, also referred to as realisation requirements, are derived from the design requirements and will serve as the basis for determining the most suitable concept for conducting the experiments. These criteria encompass the following:

Table E.1: *Design requirements regarding design of the experimental setup.*

No.	Design requirements
	Group 1: Desing
1.1	The combined product must not exceed a length of 4 meters.
1.2	The suspension system can mimic the dynamic behaviour of both the train body and the train bogie.
1.3	The system must effectively keep the train on track and guide it across the bridge.
1.4	All variants are capable of traversing the bridge.
1.5	Measurement data should remain unaffected by vibrations from the surroundings and the motor.
	Group 2: Production
2.1	The assembly can be performed in-house.
	Group 3: Performance
3.1	Experiments can be conducted by single person.
3.2	The product should operate without impairment or malfunction during experiments.
3.3	The product can be employed for a long period of time.
	Group 4: Safety
4.1	The product is equipped to automatically decelerate upon reaching the end of the bridge section.
4.2	Safety for both the operator and bystanders is guaranteed.
4.3	The product design excludes any sharp corners.

- The product should occupy the least amount of space possible.
- The product should possess the utmost reliability.
- The product should comprise the most simplest design.
- The product should have the highest level of controllability.
- The product should be as robust as possible.
- The product should be as safe as possible.
- The product should be as straightforward to manufacture as feasible.
- The product should optimally meet the desired functionality.

F | Concepts and assessment

This appendix provides additional information concerning the process of concept generation and the assessment to determine the most suitable concept. This appendix encompasses a morphological chart, concept descriptions and the assessment of concepts against the design requirements and success criteria.

F.1 Morphological chart

This morphological chart, depicted in fig. F.1, presents multiple solutions for each function. Concepts are derived from these potential solutions, with each concept features a single suspension system for simplicity. The second suspension system is omitted as it does not provide additional information for determining the optimal concept. Additionally, the motor system and fixation mechanisms are not illustrated but are mentioned, as their functionality can be evaluated without representation.

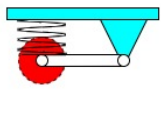
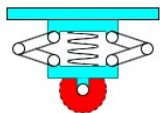
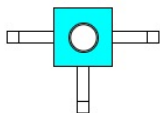
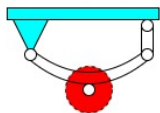
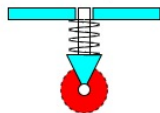
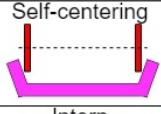
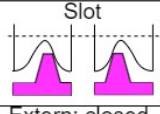
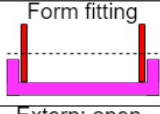
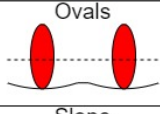
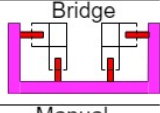
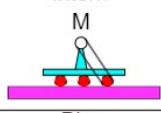
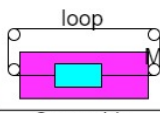
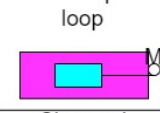
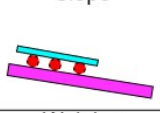
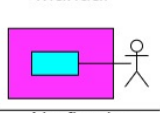
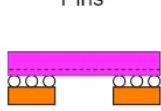
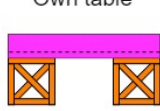
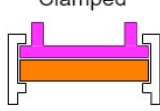
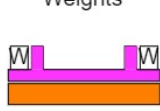
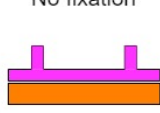
Functions	Solution 1	Solution 2	Solution 3	Solution 4	Solution 5
	Rotation arm	Double jack	Tripple jack	Leaf springs	Linear pin
1. Mimic dynamic behaviour					
2. Guiding the train	Self-centering	Slot	Form fitting	Ovals	Bridge
					
3. Moving the train (motor)	Intern M	Extern: closed-loop	Extern: open-loop	Slope	Manual
					
4. Fixating the bridge	Pins	Own table	Clamped	Weights	No fixation
					

Figure F.1: Morphological chart for the design of the experimental setup.

F.2 Concepts

The first concept mimics the dynamic behaviour by using a rotating arm, similar to a trailer suspension, as illustrated in fig. F.2. A spring, not depicted, encompasses the damper unit. Guidance relies on the self-centering effect of conically shaped train wheels, enabling point-to-surface contact. Off-center wheels are redirected toward the center due to the difference in horizontal forces. A motor in the bogie drives the axle, requiring adequate wheel-rail friction for motion. The bridge is secured to a plateau using pins.

The second concept's suspension system, illustrated in fig. F.3, is inspired by the design of a scissor jack. This concept features two opposing legs with the spring connected at their center. To ensure synchronised movement of both legs, a gear mechanism is integrated into the arms, ensuring strictly vertical motion. However,

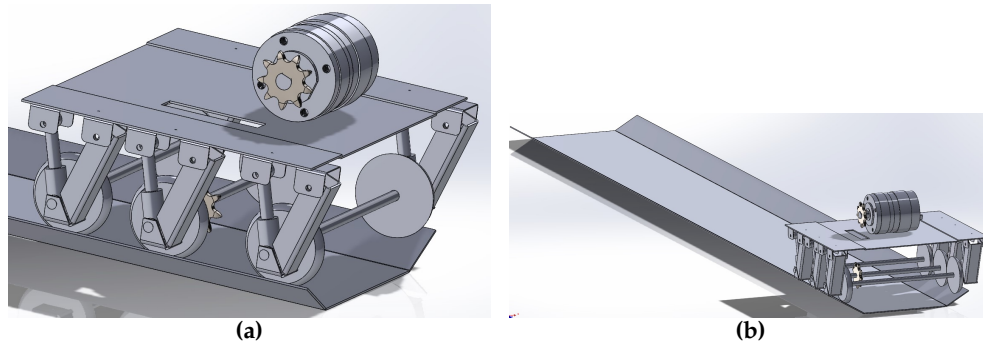


Figure F.2: Representation of concept 1 for (a) the bogie's design (b) the complete design.

it is worth noting that such gearing system often entail high forces, which may pose challenges for smaller components. Train guidance is achieved through slotted holes where the wheel makes contact with the side of the rails. A closed-loop motor system enables bidirectional movement of the train. The fixation system is custom-designed, providing design flexibility but also increasing the complexity of the concept.

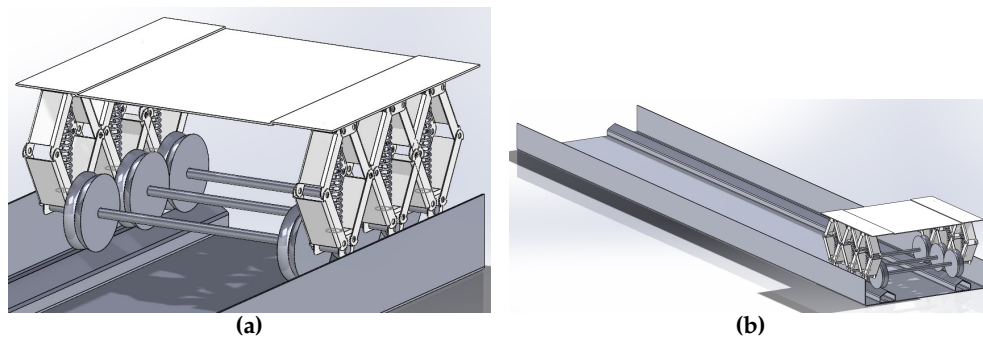


Figure F.3: Representation of concept 2 for (a) the bogie's design (b) the complete design.

Concept 3, as depicted in fig. F.4, closely resembles concept 2 in terms of mimicking dynamic behaviour. The difference lies an additional arm, eliminating the need for gearing on the arms, resulting in a more reliable design. However, this modification requires additional in-plane space, posing challenges in fitting the suspension system within the bogie. To guide the train across the bridge, this concept uses a form-fitting approach. A raised edge ensures that the train remains on the bridge, preventing derailment. The motor system is similar to concept 2, but without looping around, simplifying the design but reducing the functionality of the experimental setup. Fixation is achieved by clamping the bridge to the table, using a bar clamp. However, this introduces an additional constraint in the design process, requiring more space around the table for securing the bar clamp.

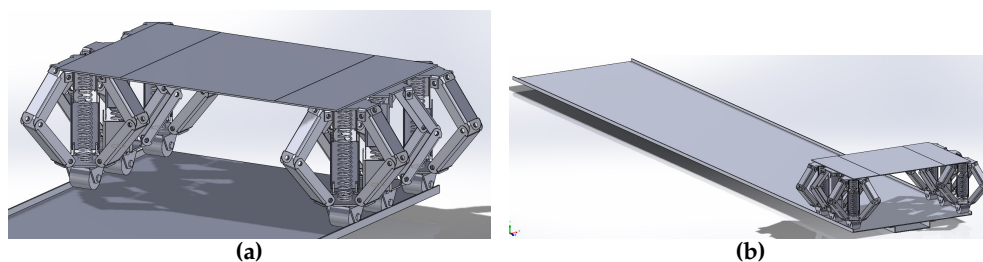


Figure F.4: Representation of concept 3 for (a) the bogie's design (b) the complete design.

Concept 4, illustrated in fig. F.5, employs leaf springs to mimic the dynamic behaviour of the train components. This concept offers the option to secure either both sides or just one side of the leaf springs, resulting in either purely vertical motion or both vertical and horizontal motion. The challenge lies in determining the appropriate stiffness coefficient for the leaf springs. Guidance is achieved through the use of oval-shaped wheels and rails with varying radii. The wheels have smaller radii than the rails, creating a self-centering effect when the wheels are positioned off-center. However, it is important to note that manufacturing such rails is more complex compared to producing bent parts. This concept relies on gravity to maintain the desired velocity, however, this approach lacks control over the setup and presents challenges in adjusting the train's velocity. Securing the bridge structure is achieved by adding extra weight.

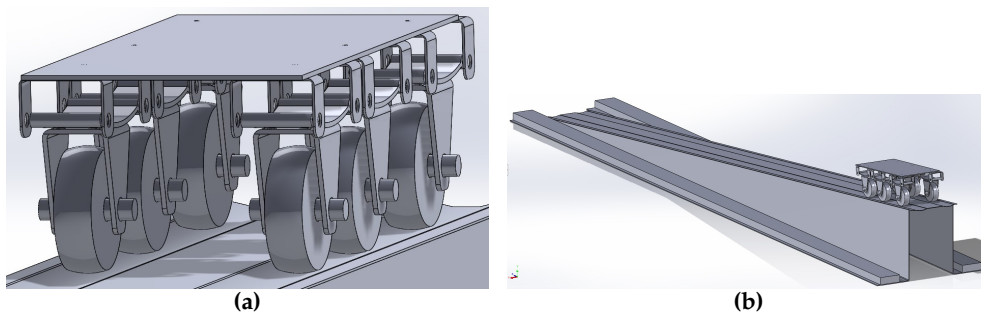


Figure F.5: Representation of concept 4 for (a) the bogie's design (b) the complete design.

The final concept mimics the dynamic behaviour using a linear pin system, as depicted in fig. F.6. This system incorporates a pin between the wheel and the bogie, allowing vertical movement. However, potential issues may arise if the pin becomes jammed in the holes due to rotation. To reduce this risk, the use of two contact points on the tube is proposed, increasing the contact area. If the bridge features a closed profile, enhancing stiffness and reducing weight, this design allows the train to be guided along the bridge itself, similar to a roller coaster. It is important to note that the middle section of the bridge structure typically has lower plate strength compared to nearby connections or bends. Contact between the wheels and bridge is likely to occur in the middle of the plate, potentially leading to plastic deformation if thin plates are used. This issue can be addressed by employing thicker plates, although proper scaling might pose challenges. In this concept, movement is manually operated, which could reduce system reliability and introduce difficulties during experiments. Additionally, the bridge is not secured to a table, potentially raising concerns related to reliability and safety.

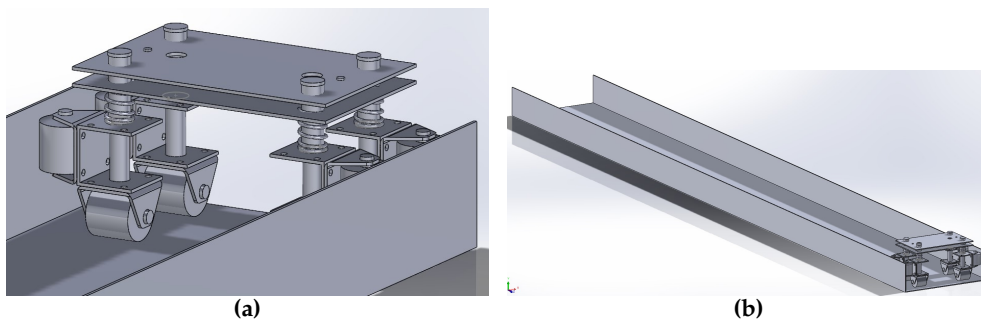


Figure F.6: Representation of concept 5 for (a) the bogie's design (b) the complete design.

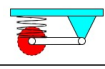
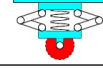
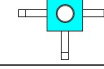
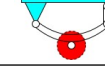
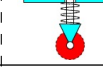
F.3 Concept assessment

To determine the most suitable concept, each concept must first undergo evaluation against the design requirements. Upon assessment, it becomes evident that all concepts align with these requirements. This alignment arises from the inherent nature of the problem (development of an experimental setup), which lacks a predefined strict requirement. As objectives like minimising cost or weight are not applicable in this context. Therefore, all concepts fulfil the requirements, and the selection of the most suitable concept depends on the success criteria.

Each success criterion is assigned a Weight Factor (WF) to denote its importance. Assessment is performed independently for each solution per function, allowing for potential combinations of solutions between concepts to achieve an optimal hybrid concept. The initial solution serves as the reference against which other solutions are compared, and the initial solution receives a final score of 0. This comparison determines whether a solution is superior (+), inferior (-), or similar (S). The highest score is obtained by subtracting the positives from the negatives, identifying the most suitable solution for that specific function.

The assessment for mimicking dynamic behaviour is presented in table F.1. It should be noted that all concepts are comparable in terms of manufacturing (utilising either bending plates or 3D printing), resulting in the same score for all. The conclusion drawn from this table is that the reference concept is the most favorable solution for this function, as all other solutions perform worse, indicated by their negative scores. The main drawback of the second solution is the anticipated reliability issues and increased complexity. The third solution, although more robust, is also more complex, space-consuming, and challenging to incorporate into the bogie. Tuning the leaf springs to achieve the desired stiffness coefficient is more challenging, and the use of linear pins carries the risk of becoming stuck, decreasing reliability.


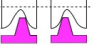

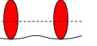
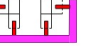
Table F.1: Assessment of mimicking the dynamic behaviour on the success criteria.

Success criteria	W F	Rotation arm 	Double jack 	Triple jack 	Leaf springs 	Linear pin 
Space	1		S	-	+	S
Reliability	3		-	S	S	-
Simplicity	3	R	-	-	-	S
Controllability	2	e	S	-	S	S
Robust	2	f	S	+	S	+
Safe	2	.	-	-	S	-
Manufacture	2		S	S	S	S
Functionality	3		+	+	S	S
		Σ^+	3	5	1	2
		Σ^-	-8	-8	-3	-5
		Total	-5	-3	-2	-3

The assessment of the guidance is depicted in table F.2. Among the various solutions, slots have been identified as the optimal choice for guidance. Incorporating an outer flange provides an additional safety feature in comparison to the self-centering approach. This solution enhances controllability and functionality while reducing the risk of derailment. In contrast, the form-fitting concept might be less secure in case of derailment. Oval-shaped wheels, although similar to the self-centering approach, introduce greater complexity in both design and manufacturing. Guiding the train onto the bridge offers higher levels of reliability and controllability compared to the

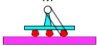


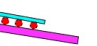
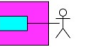
reference solution. However, a drawback of this approach is the potential for significant deformation if the point of contact is located in the middle of a thin plate, far from any reinforcement or bends.

Table F.2: Assessment of the guidance on the success criteria.

Success criteria	W F	Self-centering 	Slot 	Form fitting 	Ovals 	Bridge 
Space	1	R e f e r e n c e	S	S	S	-
Reliability	3		+	+	+	+
Simplicity	3		-	S	-	-
Controllability	2		+	-	+	+
Robust	2		S	S	-	-
Safe	2		+	-	+	+
Manufacture	2		S	S	-	+
Functionality	3		+	S	S	S
			Σ^+	10	3	7
		Σ^-	-3	-4	-7	-6
		Total	7	-1	0	3

The assessment for the motor system is presented in table F.3. The externally closed-loop motor system emerges as the optimal design. This choice offers advantages over the open-loop system due to its higher reliability and functionality, as it reduces potential issues that may arise during cable winding. The slope solution lacks control and is deemed considerably unsafe and unreliable. The manual system is not recommended due to its inconsistency and low functionality. The internal system could pose challenges related to friction and power application, potentially reducing reliability. Additionally, it is more complex to manufacture.

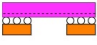
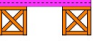



Table F.3: Assessment of the motor system on the success criteria.

Success criteria	W F	Intern 	Extern closed-loop 	Extern open-loop 	Slope 	Manual 
Space	1	R e f e r e n c e	-	S	+	S
Reliability	3		+	S	-	+
Simplicity	3		S	+	+	+
Controllability	2		S	-	-	-
Robust	2		S	S	S	-
Safe	2		S	S	-	-
Manufacture	2		+	+	+	+
Functionality	3		+	-	S	-
			Σ^+	8	5	6
		Σ^-	-1	-5	-7	-9
		Total	7	0	-1	-1

The assessment of the function's ability to secure the bridge structure is demonstrated in table F.4. The fourth solution, involving the addition of weights, receives the highest score. The main reason for not selecting the initial two options is their increased complexity and decreased functionality, resulting from additional space

restrictions in the Dynamics Lab. The third solution scores lower than the fourth due to challenges associated with fixing the bridge structure using clamps, as not all tables may be suitable for this purpose. The fifth solution receives a relatively low score as it relies on the own weight of the structure, making it less reliable for securing the setup and resulting in a lower level of safety.

Table F4: Assessment of the fixating of the bridge on the success criteria.

Success criteria	W F	Pins 	Own table 	Clamped 	Weights 	No fixation 
Space	1		-	+	+	+
Reliability	3		+	S	S	-
Simplicity	3	R e f i x e d	S	+	+	+
Controllability	2		S	-	S	S
Robust	2		+	S	S	-
Safe	2		S	S	S	-
Manufacture	2		S	S	+	+
Functionality	3		S	+	+	-
			Σ^+	5	6	9
		Σ^-	-1	0	0	-10
		Total	4	6	9	-4

Based on the design assessment, it is evident that the optimal design is a hybrid concept that combines solutions from different concepts. Specifically, dynamic behaviour is mimicked using a rotational arm, guidance is achieved through a slot, an external closed-loop motor system is employed, and additional weight is added for fixation. These integrated solutions form the new hybrid concept.

G | Design details

This appendix elaborates on the choices made during the finalisation of the design. The aim is to expand upon and refine the best concept chosen and finalise the design in preparation for manufacturing. The general choices regarding the design, production, materials, and their relation, are elaborated upon. Additionally, this appendix offers additional information regarding the subsystems is described, encompassing calculations, optimisations, and simulations.

G.1 Design, production and materials

The final design results from a series of decisions concerning design, production processes, and materials. The design adheres to relevant standards, including dimensioning according to ISO 129, geometric dimensioning and tolerances (GD&T) according to ISO 1101, and roughness according to ISO 1302. In general, tabs and slots are incorporated into the design to facilitate the positioning and assembly of multiple steel plates. Additionally, a clearance equal to half the sheet thickness is introduced to accommodate various parts and account for tolerances, especially during processes like bending.

Manufacturing can take place either at the University of Twente's workplace or through external companies. Important machines at the university include CNC laser cutting machines (equipped with fiber and CO₂ lasers), a CNC press brake, automated and manual sheet folding machines, a lathe, a milling machine, and standard machines. However, these machines have specific limitations. For instance, the press brake can handle parts up to 1200 mm in length, with a minimum leg length of 6 mm and a V-die length of 8 mm. The CO₂ laser cutting machine is suitable for materials like rubber, wood, or plastic and can cut parts shorter than 1000 mm. The fiber laser cutting machine, used for metals, operates with nitrogen or oxygen. Nitrogen, an inert gas, provides cooling effects and does not react with molten metal, preventing oxidation. Oxygen, on the other hand, reacts with metal, potentially causing slight edge burning but is more cost-effective and faster, making it suitable for thicker parts. Nitrogen cutting is preferred for smaller parts to avoid burnt edges, whereas oxygen is chosen for larger components like the bridge to minimise costs, accepting a slightly worse surface finish.

Various materials, such as steel, aluminium, stainless steel, and plastic, could potentially be chosen for the components of the design. However, plastic is unsuitable for the bridge due to its low density, leading to an excessively light structure. This would cause issues during experiments with the modal hammer, particularly in terms of structure bouncing (ensuring double hits). Additionally, the fixed quantities determined by the similarity analysis pose challenges in meeting the specified train mass limit. The choice among the remaining metals is influenced by factors like processability, price, and availability. Availability is dependent on the existing stock in the workplace, which typically includes various thicknesses of blank steel plates, aluminium plates, steel strips, and round bars. The similarity analysis underscores the need for lightweight components, requiring the use of thin plates. Only galvanised steel with a thickness of 0.5 mm aligns with the values derived from the similarity analysis and is readily available in stock. Consequently, steel is primarily chosen for its suitability in terms of required thickness, ease of processing, and cost-effectiveness.

In the design process, bolt selection depends upon available space (e.g. sufficient space around holes even when a plate is bent) and the maximum force exerted on

various components. Bolts are primarily determined by the shear force applied to the structure, which depends on bolt size and shear force. The shear force τ_{bolt} in MPa for an M2 bolt subjected to a shear force equivalent to half the train mass is given by

$$\tau_{\text{bolt}} = \frac{F}{A} = \frac{0.5M_{\text{train}}g}{\frac{1}{4}\pi d^2} = 2.65 \quad (\text{G.1})$$

This simplified equation assumes an even distribution of shear force across the entire cross-sectional area. This is a valid assumption as the shear stress remains significantly below the yield strength. In cases where the value approaches the yield strength, a more advanced equation would be consulted. For the type 50 stainless steel bolt (the weakest bolt type) with a yield strength of 210 MPa, failure would not occur under the specified conditions.

G.2 Bridge structure

The dimensions of the pillars are determined by the minimum dimensions of the press brake and its ability to withstand the applicable normal force given that the pillars are pinned at both ends. The worst-case scenario for the maximum normal force on a single pillar is assumed to be half of the train mass. As earlier mentioned, the minimum dimensions for a bent plate are 6 mm (L_{leg}) by 8 mm (V_{die}). The uniaxial normal stress ($\sigma_{\text{n,pillar}}$) in MPa for a bent plate with a thickness of 0.5 mm (t) is given by:

$$\sigma_{\text{n,pillar}} = \frac{F}{A} = \frac{0.5 \cdot M_{\text{train}} \cdot g}{(L_{\text{leg}} \cdot V_{\text{die}}) - ((L_{\text{leg}} - t) \cdot (V_{\text{die}} - t))} = 1.24 \quad (\text{G.2})$$

This calculation is based on Saint-Venant's principle, where stress is evenly distributed across the entire cross-section. This assumption is valid when the length of the bar is significantly greater than its diameter, which is the case for these pillars. The normal stress is far from reaching critical levels or exceeding the maximum stress, indicating the press brake's dimensions are leading instead of stress.

The distance between consecutive pillars is determined by A_{bridge} and I_{bridge} , leading to an iterative process to fulfil the similarity analysis. This distance also hinges on the maximum stress to prevent rail segment failure. Due to the length constraint of the press brake, the distance between two pillars (L_{pillars}) is set at 285.71 mm (calculated as 2000 mm divided by 7). This allows for pillar repetition along the bridge's length and facilitates the distribution of the train load across multiple pillars. The value of I_{rails} (961.41 mm⁴) is obtained from SOLIDWORKS using the Section Properties tool. The y -coordinate of the centroidal axis is 4.83 mm, and the total height of the rails is 13.49 mm, resulting in a maximum fiber distance of 8.66 mm (z_{max}).

To calculate the bending stress in the rails induced by pure bending, the Euler-Bernoulli beam theory (classical bending theory) is applied. This theory, neglecting transverse shear, is suitable for slender beams, as is the case with the rails. The bending stress of the rails ($\sigma_{\text{b,rails}}$) in MPa is given by:

$$\sigma_{\text{b,rails}} = \frac{M \cdot z}{I_{\text{rails}}} = \frac{0.5 \cdot M_{\text{train}} \cdot g \cdot 0.5 \cdot L_{\text{pillars}} \cdot z_{\text{max}}}{I_{\text{rails}}} = 10.73 \quad (\text{G.3})$$

where compression occurs at the top of the profile and tension at the bottom. This stress calculation indicates that the stress is significantly below the maximum allowable stress for steel, ensuring that failure will not occur in the rail structure. It also implies that factors like A_{bridge} and I_{bridge} are essential in the design process in meeting the similarity analysis, rather than the maximum stress.

The top plate of the bridge has undergone a topology optimisation process. This simulation entails analysing the structure under the specified load conditions to identify

the material contributing most significantly to those conditions. The result of this analysis guides the removal of material with low contributions and the addition of material where stress levels are high. Throughout this simulation, considerations have been made to ensure that sufficient space is maintained around holes and bend lines to facilitate manufacturability. The simulation involves applying the train mass as a load on the top plate's holes while keeping the remaining pillars fixed. Material removal occurs incrementally, ultimately resulting in the optimised top plate of the bridge section.

G.3 Train

A decision has been made regarding the manufacturing method for the train, considering additive manufacturing versus bent steel plates. Additive manufacturing typically produces plastic parts, while conventional processes like cutting and bending yield metal parts. These different materials result in differences in the strength-to-weight ratio of the parts. Additive manufacturing allows for more design flexibility compared to conventional methods. Multiple designs are explored, with the steel plate design meeting the similarity analysis criteria and being easy to manufacture. The additive manufacturing design could not meet the mass requirements due to the substantial material needed, especially at connection points like the axles. Consequently, steel plates are chosen for the primary train components to fulfil the requirements.

The bogie's components are illustrated in fig. G.1. A spring cap is placed to secure the spring's position and the spring has been glued during assembly to prevent displacement. The cap's diameter is larger than that of the spring, allowing for free expansion during compression. The control arm is designed as a single bent part to enhance strength and reduce part count. While this configuration restricts independent movement of both sides of an axle, it is considered sufficient since movement is anticipated to be limited.

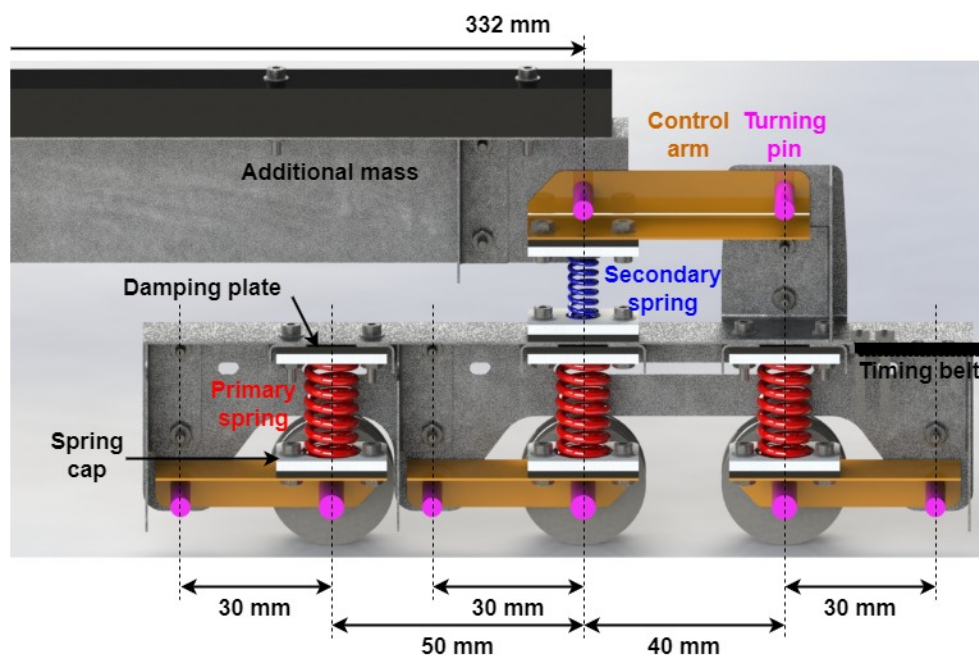


Figure G.1: A section view of the bogie and its main components.

The control arms are oriented outward to create additional space for both design

and assembly considerations. Furthermore, U-profile plates are incorporated into the bogie outer frame and body frame to enhance stiffness in longitudinal, lateral, and torsional directions. Bolts are used to attach the timing belt to both sides of the train. A hole pattern is introduced to enable proper tensioning of the timing belt, ensuring sufficient friction between the belt and the pulley.

To meet the mass requirement stipulated in the similarity analysis, the wheels are placed around the outer frame of the bogie. These wheels are equipped with bearings to minimise friction. Steel wheels are utilised to withstand the high contact force, as plastic wheels are prone to plastic deformation. The steel wheels are manufactured using a lathe, and a protrusion is added to prevent collisions by creating space between the control arm and the wheel. Moreover, the hole in the wheel is bigger than the inside diameter of the bearings, ensuring contact only occurs between the bearing and the axle.

G.4 Motor system

The selection of the electric motor depends on the train's velocity and entrance length, as determined by the following equation:

$$P_{\text{motor}} = v_{\text{final}} M_{\text{train}} \left(\frac{v_{\text{final}}^2 - v_{\text{initial}}^2}{2L_{\text{entrance}}} + g\mu \right) \quad (\text{G.4})$$

This equation is based on second law of Newton, where the force is a combination between frictional forces and accelerations forces.

The choice of the pulley is determined by the required diameter to achieve the desired surface speed, which equals the train's velocity. The surface speed is given by:

$$v_{\text{surface.speed}} = \frac{\pi \cdot d_{\text{axle}} \cdot \text{RPM}}{60} \quad (\text{G.5})$$

Where RPM represents the motor's revolutions per minute. For a specific velocity of 2.0 m/s and an electric motor with an RPM of 1425 revolutions per minute, a pulley diameter of 26.8 mm is required.

G.5 Challenges

Designing the bridge presents challenges in achieving the specified A_{bridge} and I_{bridge} values from the similarity analysis while maximising the space between pillars. Additionally, designing the rail segment poses difficulties, with various approaches considered, including a single component, custom tools, and multiple parts.

For the train, the primary challenge involves accommodating all components within the constrained space of the bogie. This space is dictated by the bridge's design width. This requires an iterative approach to reach an optimal design. Ensuring the desired mass for the bogie and wheels proved challenging, although achieving the desired body mass is relatively easier due to the addition of an extra strip (added mass).

H | Validation experimental setup

This appendix provides additional details regarding the validations performed for the experimental setup. The first validation involves a comparison between the physical quantities of the prototype and those of the SOLIDWORKS design. The second validation involves a comparison of the frequency and mass ratios between the model and the design.

H.1 Validation prototype and design

The comparison between the prototype and design is presented in table H.1. The mass, inertia and length quantities are directly extracted from SOLIDWORKS. The values for I_{bridge} and A_{bridge} are approximated using the Section Properties tool in SOLIDWORKS. I_{bridge} is approximated by calculating the second moment of area at 2.5 mm intervals along the bridge and then averaging these values, similar to performing a Riemann sum. Meanwhile, A_{bridge} is estimated by dividing the free-hanging bridge mass by the material density and bridge length, resulting in an average cross-sectional area.

It is assumed that the material properties are consistent in both cases. The selection of springs for the design relies on their spring coefficient, initial length, and maximum force capacity. A spring is chosen based on its closest match to the desired spring coefficient while satisfying the other two criteria. The analysis of the relaxed model indicates that damping has negligible influence and, as a result, is not subjected to further verification.

Table H.1: Validation of the physical quantities between the prototype (similarity analysis) and SOLIDWORKS design with associated differences.

Quantity	Unit	Prototype	Design	Difference
E_{bridge}	Nm ⁻²	$2.050 \cdot 10^{11}$	$2.050 \cdot 10^{11}$	0%
I_{bridge}	m ⁴	$4.586 \cdot 10^{-7}$	$4.877 \cdot 10^{-7}$	6.35%
L_{bridge}	m	2.000	2.000	0%
ρ_{bridge}	kgm ⁻³	$7.850 \cdot 10^3$	$7.850 \cdot 10^3$	0%
A_{bridge}	m ²	$9.197 \cdot 10^{-5}$	$9.727 \cdot 10^{-5}$	5.76%
\bar{M}_{tb}	kg	$9.790 \cdot 10^{-1}$	$9.872 \cdot 10^{-1}$	0.84%
J_{tb}	kgm ²	$1.864 \cdot 10^{-2}$	$1.084 \cdot 10^{-2}$	41.85%
M_{b}	kg	$1.546 \cdot 10^{-1}$	$1.546 \cdot 10^{-1}$	0%
J_{b}	kgm ²	$1.075 \cdot 10^{-4}$	$4.685 \cdot 10^{-4}$	335.81%
M_{w}	kg	$6.862 \cdot 10^{-2}$	$6.887 \cdot 10^{-2}$	0.36%
J_{w}	kgm ²	$4.208 \cdot 10^{-5}$	$1.6488 \cdot 10^{-6}$	96.08%
\bar{K}_{p}	Nm ⁻¹	$3.640 \cdot 10^4$	$3.630 \cdot 10^4$	0.27%
\bar{K}_{s}	Nm ⁻¹	$1.560 \cdot 10^4$	$1.610 \cdot 10^4$	3.21%
\bar{R}_{w}	m	$1.258 \cdot 10^{-2}$	$1.250 \cdot 10^{-2}$	0.64%
L_{wb1}	m	$4.182 \cdot 10^{-2}$	$4.000 \cdot 10^{-2}$	4.35%
L_{wb2}	m	$5.000 \cdot 10^{-2}$	$5.000 \cdot 10^{-2}$	0%
L_{b}	m	$3.320 \cdot 10^{-1}$	$3.320 \cdot 10^{-1}$	0%

A slight deviation exists between the values of I_{bridge} and A_{bridge} , as is illustrated in table H.1. This difference arises from a combination of factors, including the min-

imum dimensions of the press brake and the necessity to maintain adequate space between the pillars for train passage. Consequently, there is a greater difference in the mass of the bridge, as illustrated in table H.2. However, the variation in the bridge's fundamental frequency remains minimal and is therefore deemed acceptable.

The train's mass quantities remain similar between the design and prototype, as indicated in table H.1. On the other hand, there is a relatively higher error in the inertia terms. Nevertheless, as discussed in the relaxed model, these terms have a negligible impact on the bouncing frequency of the train components. The selection of spring coefficients closely aligns with the desired values. The decision to modify the wheel radius to a standard size of 25 mm was driven by manufacturing considerations and the negligible impact of this quantity on the final result. Variations in the wheel-base are attributed to practical considerations. As demonstrated in table H.2, the bouncing natural frequencies are similar, with only a slight deviation.

Table H.2: Frequency and mass ratios between prototype (similarity analysis) and SOLIDWORKS design with associated differences.

Quantity	Unit	Prototype	Design	Difference
f_{bridge}	Hz	141.715	142.098	0.27%
f_{body}	Hz	26.514	26.740	0.86%
f_{bogje1}	Hz	143.033	142.978	0.04%
f_{bogje2}	Hz	143.205	143.619	0.29%
M_{bridge}	kg	1.444	1.527	5.75%

H.2 Validation model and design

The final validation requires several frequency and mass components, which can be found in table H.3. The calculation of these frequencies adheres to the matrix definitions outlined in appendix B. The model quantities are grounded in the Boyne Viaduct and locomotive train configuration provided in appendix A and appendix B, respectively. The specific design values can be found in table H.1.

Table H.3: Frequency and mass values of both the model (Boyne Viaduct) and SOLIDWORKS design.

Quantity	Unit	Model	Design
f_{bridge}	Hz	3.510	142.098
$f_{\text{b.body}}$	Hz	0.656	26.742
$f_{\text{b.bogje1}}$	Hz	3.532	142.978
$f_{\text{b.bogje2}}$	Hz	3.536	143.619
M_{bridge}	kg	95106.675	1.527

I | Settings experiments

This appendix offers more detailed information on the conducted experiments and is divided into two sections. The first section outlines the equipment and settings used in the Sound and Vibration Measurement System for the natural frequency analysis, while the second section delves into the settings for the dynamic analysis.

I.1 Natural frequency analysis

Tools has been designed to capture the bouncing frequencies of the body and bogie, as highlighted in red in fig. I.1. These tools separate the system into distinct parts, allowing for precise capture of the specific (bouncing) frequencies.

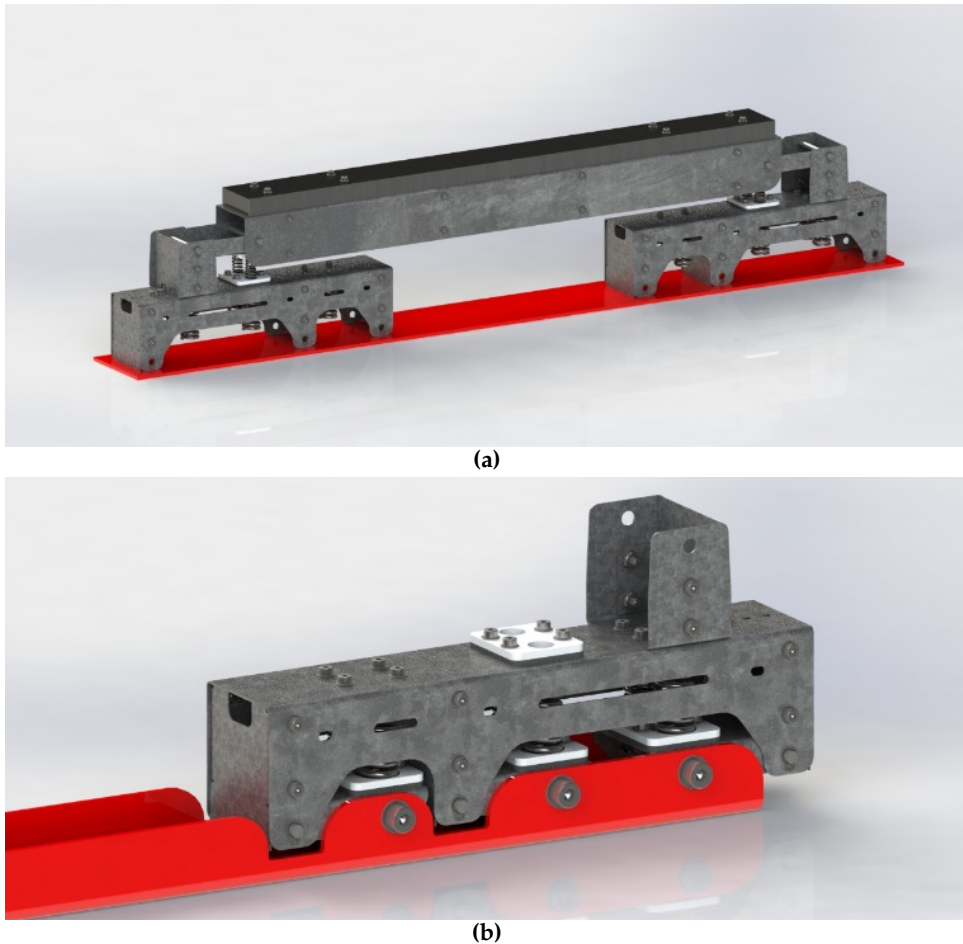


Figure I.1: Tools employed for obtaining the natural frequency of (a) the body or (b) the bogie.

The settings applied in the Sound and Vibration Measurement System are outlined in table I.1. The selected frequency range should encompass the expected observed frequencies. While the highest frequency observed in these experiments is around 145 Hz, a broader range up to 1000 Hz ensures capturing any deviations effectively. The frequency step, also known as resolution, crucially impacts the quality of the acquired response and is determined experimentally for a smooth response. When obtaining natural frequencies, using a window (and thus overlap) is unnecessary for

satisfactory results. Default settings for averaging, weighting, linear mode, slope, and pre-sample are used. A minimum of three averages is required for valid results. Activating the analog trigger is vital for initiating recording; otherwise, measurement starts only after pressing the start button. The trigger level should be set to prevent accidental triggers due to movements like handling the hammer, and should only activate when the structure is struck.

Table I.1: *Measurement settings for the Sound and Vibration Measurement System.*

Setting	Input
Frequency range	0 - 1000 Hz
Frequency step	1.0 Hz
Window	none
overlap	0 %
Averaging	RMS averaging
Weighting	Linear
Averages	3
linear mode	one shot
Analog trigger	on
trigger channel	Dev3/ai0
slope	Rising
level	0.2
pre-sample	1000

For initial experiments, a recording time of 1 second is chosen, considered adequate for capturing the complete response before its decay. This duration is determined through experimental testing, observing when the response has sufficiently decayed. The default sampling frequency of 48000 samples per second (S/s) is employed.

I.2 Dynamic analysis

During this experiment, it is essential to specify both the motor input and the sampling frequency. The motor voltage starts at 3 Volts and is adjusted in various experiments to vary the train's velocity. The current is fixed at 2 Amperes, controlling the initial acceleration. Lower current reduces motor power, limiting acceleration. However, it must be sufficiently high to ensure consistent velocity before entering the bridge section. Moreover, the sampling frequency is set at 1600 samples per second (S/s) to capture adequate signal information. It adheres to the Nyquist criterion, being at least twice the signal's highest frequency. This frequency is lower than the natural frequency analysis because data will be processed in MATLAB, and excessive amount of data is counterproductive.

J | Numerical model development

This appendix focuses on the development of the numerical model, encompassing both train and bridge components, and provides additional details beyond those presented in the main text. The development of the three train variants, namely bogie, half-train, and train, is achieved in four stages. The bridge development addresses the element type and beam theory.

J.1 Train

The development of the train model unfolds in four stages, as illustrated in fig. J.1. The first stage primarily involves reorganising the benchmark model. The second stage entails expanding this model to incorporate two suspension systems, with a velocity boundary condition applied at all nodes. The third stage involves reducing the velocity boundary condition to a single node by introducing link connectors. The final stage extends the bogie model with a secondary suspension system, forming the half-train model and train model. The remainder of this section delve into the decisions made and challenges faced during these stages.

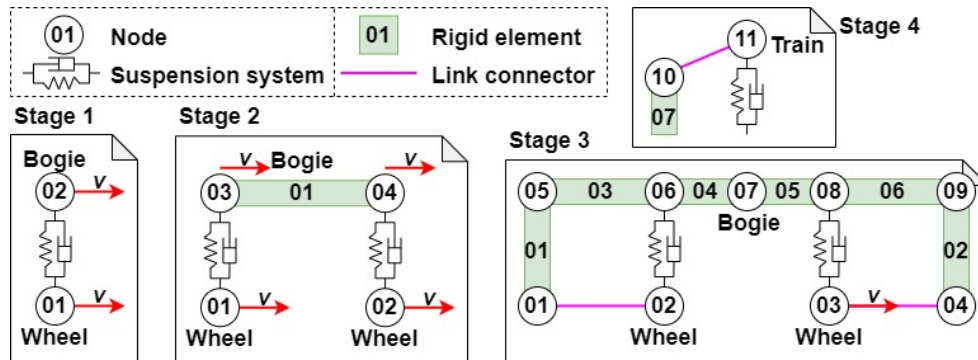


Figure J.1: The four stages of the model development of the train part.

Stage 2:

The model is expanded by incorporating an additional suspended mass and connecting both sprung masses. The nodes are linked using a rigid element, see fig. J.1 the green element 1, along with a rigid body. It is noteworthy that a damper element must be introduced in the assembly definition rather than within (train) part to prevent an error where a rigid element and a connector (damper element) can not be combined within a part. The rigid body comprises nodes and elements, and its movement is determined by a single node's motion [53]. Consequently, employing a rigid body with a rigid element ensures uniform motion across all nodes when a velocity boundary condition is applied to a specific node in the model.

Stage 3:

The subsequent step involves reducing the velocity boundary condition to a single node, which is more representative of the actual case. However, employing the model developed so far and reducing the velocity boundary condition to a single node leads to an unrealistic motion of the train model. This motion is characterised by a circular motion of the bogie and wheel (node 1) around the driving wheel (node 2), as depicted in fig. J.2. This motion is chaotic, with the rest of the train model

(bogie and wheel) oscillating back and forth around the first wheel. This behaviour arises because the suspension system fails to remain upright, causing the angle between the wheel and bogie to deviate from perpendicularity.

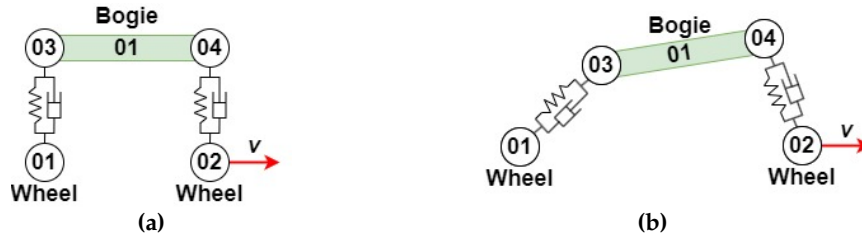


Figure J.2: Crash cases with the velocity boundary condition applied at the wheel node (node 2) for (a) before simulation or (b) during simulation.

To overcome this behaviour, several options were explored, such as combining all nodes into a single rigid body. However, this approach failed proved ineffective because the rigid body links all degrees of freedom of the nodes and the applied boundary condition. Consequently, this approach led to a scenario where the velocity boundary condition affected all nodes, mirroring the initial problem encountered. Another approach involved implementing a kinematic coupling constraint. This constraint restricts the motion of a group of nodes to follow the rigid body motion defined by a reference node [53]. A specific degree of freedom can be allocated, connecting the nodes within the constraint. The expectation was that linking the in-plane rotational degree of freedom (denoted as 6 in Abaqus) would maintain consistent rotation for both wheels and the bogie, thus keeping the suspension system upright. However, controlled circular motion of the bogie around the wheels was observed, as depicted in fig. J.3. It became evident that the suspension system (spring and damper) did not link the rotational degree of freedom of nodes, causing node rotation to remain independent of the suspension system's rotation. Various other constraint options were explored, but they yielded similar failures in the model.

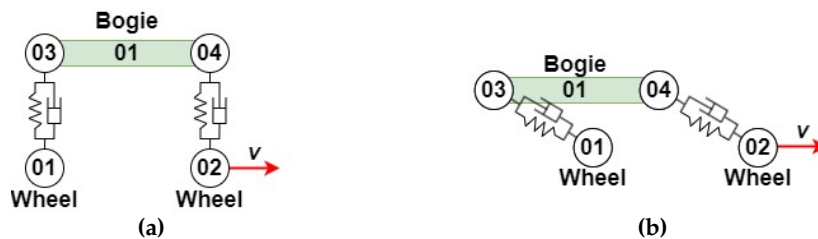


Figure J.3: Crash cases with the velocity boundary condition applied at wheel (node 2) and a kinematic constraint applied to all nodes w.r.t. degree of freedom 6 for (a) before simulation or (b) during simulation.

Stage 4:

Developing the other two train configurations requires incorporating a secondary suspension system. However, attempting to add the second suspension system and links in a similar manner to the existing bogie model leads to a crash during simulation. This crash, illustrated in fig. J.4, depicts the train (node 11) rotated below its original position. This representation remains consistent throughout the simulation. It is important to note that the altered link length in the figure merely serves to highlight the crash type; in the simulation, this distance remains constant. The crash occurs due to the instantaneous application of velocity to the model, resulting in high acceleration. To prevent this crash, two modifications are made to the model.

A ramp, referred to as 'amplitude' in Abaqus, is incorporated into the velocity boundary condition. This ramp ensures a gradual increase in velocity from zero to its fi-

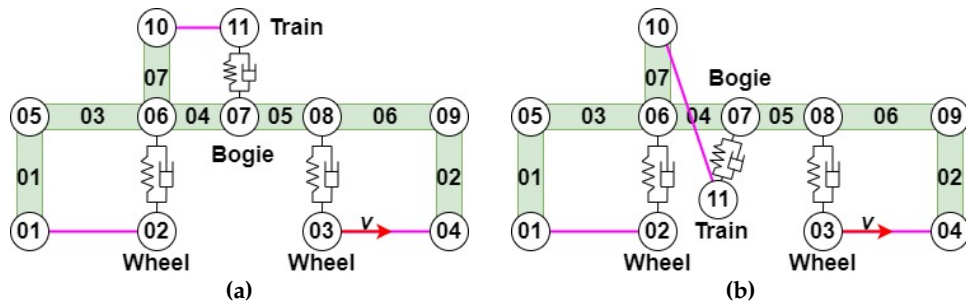


Figure J.4: Crash case after solely adding the secondary suspension system for (a) before simulation or (b) during simulation.

nal value over a specific period. This modification reduces system disturbances, although it's important to note that a longer entrance length is required to attain the final velocity before entering the bridge section.

Additionally, upon applying gravity in the model, compression occurs in the train node (node 11) due to the train mass. This compression reduces the available length to absorb the initial acceleration caused by the applied velocity. This effect is more significant in the secondary suspension due to its lower spring coefficient. Therefore, the second adjustment involves elevating the initial height of the train node (node 11) by the compression length (the force generated by the train mass divided by the spring coefficient), as depicted in fig. J.1. This increase in height ensures a neutral position is achieved after applying the train body mass load to the spring, ensuring the model functions as intended.

J.2 Bridge

Various elements can be utilised in modelling bridge structures, including rigid elements, as well as solid, shell, beam, or truss elements. Each element type serves a specific purpose, with solid elements being commonly employed. Although these elements are suitable for complex designs, their usage significantly prolongs the solution time due to the high element count in the model. Hence, it is necessary to select an element type that reduces the number of elements while ensuring a viable solution. Beam elements are specifically engineered for parts where one dimension is considerably larger than the other two, a characteristic often seen in slender structures like bridges subjected to transverse forces. In such cases, beam elements enable simplification and acceleration numerical problem-solving.

In Abaqus, different beam formulations are available concerning beam type and geometric order, where geometric order denotes the interpolation function. For linear geometric order, the beam type options include 'shear-flexible' and 'cubic formulation'. 'Shear-flexible' corresponds to a B21 beam element rooted in Euler-Bernoulli beam theory, while 'cubic formulation' corresponds to a B23 beam element based on Timoshenko beam theory. The quadratic geometric order represents the B22 beam element, which features 3 nodes instead of the 2 nodes present in the other two beam elements. Both theories offer accuracy for slender beams; however, when the aspect ratio (length over thickness) is relatively low, Euler-Bernoulli beam theory deviates from the accurate solution. This deviation occurs because Euler-Bernoulli beam theory does not consider shear distortion and rotational inertia effects. In contrast, Timoshenko beam theory incorporates these effects, providing a more precise solution for higher aspect ratios.

K | Simulations locomotive

This appendix provides information on dynamic simulations of various subsystems of the bogie variant. The dynamic simulations based on the vertical acceleration of the bridge's quarter node and three-quarter node are depicted in K.1 and K.2, respectively. Both results exhibit behaviour similar to that of the mid-span node on the bridge. However, differences in energy distribution and intensity are evident during the phase transitions.

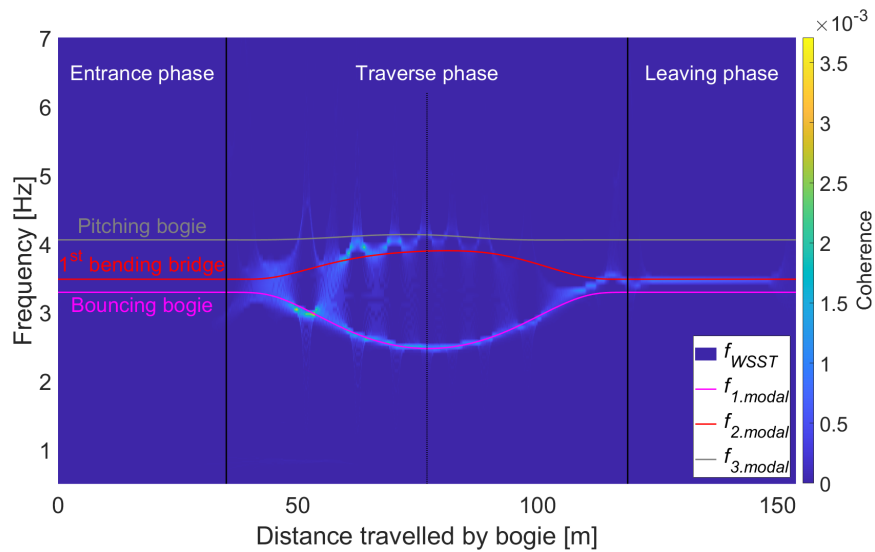


Figure K.1: A comparison for the bogie variant between the modal analysis, and the dynamic analysis based upon the vertical acceleration of the quarter node and a velocity of 10 m/s.

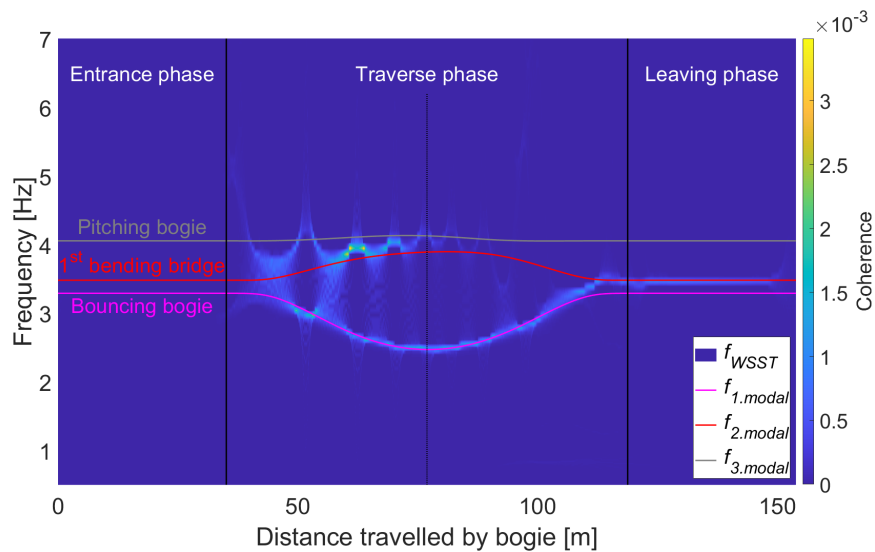


Figure K.2: A comparison for the bogie variant between the modal analysis, and the dynamic analysis based upon the vertical acceleration of the three-quarter node and a velocity of 10 m/s.

Similarly, the dynamic simulation based on the vertical acceleration of the bogie is depicted in K.3. This result closely resembles the behaviour of the bridge's mid-span

node, except for the absence of the bridge's fundamental frequency in the leaving phase.

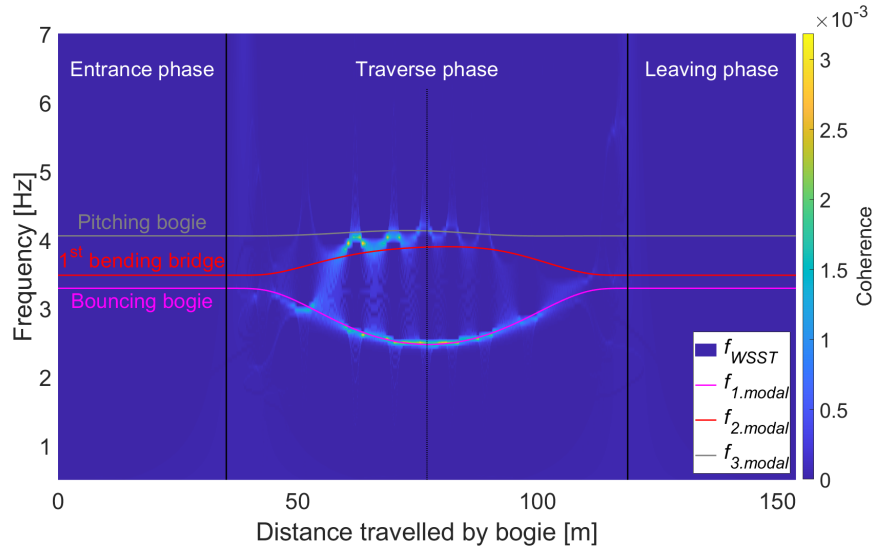


Figure K.3: A comparison for the bogie variant between the modal analysis, and the dynamic analysis based upon the vertical acceleration of the first wheel and a velocity of 10 m/s.

Moreover, the dynamic simulation based upon the vertical acceleration of the bogie is depicted in fig. K.4. Notably, spikes emerge during the entrance phase, although the limited interaction between the train and the bridge. Moreover, there is a lack of energy during the traverse phase, although a similar behaviour to that of the bridge's mid-span node is observed when intensity is adjusted.

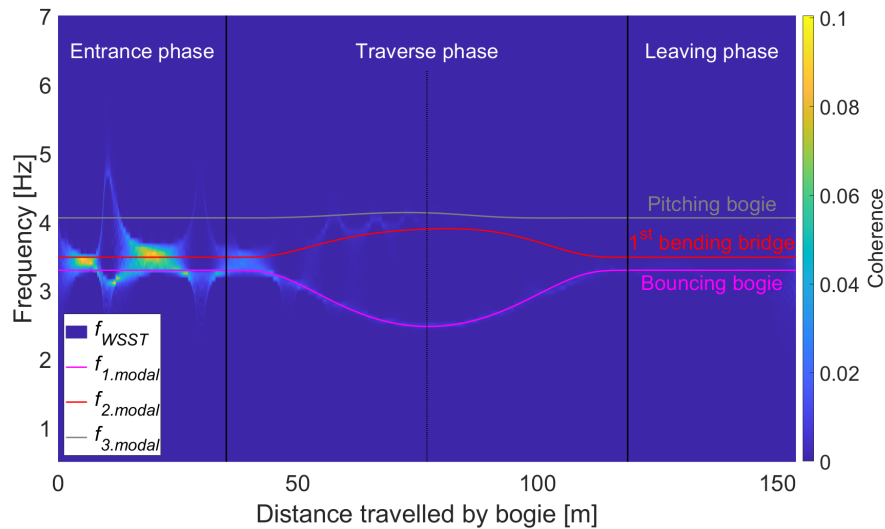


Figure K.4: A comparison for the bogie variant between the modal analysis, and the dynamic analysis based upon the vertical acceleration of the bogie and a velocity of 10 m/s.

L | Variation study: Velocity

This appendix provides information on the variation study of the bogie variant with varying velocity. A simulation conducted at a velocity of 5 m/s is presented in fig. L.1. This figure depicts vertical lines corresponding to the points where the wheels enter and exit the track. Additionally, the in-phase frequency is visible, although the out-of-phase frequency is not distinctly observable at lower velocities.

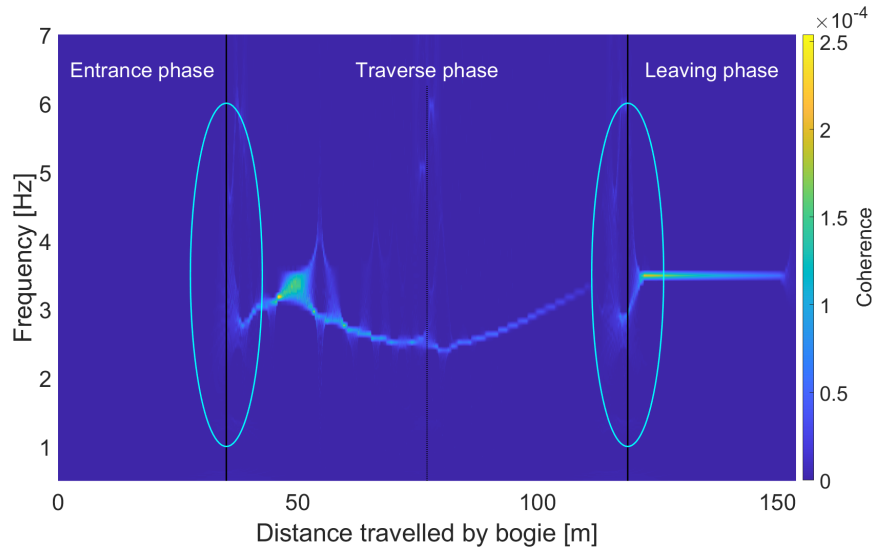


Figure L.1: Dynamic simulation of the bogie variant, grafted upon the locomotive, with a velocity of 5 m/s.

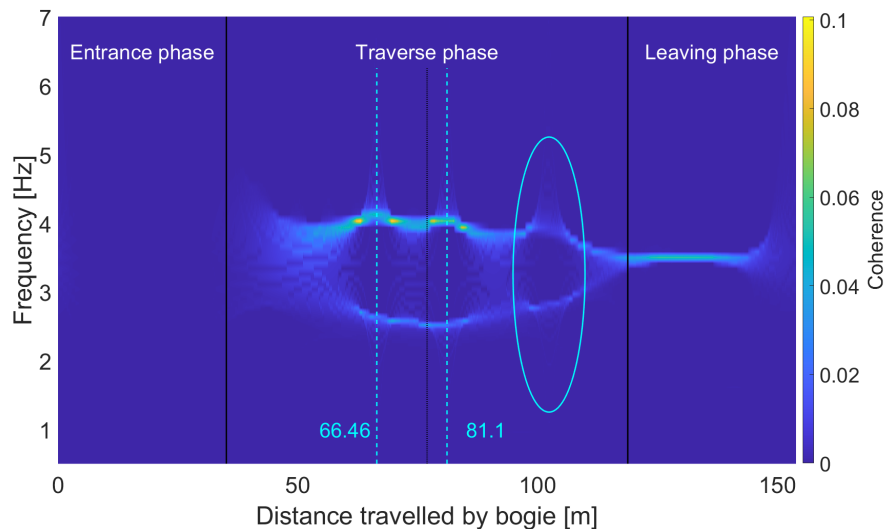


Figure L.2: Dynamic simulation of the bogie variant with a velocity of 23 m/s.

It has been observed that spikes in the frequency content move from left to right across the phases. At a bogie velocity of 23 m/s, as illustrated in fig. L.2, three spikes are visible, with the spikes of interest highlighted using cyan circles. Upon increasing the bogie's velocity to 24 m/s, as depicted in fig. L.3, all spikes shift rightward during the traverse phase. Further elevating the velocity to 25 m/s, as presented in fig. L.4,

results in only two spikes remaining within the traverse phase, while the third spike has exited this phase. Notably, these figures also demonstrate that the two remaining spikes continue to exhibit a left-to-right movement, as indicated by the dotted lines.

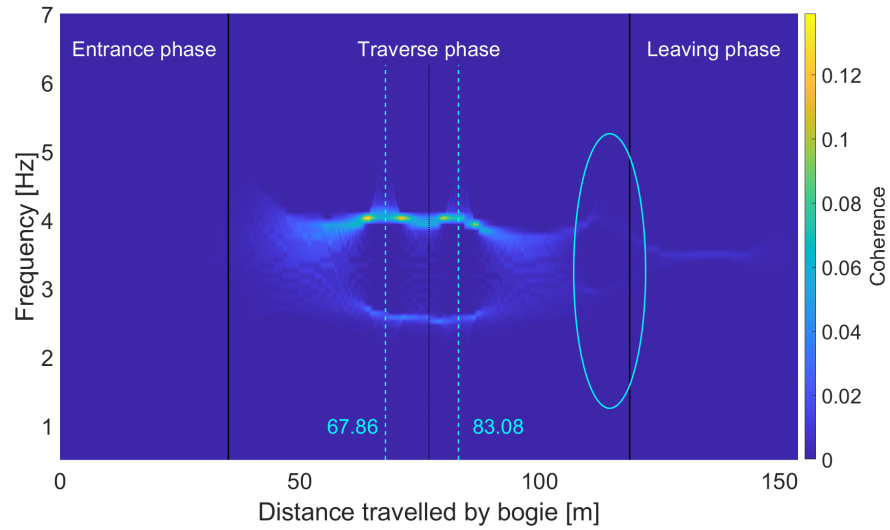


Figure L.3: Dynamic simulation of the bogie variant with a velocity of 24 m/s.

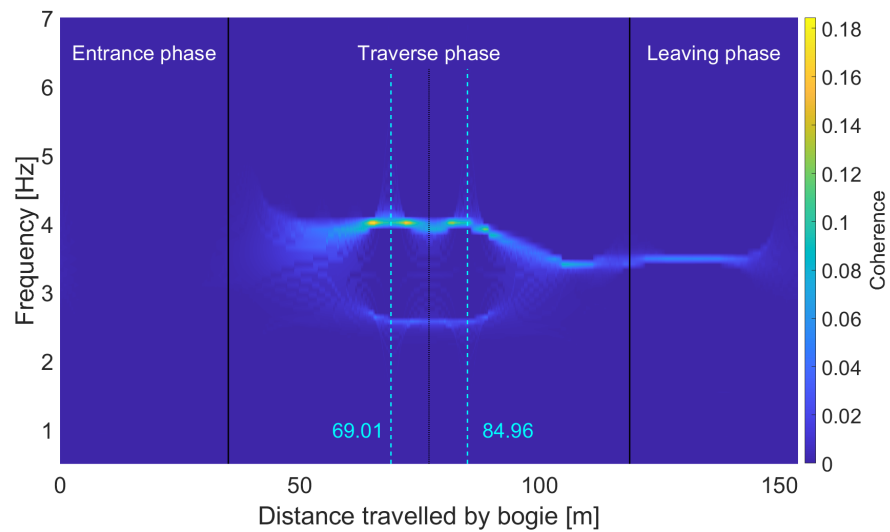


Figure L.4: Dynamic simulation of the bogie variant with a velocity of 25 m/s.

M | Simulations DMU

This appendix provides information on dynamic simulations for various variants. Introducing unequal axle spacing erases the distinct behaviour observed at the mid-span and results in a smoother alignment of the resonance frequency with this location. This behaviour is shown in M.1. This result closely aligns with the modal analysis results, and the occurrence of spikes is less frequent compared to the locomotive variant.

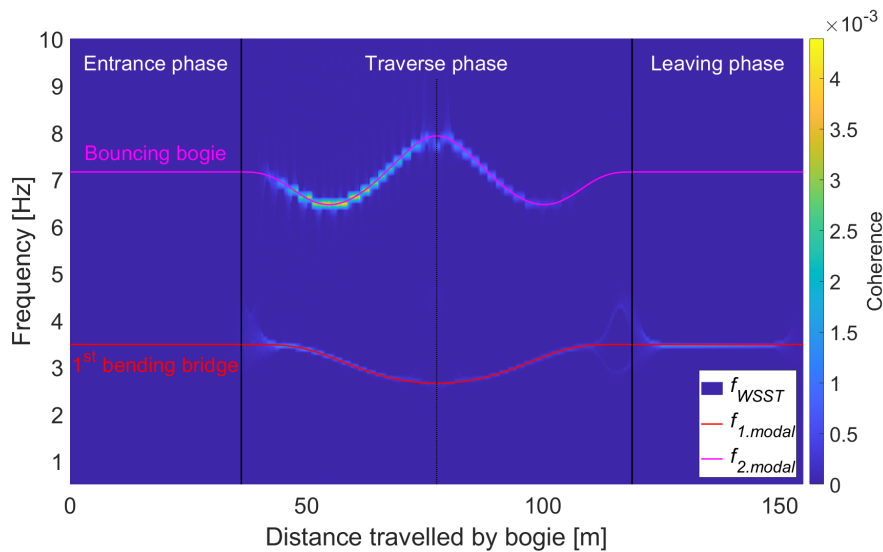


Figure M.1: A comparison for the bogie variant between the modal analysis, and the dynamic analysis based upon the vertical acceleration of the mid-span node, a velocity of 10 m/s, and by equating the damping coefficient, mass ratio and frequency to the locomotive, and introducing unequal axle spacing.

The dynamic simulation of the half-train variant is illustrated in fig. M.2. Here, a single resonance frequency is observed, although the energy in the latter part of the traverse phase exhibits lower intensity. Additionally, a lower frequency is visible, corresponding to the resonance frequency of the body.

The dynamic simulation of the train variant is depicted in fig. M.3. This plot reveals multiple resonance frequencies, although they are not consistently maintained throughout the entire traverse phase. Furthermore, this result displays pronounced wave-like behaviour, which is distinct from the patterns observed in other variants.

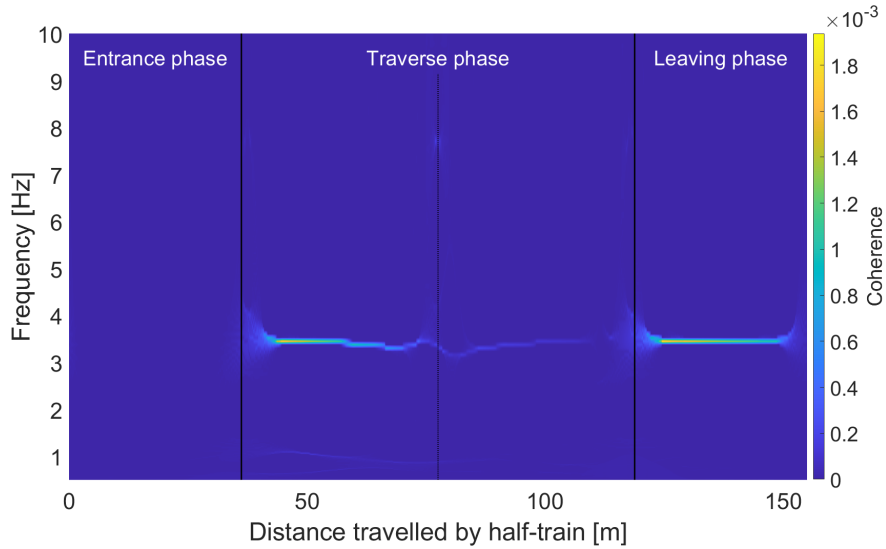


Figure M.2: A comparison for the half-train variant between the modal analysis, and the dynamic analysis based upon the vertical acceleration of the mid-span node and a velocity of 10 m/s.

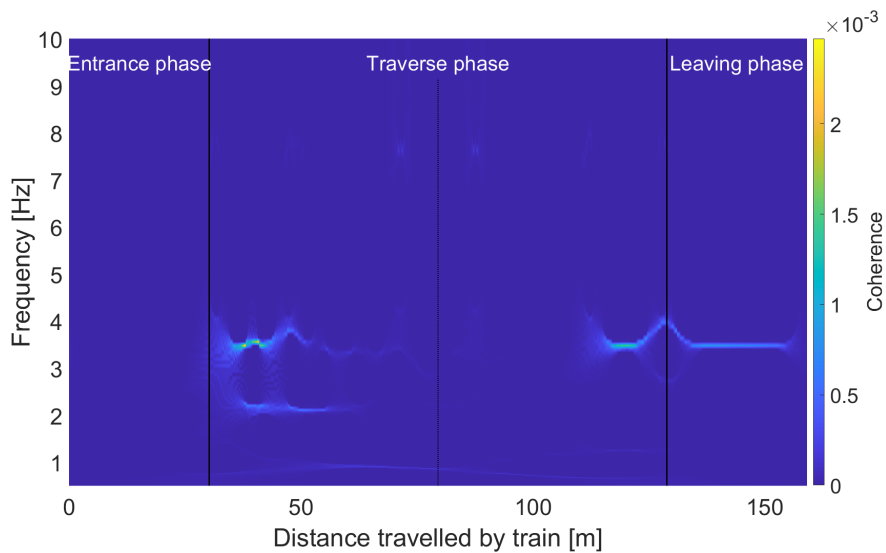


Figure M.3: A comparison for the train variant between the modal analysis, and the dynamic analysis based upon the vertical acceleration of the mid-span node and a velocity of 10 m/s.

N | Experimental results

This appendix provides information on the modal and dynamic analyses conducted on the half-train and train variants. The modal analyses for these variants can be observed in fig. N.1 and fig. N.2, respectively. These results exhibit similarities to those of the bogie variant, as they depict a decrease in the lower limit toward the bridge's mid-span, followed by a return to the original value. Moreover, these variants exhibit an extended range between the lower and upper limits, resembling the characteristics observed in the bogie variant. The experimental results for the half-train exhibit an undesirable spikes at the mid-span, likely attributable to the employed experimental methodology. In contrast to the other variants, the train variant does not maintain a consistent bridge's fundamental frequency throughout the entrance and leaving phase, making it an unsuitable method for this purpose.

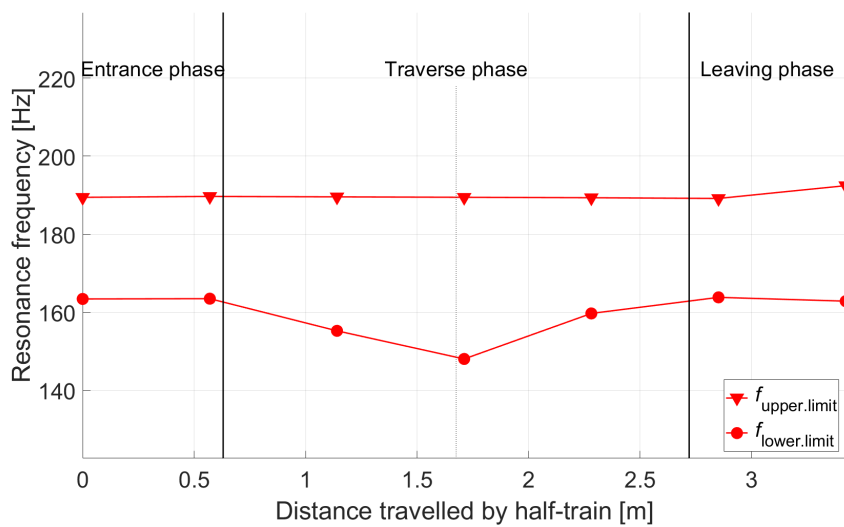


Figure N.1: Modal analysis of the half-train variant across the bridge.

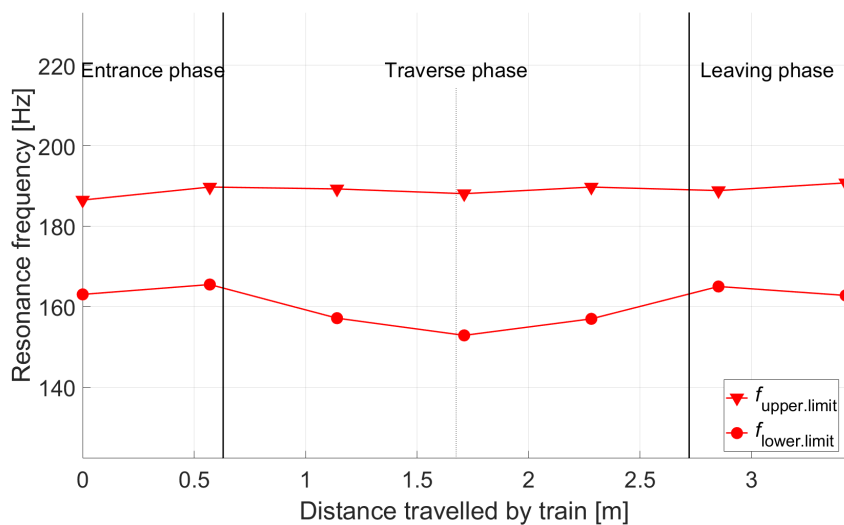


Figure N.2: Modal analysis of the train variant across the bridge.

The dynamic simulation based on the vertical acceleration of the half-train, is displayed in N.3. This result reveals more pronounced frequency content, although none of it aligns with the expected results. Notably, certain frequency content is evident even prior to the train entering the bridge section.

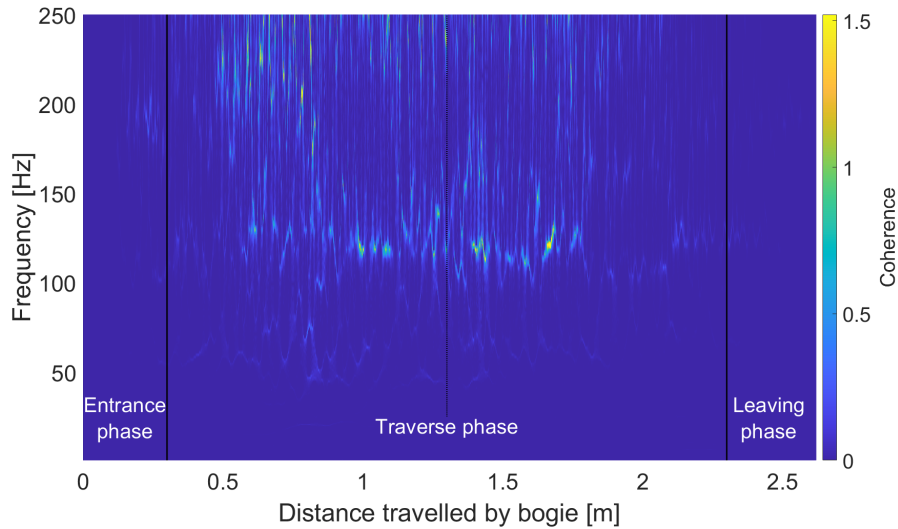


Figure N.3: Dynamic analysis of the half-train variant based upon experimental data from the vertical acceleration of the mid-span node.

The dynamic simulation based on the vertical acceleration of the train is illustrated in N.4. This result exhibits a considerable amount of noise in the frequency content, characterised by vertical lines. However, unlike the numerical simulations, no distinct resonance frequency appeared. Again, there is notable frequency content even prior to the train entering the bridge section, and frequency content during the leaving phase does not align with the bridge's fundamental frequency.

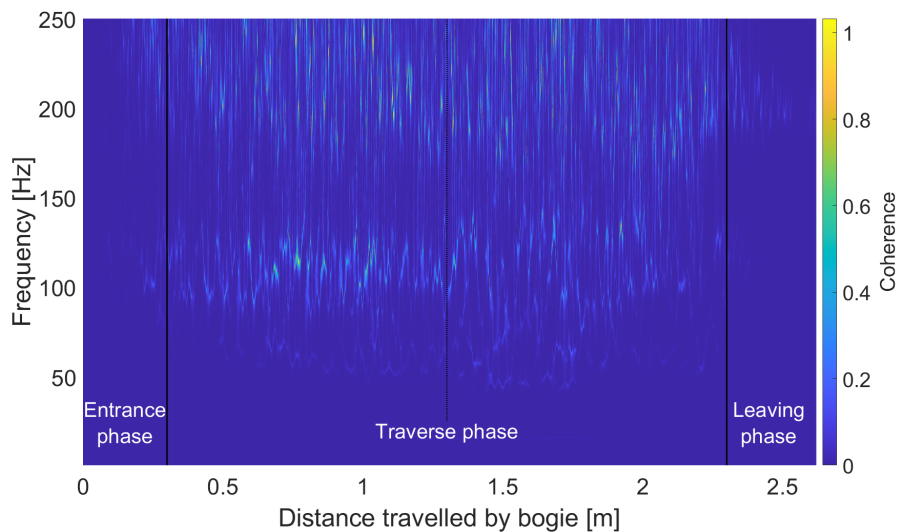


Figure N.4: Dynamic analysis of the train variant based upon experimental data from the vertical acceleration of the mid-span node.

O | Simulations experimental setup

This appendix provides information on modal analysis for various variants. Modal analyses for the half-train and train variants are depicted in O.1 and O.2, respectively. Both figures demonstrate similar behaviour to the bogie variant, where an increased bridge's fundamental frequency leads to similarities between experimental and numerical results. Furthermore, these results indicate a significant difference in the determination of the bridge's fundamental frequency, which appears to be excessively high.

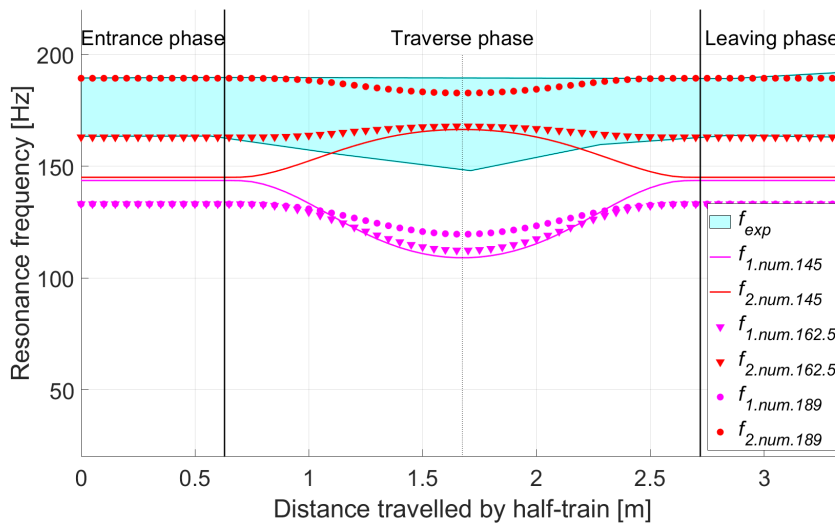


Figure O.1: Modal analysis of the half-train variant across the bridge.

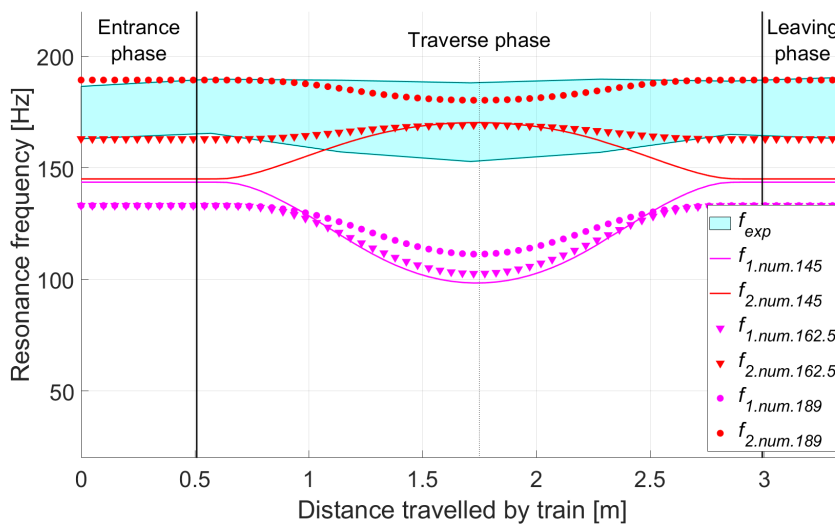


Figure O.2: Modal analysis of the train variant across the bridge.